Diploma Thesis

Operational Optimization of the Geothermal Power Plant Unterhaching

Anastasios Petrou

DA 399
2014/10

Lehrstuhl für Energiesysteme

Supervisor:	Dipl.-Ing. Christoph Wieland Technische Universität München Lehrstuhl für Energiesysteme Boltzmannstr. 15 85748 Garching b. München
Issued:	15.04.2014
Submitted:	15.10.2014

Statutory Declaration

Hiermit versichere ich, die vorliegende Arbeit selbständig und ohne Hilfe Dritter angefertigt zu haben. Gedanken und Zitate, die ich aus fremden Quellen direkt oder indirekt übernommen habe sind als solche kenntlich gemacht. Diese Arbeit hat in gleicher oder ähnlicher Form noch keiner Prüfungsbehörde vorgelegen und wurde bisher nicht veröffentlicht.

Ich erkläre mich damit einverstanden, dass die Arbeit durch den Lehrstuhl für Energiesysteme der Öffentlichkeit zugänglich gemacht werden kann.

All the work enclosed was done by me except where otherwise stated. Every section that reports or paraphrases work by other authors indicates who the other authors are and gives a reference to the article, book, or other source. All quotations from other work are explicitly indicated as such and a reference to the original is given. This work has not yet been published or presented to any academic institution.

I agree that this work can be published by the Institute of Energy Systems.

_____, den _____ _____

Unterschrift

Every human has thousands of paths to be opened in front of him during his life. But his really own path is that one, which if he decides to follow, it makes his fears grow.

Make your fears your motivational power and success is coming.

(*Petrou A., Munich 2014*)

Thanksgiving

The present thesis was conducted at TU Munich in Garching, at which I was member as an exchange student from Erasmus program, during the tenth semester of my studies in Mechanical Engineering in NTU Athens.

First of all, I would like to thank the Assistant Professor of the Laboratory of Steam Boilers and Thermal Plants at NTUA Dr. Mechanical Engineer Sotirios Karellas for being next to my important academic steps and offering me the possibility to write my thesis at TU Munich.

Furthermore, I would like to give my thanks to my supervisor Dipl. Mechanical Engineer Christoph Wieland for his patience, confidence, guidance and great cooperation during the conduction of my thesis.

Also, many thanks to the candidate Mechanical Engineer Lukas Schwan, who wrote his thesis on the same project, for the friendly collaboration and his help on my general adaptation in university and daily life Munich.

Finally, I seize the opportunity to thank my family and especially my parents for all their support throughout my life and particularly throughout my academic steps.

Abstract

Geothermal energy constitutes one of the most widely approved renewable sources to provide heat or produce electric power. Geothermal brines exist also in the area of Unterhaching in south Germany, where proper industrial facilities have been installed to supply with heat nearby households. Simultaneously, electrical energy is produced through a 5-year operated Kalina cycle power plant that exploits the excess of the geothermal hot fluid. Kalina cycle is considered as an efficient power cycle that uses an ammonia-water mixture as working fluid. The high energy consumptions, required for the operation of the power plant in Unterhaching, prevent it from being more profitable. This thesis is based on analyzing the data acquisition system's values and on deriving the specific parameters that influence the several efficiencies and power consumptions. The closed-loop indirect cooling system has been investigated, as pumps and fans constitute high energy consumers. Detailed models that simulate the cooling system have been developed, in order to evaluate the proposed technical solutions and confirm the improvement in the power generation process. Underground cooling of the ambient air that enters the cooling towers, through a buried pipe, has been proposed. This idea has been evaluated through the development of a model that simulates the heat transfer between the sub-soil and the air that flows along the pipe. Calculations verified that, through such an installation, the low temperature of the Kalina cycle can be reduced resulting in an increased power generation and constituting the buried pipe a profitable investment.

Key Words: Geothermal energy, Kalina cycle, Wet-cooling towers, Underground cooling, Buried pipe

Table of contents

List of figures

List of Tables

List of Abbreviations

EAHE	Earth to Air Heat Exchanger
IRR	Internal Rate of Return
LCOE	Levelised Cost of Energy

Nomenclature

A	Area [m^2]
AC	Annual cost [€]
a_c	Convection heat transfer coefficient [W/m^2K]
a_D	Mass transfer coefficient [m/sec]
A_s	Amplitude of the soil surface temperature variation [°C]
B	Breadth [m]
C	Cost [€]
C_D	Drag coefficient
C_p^0	Purchased cost [€]
c_p	Specific heat at constant pressure [J/kgK]
c_{pma}	Specific heat of the air-water vapor mixture [J/kgK]
$ConPerArea$	Unit cost for the condenser per installed unit of heat transfer area [$€/m^2$]
D	Diameter [m]
D_{con}	Concentration gradient [mol/m^3]
D_f	Diffusion coefficient [m^2/s]
D_{pen}	Penetration depth [m]
dV_x	Difference between the partial pressure at water surface and saturation and the partial pressure in air
dz	Discrete element in z-direction
E_y	Power generation in year y

f	Fraction of evaporation rate
F	Force [N[]
F_y	Fuel expenditures in the year y
g	Gravity acceleration [m/s^2]
G	Mass velocity [kgm/s]
h	Enthalpy [J/kg]
H	Height [m]
h_{fg}	Latent heat of water vaporization [J/kg]
h_{ma}	Enthalpy of the air-water vapor mixture per unit mass of dry air [J/kg]
h_{masw}	Enthalpy of saturated air [J/kg]
h_v	Water vapour enthalpy [J/kg]
I_y	Investment expenditures in the year y
j	Runge Kutta variable
J	Diffusion flux [mol/m^2 s]
k	Runge Kutta variable
K	Loss coefficient
l	Runge Kutta variable
L	Length [m]
$LCOE$	Levelised cost of energy
Le_f	Lewis factor
lf	Lifetime of the system

$\dot{m}$	Mass flow rate [kg/sec]
m	Mass [kg]
Me_P	Merkel number
M_{H_2O}	Molar mass of water, $18\ g/mole$
M_y	O&M costs in the year y
N	Number of
N_v	Number of droplets per unit volume
Nu	Nusselt number
OC	Operational cost [€]
p	Pressure water vapor [Pa]
Pr	Prandtl number
P	Power [W]
$\dot{Q}$	Heat flow [W]
Q_c	Sensible heat transfer [W]
Q_m	Enthalpy transfer due to difference in vapour concentration between the saturated air at the interface and the mean stream air [W]
r	Discount rate
R	Radius [m], Thermal resistance [°C/W]
R_g	Gas constant 8.314 [J/kg mol]
Re	Reynolds number
RH	Relative humidity

$Ry_{de}^{b_{de}}$	Characteristic flow parameter
S	Surface area [m^2]
Sc	Schmidt number
S_m	Average solar radiation (W/m^2)
S_v	Amplitude of solar radiation (W/m^2)
T	Temperature [°C]
T_m	Mean ground surface temperature [°C]
U	Overall heat transfer coefficient [W/m^2 K]
u	Velocity [m/s], Annual average value of wind velocity (m/s)
V	Volume [m^3]
$\dot{V}$	Volume flow rate [m^3/s]
v	Kinematic viscosity [m^2/s]
w	Humidity ratio [kg/kg dry air], Annual angular frequency, 1,992x10^{-7}rad/sec
W	Width [m]

Greek Letters

β	Absorption coefficient
Δ	Difference
ΔR	Radiation constant, 63W/m^2
ε	Hemispherical emittance of ground surface, 0.93 to 0.96

θ	Plate inclination angle
$\xi_{T_{de,out}}$	Temperature lapse rate inside the cooling tower
ρ	Density [kg/m^3]
λ	Thermal conductivity [W/m^{o}C]
π	Constant 3.14
μ	Dynamic viscosity [kg/m s]
φ	Concentration [mol/m^3]
φ_I	Phase angle between the insolation and the air temperature (rad)
φ_s	Phase angle difference between the air and soil surface temperature (rad)

Subscripts

a	Air
abs	Absolute
air	Ambient Air
av	Air-vapor
con	Condenser
cs	Cold side
ct	Inlet loss coeffient
eff	Efficiency

eff	Efficiency
elec	Electricity
ev	Evaporation
$F/difst$	Fan-Diffuser static
fdm	Specified fill
fi	Actual fill
$fill$	Fill packing
fr	Frontal area
fs	Fill support system
g	Gravitational
HE	Heat exchanger
hs	Hot side
iL	Inlet louvers
in	Inlet
int	Interval
$longrad$	Long-wave radiation
$made$	After spray zone – drift eliminator
out	Outlet
p	Pipe
phe	Plate heat exchanger
rej	Rejection

rz	Rain zone
s	Soil
$solrad$	Solar radiation
sp	Spray zone
$spfill$	Spray zone
ss	Superasaturated
$ssfill$	Support structure of the fill
st	Static
sur	Surface
sw	Saturated moist air at water temperature
tot	Total
tr	transfer
up	Upstream
$upfill$	Upstream of the fill packing
v	vapor
$vcfi$	Vicinity of the fill
vwb	Water-vapor
w	Water
wb	Wet-bulb
wd	Water distribution system
$wdfill$	Water distribution system
wf	Working fluid

1 Introduction

1.1 Motivation

Geothermal energy constitutes one of the most widely approved renewable sources to provide heat or produce electric power, due to several factors, such as low operational costs, no dependence on fossil fuels, no environmental pollution and its direct use from the heat source. In south Germany, and particularly in south Munich in the area of Unterhaching, a hot water sink with temperatures up to 140°C has been located. Since 2009, there operates a Kalina cycle power plant, which is supplied with geothermal fluid pumped from this source in order to generate electric power and provide it to the grid. The power plant is capable to produce up to 3.5MW. Although it owns to the municipality of Unterhaching, it constitutes an enterprise that has to be profitable and return the capital that has been invested. On the one hand such geothermal binary fluid power plants are characterized by a long lifespan that may exceed the 25 years, but on the other hand their high energy consumption required for the process prevents them from being directly profitable. The main goal of this thesis is to identify which are the main energy consumers during the operation of the plant, to derive the parameters that may influence them, to figure out whether technical solutions could be implemented in order to improve their efficiencies and to evaluate, finally, these ideas. Of course, there exist two ways to make the power plant more financially beneficial. One is by reducing the existing energy consumption, while the other, which is based on the Carnot's theorem, is to improve the total power cycle's efficiency and result in a higher power output by reducing the cold temperature of the cycle, i.e. the working fluid's temperature at the condenser's outlet. For the second way of improvement, the higher price of the electricity that is sold than this that electricity is purchased should be taken into account.

1.2 Task

As aforementioned in „Motivation" paragraph, the main goal of this thesis is to figure out solutions that can be implemented in the since 2009 operating Kalina cycle power plant in Unterhaching, in order to optimize or even improve its operation concerning either the produced output or the energy consumption. As the power plant has already been constructed, it is preferable to look for a solution that would have a quick return of investment, be easy to install without obstructing the normal plant's operation, result in an efficient improvement on a specific problem and do not add another energy consumer that is affected by other factors. For this purpose, the data received from the Unterhaching power plant concerning the sensors' values throughout a certain period of the year 2013 and the design specifications of several process equipment were thoroughly analysed and the great influence of the indirect cooling system was observed. Models that simulate the heat and transfer phenomena that take place in the cooling tower between air and water and the heat transfer between air and sub-soil during underground cooling have been developed. Moreover, algorithms content also equation for calculating firstly the pressure losses in the cooling towers, the rest cooling system and the buried pipe and finally evaluate the required power consumption for a specific cooling performance. An algorithm that takes into account all energy consumer by combining the several models has been constructed and an evaluation of the EAHE operation has been conducted.

1.3 Thesis Outline

After the Introduction part in the present chapter 1 and the Summary/Outlook in chapter 2, the thesis starts on chapter 3 with a general overview of the geothermal energy. The nowadays situation of renewable sources and especially geothermal energy is primarily presented and continues with a reference on the geothermal fluid and the different geothermal applications that have been developed depending the available heat sources and the desired power output. A financially-wise aspect of a geothermal power plant is, also, quoted regarding its capital cost and the feed-in tariffs that exist in Germany.

Chapter 4 focuses mainly on the Kalina power cycle by reviewing the binary cycles developed until now, explaining its process, the thermo-physical features of ammonia-water mixture and its special behaviour throughout the power cycle. A cost estimation of Kalina power plants and various possible equipment arrangements are also included, as well as a table with the relative technology installations around the world.

A presentation of the Unterhaching power plant can be found on chapter 5. The route of constructions and operational milestones in the area of south Munich are noted down and the problem of the high energy consumption is numerically verified. Furthermore, this chapters contents the illustrative depiction of the parameters' fluctuations throughout the given period of the year, concerning the cooling – condensing system. A correlation coefficient analysis has also been conducted in order to investigate possible correlation among the several variables.

Chapter 6 includes the first simulation model regarding cooling towers, after describing shortly their principles. The whole thermodynamic and mathematical background for each zone of the tower, where the algorithm is based on, is explained here in detail. The way of calculating the pressure losses in the whole cooling system is presented in order to define the pump and fan power consumptions. A parameters' variation is conducted for each model, to investigate further how they reflect in several changes and the cooling tower's model is compared with real registered from the power plant values. In addition, an algorithm that combines all the models has been created, for the illustrative overview of the main consumers behaviour depending on the cooling performance required. The relative figures that characterize the cooling towers' performance are also extracted and depicted.

Finally, in chapter 7, the solution of underground cooling of the ambient air, that can bring improvement in the operation of the power plant, is presented. Particularly, a simulation model that estimates the sub-soil's temperature throughout the year on an hourly basis is primarily described. Then a model that evaluates the heat transfer phenomenon between earth and a buried pipe is detailed explained in order to develop the relative simulation program. The model is used to investigate the several parameters of the EAHE system and for this purpose relative graphs are presented. An optimization algorithm that extracts the specifications of the pipe that achieves the minimum capital cost of an EAHE system for a given cooling performance. Finally, a financial evaluation of such an investment is presented regarding the improvement that an EAHE system can present on the cooling system and on the power plant production in general.

2 Summary / Outlook

In this thesis, an effort to optimize the operation of geothermal, but also any kind with similar cooling systems, power plants has been made. For this purpose, several models that simulate the process have been developed and combined in such a way that information regarding optimum operation can be extracted. The cooling system has been investigated as a system whose energy consumption can be reduced by taking into account both pump and fan power consumptions. Any power plant that uses such an indirect cooling system can benefit from these algorithms, by combining with suitable control systems. A technical solution has also been proposed, called earth-to-air heat exchanger that can enhance the cooling performance of the cooling tower. Such an installation is able on the one hand to reduce the pump's and fan's power consumptions and on the other hand and even better to increase the possible, for the regarding ambient conditions, power output by decreasing the low temperature of the Kalina cycle. The EAHE solution has been financially evaluated and the results were quite promising. For power plants that operate in hot and dry climates, the exploit of the sub-soil's cooling properties during hot periods of the year can prove to be even more beneficial and enhance substantially their power generation. Regarding the models, much attention should be paid on the assumptions that have been made and the parameters that are defined based on the case of Unterhaching power plant's facilities. Taking all these into account, the models can prove to be a useful tool for evaluating such installations, even for other uses, or investigating any proposed changes on the process. Particularly for the EAHE model, the heat absorption from the soil has also been considered, a phenomenon that was mostly neglected in previous relative studies for buried pipes, making the simulation model and the results be closer to real operation.

3 Geothermal Energy

3.1 Renewable sources

It is widely approved that a renewable revolution is underway. The rapid evolution of renewable power generation applications and simultaneously the rapid reduction in the investment cost of relative technologies constitute a sustaining virtuous circle. The average lifetime levelised cost of electricity generation (LCOE) is descending for wind, solar PV, CSP and biomass technologies, while hydro- and geothermal energy produced under viable conditions are characterized as one of the most cost efficient ways to generate electric power.

The definition of high-quality resources are a very important factor in order to exploit efficiently the geothermal energy, through the mature and base-load generation technology existing nowadays. Financial evaluations concluded that the LCOE of a conventional geothermal project ranges from 0.07€/kWh to 0.1 €/kWh, including a 10% capital cost. Contemporary technologies, able to eliminate the development risks and utilize well-documented or adjacent resources, have been observed to present a competitive LCOE that meets as low as 0.04€/kWh.

3.2 Introduction to geothermal power generation

Geothermal energy is stored in the Earth's interior, in the forms of heat inside the rocks, steam or hot water in the surface's crust or even among Earth's surface, where active geothermal sources exist.

For electricity production purposes, high-temperature water or steam resources (>180°C) seem to be the most efficiently exploitable, through "flashing" technologies, that use steam to drive a turbine. In case of medium-low temperature geothermal fluids, the "binary" plants are the determined way to generate power. The fact that heat exchangers are required to produce steam from a liquid with low boiling point in order to rotate the turbine makes them significantly expensive.

The process of a geothermal project begins with the initial exploration of the Earth's content, so that the available geothermal reservoirs are clearly defined. These first estimations will soon confirmed through the drilling works, which constitute a barrier to the uptake of geothermal power plants, as they are followed by high expenses and time-consuming processes. Then, the next steps involve field construction projects regarding injection and reinjection wells, reservoir management, infrastructure and power plant design.

Geothermal fluid

Geothermal energy is transferred from the deep well up to the surface through the geothermal fluid. It can be either liquid or vapor, hot, sometimes salty and mineral-rich. It is pumped by the feed pumps from the reservoir and isolated during production, in order to

supply geothermal plants and produce power generation. After the exploitation of its heat energy, it is re-injected back into geothermal reservoir that exists in a significant distance from the injection well, so as to be reheated. This kind of resource that is based on the accumulation of existing hot water or steam is called “hydrothermal” resource. Although, also, other types do exist, the majority of geothermal power plants exploit hydrothermal resources. In order to determine the final design specifications of the power plant, basic characteristics of the geothermal fluid, such as temperature profile, content of non-condensable gases and chemistry, should be primarily investigated.

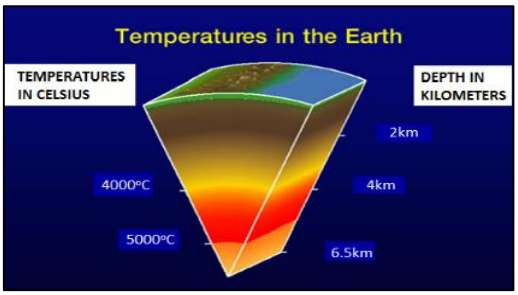

Figure 1: Earth’s temperatures (source: Geothermal Education Office (GEO))

As illustrated in Figure 1 the heat that exist underground in Earth can reach up to thousands of degrees. However, concerning power generation the suitable temperatures are on the one hand 90°C for low-temperature applications and on the other hand 200°C for high-temperatures technologies. Depending the heat provided by the geothermal fluid, the suitable conversion technology is selected, followed by the required process for optimizing the design parameters, such as the size of cooling towers and heat exchangers. It has also to be mentioned that the higher the geothermal source’s temperature the better efficiency can be achieved.

3.3 Geothermal applications

The several geothermal applications that exist nowadays can be divided into two main categories, further described in following paragraphs: the direct and the indirect use.

Direct use

Geothermal resources, through geothermal hot wells, have been used directly for centuries. Geothermal fluid from hot springs can be exploited directly (known as “direct use”) for a wide variety of application. Figure 2 depicts a completely overview of some of the most common direct use geothermal applications regarding the available source’s temperature.

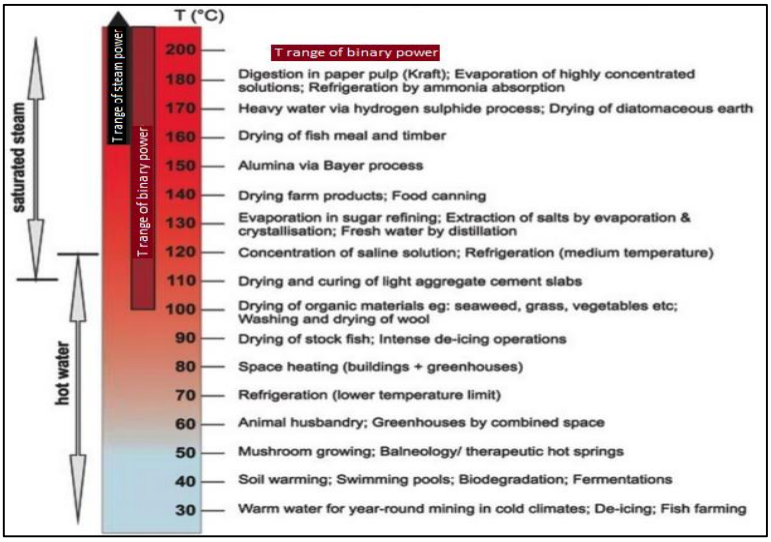

Figure 2: Temperature ranges for direct heat applications (source: www.ecogeneration.com)

Contemporary direct use applications are listed below:

1. Bathing and balneology (hot spring, medical – and Spa bathing)
2. Agriculture (greenhouse, soil sterilization, drying processes, warming processes)
3. Agriculture (fish-, prawn- etc. farming, breeding, cultivation of mushroom farms etc.)
4. Industrial use (product drying or warming, linen and clothes blanching, process steam applications, smelter processes in metallurgic industries like aluminum and Zinc smelter industries)
5. Residential – and district heating or – cooling (including hotels, schools, hospitals, factories, office buildings)
6. Shallow geothermal use applications (residential heating, heat pumps etc.)

The benefits coming from direct use of geothermal energy have spurred its development and as a result more than 15.000 thermal MW are produced worldwide. Even in countries with less amount of heat rates available, like Germany, direct use applications, such as district heating, experience great demand and is predicted to play a significant role in the energy field in the future. For this kind of technologies, less than a year is needed before the project takes its total shape, projects that range from small ("mom and pop operations") to large (district heating/cooling) scale.

Geothermal water is normally oxygen free, so much attention should be taken so that oxygen entering one of the direct use applications presented above is avoided. Proper technology has also been developed in order to remove dissolved gases and minerals such as boron, arsenic, and hydrogen sulfide that provoke corrosion, scaling to materials and even harm plants and animals. In addition, the content of carbon dioxide in geothermal water can be extracted and exploited either for carbonated beverages or for enhancing growth in greenhouses.

The main equipment required in a direct use application consists of both a feed and a circulation pump, heat exchangers, transmission and distribution pipelines, peaking or redundant generators (usually fossil fuel fired) to reduce the use of geothermal water and the number of wells required, and water disposal systems (injection wells).

Indirect use

The category of indirect use consists of three different geothermal technologies that are implemented to convert fluids to electrical energy. Power plants that use these technologies are characterized as below:

a. Dry Steam Power Plants,
b. Geothermal Flash Power Plants
c. Binary Cycle Power Plants

The main factors that define the proper technology's selection concern the state of the fluid (wet or dry steam, a steam/water mixture or hot water, called as brine) and the physical variables of pressure and temperature.

The first type of geothermal power plants was the dry steam power plants. This kind of technology is able to exploit immediately the hot steam that comes from the geothermal source and supply directly the turbine in order to generate electricity.

One very common geothermal application nowadays seem to be the "flash steam" power plants, which feed the plant's facilities with high pressure and temperature (>180°C) water.

As for the "binary" power plants, they are differentiated from the previous technologies by the fact that the heat energy of the geothermal fluid is transferred through heat exchangers to a secondary medium that, once the working medium of the power plant's cycle, is evaporated and used for rotating the turbine. They use sources with medium-temperature fluids (<150°C), fluids that exist in the majority of geothermal areas, which are known to present much lower boiling point than water. They are, also, characterized by no harmful emissions to the environment, as they are closed-loop systems. Taking into account all the above, in conjunction with the wide existence of moderate-temperature bines, it is obvious why the binary plants seem to be the most preferable in the future. An example of binary installation is illustrated in figure 3.

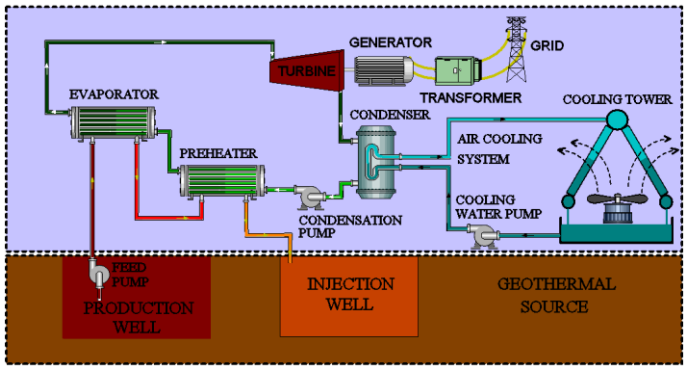

Figure 3: Binary air-cooled tower geothermal power plant

The binary systems can be categorized into ORC technology, which uses a single fluid, such as an organic and Kalina technology which uses the secondary side of the heat exchanger or a mixture, such as a water-ammonia mixture. The ORC systems, depicted in figure 4 depend on the vaporization of the working medium, which takes place in the heat exchangers. Then the vapor is driven in the turbine to generate and power and afterwards passes through the condenser to become liquid and be pumped again to the

constituting a closed-loop thermodynamic cycle. In case that high temperature sources are available, thermal oil can be used as heat transfer medium. Then the installation of a regeneration unit can result in improving the cycle's coefficient of efficiency. Choosing the suitable ORC fluid is an important process that influences the total performance, considering that due to the low temperature, any heat losses can become very prejudicial for the plant. Therefore, refrigerants and hydrocarbons are the most preferable for such applications and present high potential GHG emissions in case of contact with the environment. There are also occasions where the iso-pentane is preferred as working medium. ORC binary plants are widely installed in a worldwide scale, not only because of their satisfactory efficiency but mainly because of the more know-how and experience that has been developed among the technology community.

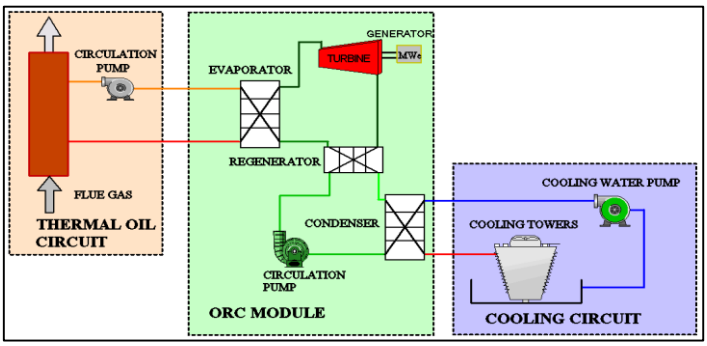

Figure 4: ORC installation for biomass application

Kalina technology will be further and detailed described in the next chapter. Generally, in Kalina cycles the working ammonia-water mixture boils and condenses at variable temperature, for a given pressure. This is very beneficial as the working medium can better exploit the temperature gradient of the heat source fluid, fact that increases significantly the heat transfer efficiency. Particularly, Kalina technology seems to have 20% to 50% higher efficiency than the ORC technology. However, it is not yet widely accepted as it was invented in the last decades, but its evolution in the energy market is remarkable. Countries like USA and Iceland, which dispose many low-temperature geothermal sources are tending to invest on this technology, tension that is based on its efficient, effective and profitable performance.

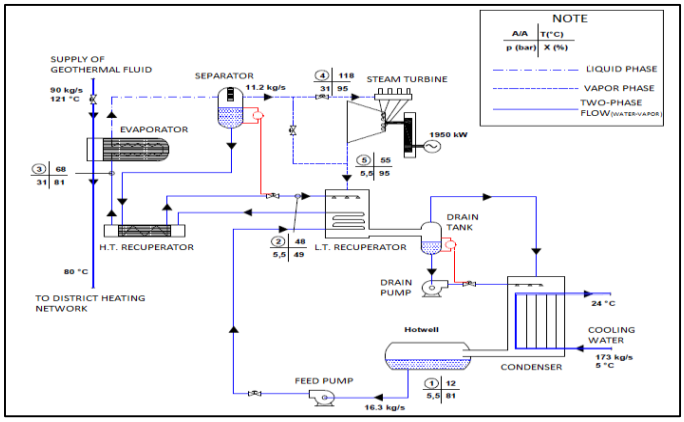

Figure 5: A process diagram of a binary Kalina plant at Husavik, Iceland [Lolos, 2010]

Combined cycle geothermal power plant

It is also beneficial to combine the technologies of “Flash” and “Binary” plants in order to produce more electricity by exploiting the heat from the hot spring from the separator and the well. This kind of power generation is known as Combined Geothermal Power technology and increases the efficiency of the power plant at higher investment costs.

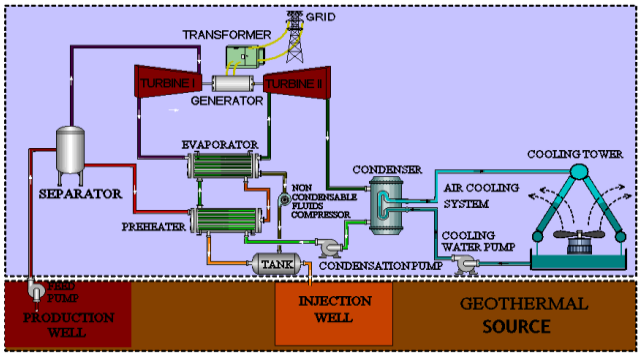

Figure 6: Combined cycle geothermal power plant

Hybrid power plants using geothermal power

Hybrid power plants constitute a flexible geothermal power plant that is able to optimize the exploited temperature of the steam, independently of the available temperature of the production well. This fact contributes to their being characterized as significantly reliable systems. Basic characteristic is that they are able to increase the efficiency and therefore generate more power without expanding the use of the geothermal resource. A typical hybrid application uses the heat from the geothermal source for the first heat exchangers, while the heat required for the “superheating” that follows can emanate from any source, such as biomass, hydropower, solar power or even coal. In this way, the capacity that is generated by the combined power primary-plant is enhanced by an additional heat source.

There are countries, such as Greece, that dispose great amounts of available solar power, while other like Indonesia have excess of biomass (sugar cane or rice hulls) or hydropower, sources that can be combined with geothermal power in a hybrid power installation, which will be operating totally with renewable sources.

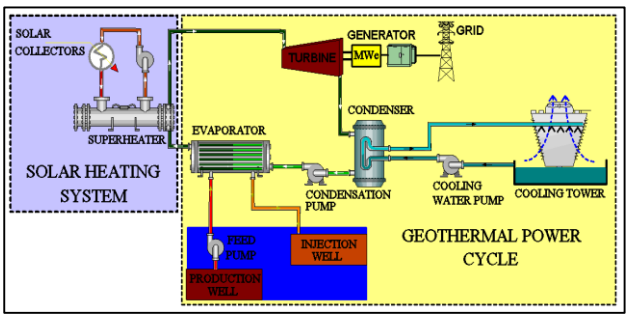

Figure 7: Schematic diagram of the hybrid solar-geothermal power plant

Geo-pressured resources

One very promising for the future hybrid application, including the use of both natural gas and geothermal fluid, is called “geo-pressured” system. It was in the 1980s when the first application based on geo-pressured resources was successfully demonstrated at Pleasant Bayou in Texas, supported by the Department of Energy. The project exploited the following types of energy:

a. heat from the geothermal resource (thermal energy),
b. energy from natural gas in the reservoir (chemical energy)
c. well head pressure (mechanical energy)

Taking into account the cost factor, only the thermal and chemical energy were captured. In addition, it was possible to increase the cycle’s performance by exploiting the waste heat from the onsite burning process of the natural gas. Nowadays, the fact that oil and gas prices follow an inclined way makes geo-pressured applications to present remarkable development.

Geothermal power plants combined with direct use

A way to maximize the efficiency of a geothermal application would be to feed with the geothermal fluid primarily the power plant and subsequently one or several direct users, such as district heating, industries, agriculture, balneology etc. The proposed simultaneous direct and indirect use of geothermal springs, i.e. the cascade integrated development illustrated in figure 8, constitutes an efficient and cost competitive way to exploit a geothermal source. In addition, this cascade arrangement, based on renewable sources, is reasonable preferable as it does not emit any harmful GHG and of course provides a great potential to create jobs.

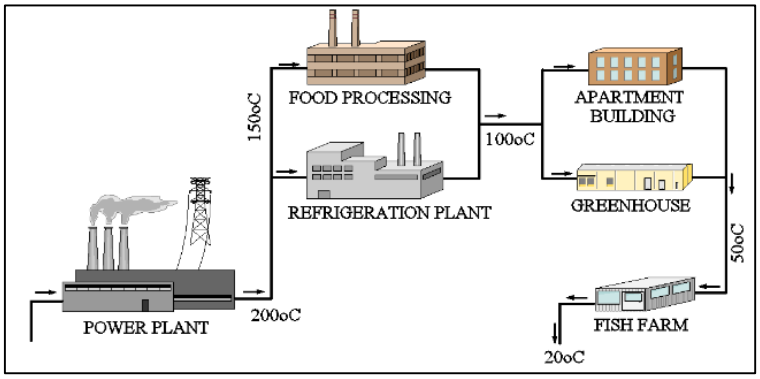

Figure 8: Example of a cascade utilization of a geothermal reservoir in Iceland

Enhanced geothermal systems (EGS)

Enhanced Geothermal Systems (EGS) have experienced great approval as technology for geothermal applications. According to MIT research, EG systems can work together with already installed geothermal power plants, such as binary, flash-binary combined cycle

and double or single flash plant. The resources required differ from the typical hydrothermal resources only by the fact that they are characterized by one or all of the followings:

1) dense rock reservoir from which liquid is difficult to be pumped (lack of the usual porosity and permeability that is needed),
2) insufficient quantities of steam and/or hot water and,
3) deeper than usual drilling depths (even more than 7.5km)

Wells that can provide high temperature geothermal heat, are known as “triple-expansion systems” and constitute actually supercritical systems. Such examples exist on double-flash power plants by adding a fluid with high density and a back-pressure turbine. The role of this turbine is to handle the extremely high pressures that derive from the EGS geothermal fluid. EGS technology is still upon investigation phase and the researchers can only estimate about the power plants’ design specification. Therefore, it is possible to recognize the factors that are influenced by such an application. These factors are the fluctuations in non-condensable gas content, the variable temperature that comes from the hot spring, the variable flow that is available, and the size of the several equipment of the power plant.

Oil and gas co-production

An oil and gas co-production application included the exploitation of wells that have already been drilled for the purpose of oil and gas industries. Sometimes these wells are deep enough to meet hot water sources, while other times drillings works have to be implemented in order to go deeper and reach the hot zone. It has been observed in the Gulf Coast region of the United States that 95% of the production wells for oil and gas, consist of water. In oil-industry, pumping and re-injecting the geothermal fluid is a very cost consuming process, that can be extenuated by exploiting the waste heat of the fluid through a binary power plant. This process is cost-effective even for small scale installations due to the elimination of upfront costs, i.e. no drilling and resource investigation required, and could drive to remarkable development the geothermal energy’s national and global reach. An example of oilfield co-production is offered by Ormat Technologies at the DOE Rocky Mountain Oilfield Testing Center (RMOTC), near Casper Wyoming. RMOTC disposes available hot water sources that range up to 88oC and flow rates sufficient for generation of about 200 kW.

3.4 Financial aspect of geothermal power production

Geothermal power generation installed costs

Although the geothermal applications are characterized as capital – intensive, it can be balanced by the very low and predictable operation costs. The high construction costs derive from the increase of prices regarding EPC, commodities and drilling, as occurs in the oil and gas sectors and are around 60% to 70% higher than in 2000. The capital cost can be split into the following topics:

I. Exploration and resource identification estimation costs.
II. Drilling works regarding injection and re-injection wells.
III. Field infrastructure and other surface treatment and installations
IV. The power plant conceptual and detailed design and regarding costs.
V. Project execution and grid connection costs.

As aforementioned the investment of "binary" plant applications is much higher that this of "flash" technology, with costs ranging from 1,650€ to 4,000€ per kW, while typical "flash" plants are evaluated from 1,400€ to 2,800€ per kW. An analysis made in USA, illustrated in figure 9, compares the two technologies and concludes that binary plants are more efficient for low temperature sources, regarding only the power plant costs (i.e. excluding production and injection wells).

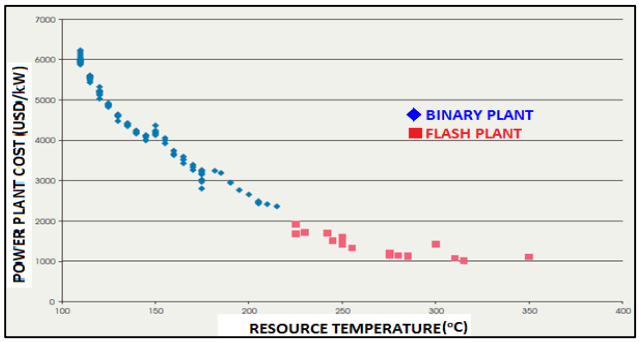

Figure 9: Power Plant only costs for Geothermal Projects by reservoir temperature (source: NREL, 2012)

The LCOE of geothermal power generation

Factors that influence the LCOE of a geothermal project are as usual the capital, operation and maintenance costs, as well as the economic lifetime and the weighted average cost of investment. But the development risk that derives from the uncertainty of production wells' performance (e.g. reservoir degradation) makes the analysis of geothermal projects and the production expectations quite dynamic. This uncertainty leads to cost increase, fact that constitutes geothermal applications much more expensive than other renewable sources, such as wind. A simple example of a financial evaluation for a geothermal power plant starts with the assumption of the capital cost up to 10%, a 25-year lifetime and annual operation and maintenance costs up to 100€/kW. A reasonable capacity factor would be 90% and the capital costs ranges from 1,650€ to 4,000€ per kW for binary plant. After calculations conducted, the LCOE can vary from as low as 0.03€/kWh for second-stage development of a field and up to 0.1€/kWh for greenfield construction. In addition, if the well's performance ends up to be less than expected, these costs can rise up to 0.14€/kWh, price that involves average capacity factors 20% lower than assumed.

The formula used for calculating the LCOE of renewable energy technologies is:

$$LCOE = \frac{\sum_{y=1}^{lf} \frac{Iy+My+Fy}{(1+y)^y}}{\sum_{y=1}^{lf} \frac{Ey}{(1+r)^y}} \quad (3.1)$$

Where I_y is the investment expenditures in the year y, M_y the O&M costs in the year y, F_y the fuel expenditures in the year y, E_y the power generation in year y, r the discount rate and lf is the lifetime of the system.

Geothermal feed-in tariffs in Germany

Geothermal energy presents remarkable development in Germany and the good economic framework conditions constitute a main factor on this result. As widely known, the Renewable Energy Sources Act has guaranteed to the plants' operators fixed payments for geothermal power generation supplied into the national grid. Since January 2009, it has been set that geothermal plants up to 10MW earn 0.16€/kWh and above 10MW around 0.105/kWh for feeding with electricity the grid. Furthermore, a bonus of 0.03€/kWh has also been instituted for geothermal CHP applications, while an additional bonus up to 0.04€//kWh exists in case that plant's operation started before the 1st of January 2016. The EGS technology is also more preferable and that is reflected by an additional amount 0.04€/kWh that is available on the market. To sum up, the most profitable scenario concerns a geothermal CHP plant, got into commercial operation during 2015 or before, which uses EGS technology to produce up to 10MW. Such a power plant is able to receive up to 0.27€/kWh from its grid-feed-in tariffs. Since these beneficial financial and political conditions in Germany exist, the geothermal applications have experienced great growth, with many CHP plants being under construction in the Rhine Graben and Molasse Basin region and even more permissions for exploration to have been submitted for about 150 sites.

4 Kalina Cycle

4.1 Introduction to Kalina cycle, operating principles and literature review

Heat from low and medium temperatures can be found in every process but is being exploited in a very small degree. Oil refineries are worldwide one of the largest and most concentrated sources of useful heat rejection to the environment. As a result of a study (Mlcak, 1996), only in U.S.A. is discarded from these industries in the environment an amount of heat that reaches up to approximately 2,000,000 MWh per year, in a temperature range of 130-500oC, which could be converted by several technologies into useful energy. Other large industrial sources of waste energy are the chemical and woodworking industries, while large low-temperature heat sources are encountered in geothermal fields or biomass sources, as well as in the form of solar energy. Taking into account the conventional technologies for power generation, it is not possible to convert efficiently in energy this moderate temperature heat coming from these sources. Therefore, as it was of great significance to produce electrical power from these low and medium-grade temperature, some technologies have been developed over the last century.

One technology of great use nowadays is the Organic Rankine Cycle (ORC) which applies the principle of the steam Rankine cycle, with the main difference of using an organic fluid as working fluid, i.e. fluid whose chemical composition consists of at least one carbon atom. The great benefit of these fluids is that they have low boiling points, fact that constitutes them ideal for recovering heat from lower temperature heat sources.

A newly invented and developed thermodynamic cycle suitable for such applications is called Kalina Cycle. This cycle, named after its inventor Dr. Alexander Kalina, constitutes actually a modification of a typical Rankine process, but with an important diversification of using a binary mixture consisting of ammonia and water as a working medium. Alexander Kalina came up with this invention in the early eighties and since then, many scientists have been motivated to go deeper on this cycle and a variety of different circuit models have been investigated.

It took a great amount of years before this technology comes into market. Nowadays, there exist many installed applications of Kalina cycle worldwide, either in functional mode or in phase of design. Through this thesis a Kalina cycle Power Plant, that is located in the area of Unterhaching in south Munich and exploits geothermal sources, is being analyzed and investigated. More information about the plant's operation and process are presented in following chapter.

Operating principles of the Kalina power cycle

As aforementioned, Kalina cycle constitutes an evolution of typical Rankine cycle and is mainly characterized by its binary mixture that is used as working fluid.

The schematic diagram presented below (10) describes an example of a conventional Kalina cycle application. A geothermal source is being exploited and by the use of a high

consumption pump the evaporator of the system is being fed with hot geothermal water (14). There the working medium of the cycle is being partially boiled and evaporated. After the heat transfer in the evaporator is completed the geothermal water (15), on the one hand, comes out in a lower temperature and returns underground far away from the basic hot sink. On the other hand, being in a two-phase condition the ammonia-water mixture (1) leaves the evaporator in a saturated statement and enters the separator.

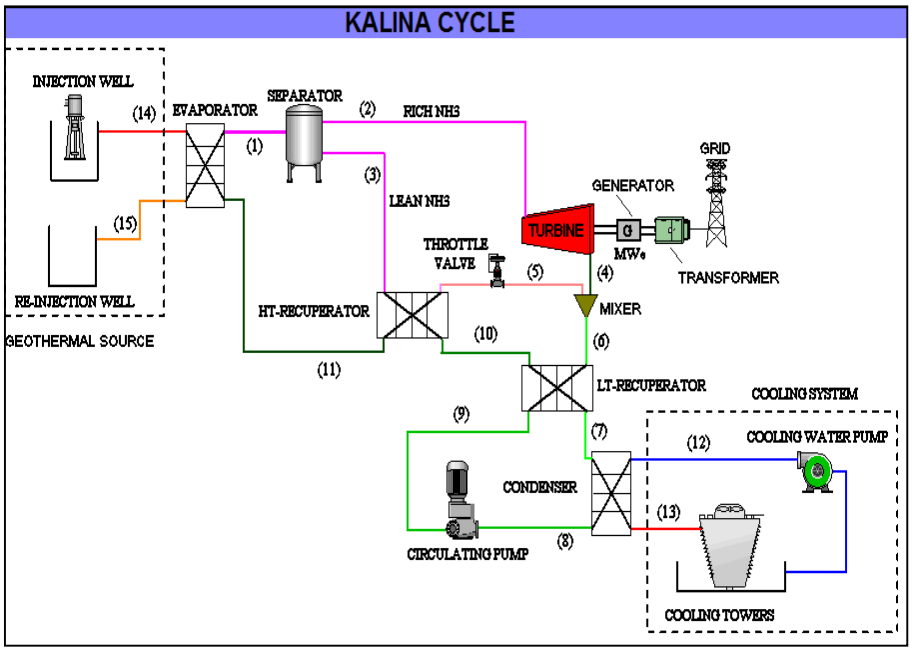

Figure 10: Schematic diagram describing a Kalina cycle process

The separator is capable of separating the main medium into two different conditions. The one is the rich in ammonia vapor (2) that comes out from the top of the separator and is expanded in a power generator in order to produce electricity. The other is the lean in ammonia liquid (3), which passes through a recuperator first to be cooled down and a throttle valve afterward to be depressurized.

The expanded fluid (4) is mixed then with the low pressure poor ammonia liquid (5) and are driven as mixture, characterized poor in ammonia, in the low temperature recuperator. The outlet fluid (7) of the LT recuperator enters the condensing system, where it can be condensed through the heat exchange that takes place with the cooling water (12). The water recirculates in the cooling system and in order to be re-used it is being cooled through the cooling towers. The working medium leaves the condenser in a saturated condition and is compressed by the main circulation pump to a high pressure (9). Before the working fluid re-enters the evaporator in order to start the whole process again, it passes through the HT and LT recuperators mentioned above in order to be preheated.

A typical T-s diagram of such an application is illustrated in figure 11. The variable boiling and condensation temperatures, the reason and benefit of which will be described in following paragraphs, result in a non-parallel curve of the working fluid with the heat source curve.

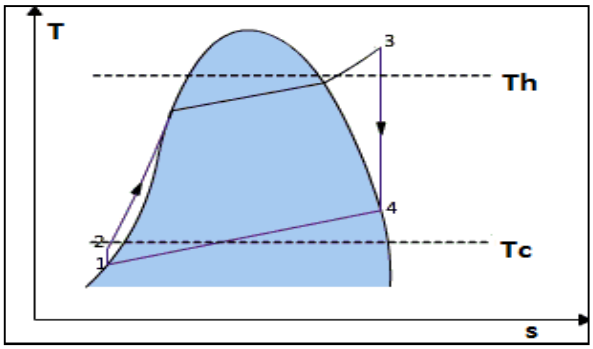

Figure 11: T-s Diagram of a Kalina cycle

Review of ammonia-water mixture cycles in literature

Ammonia – water combined cycles have been extensively studied and used as primary or secondary cycles for power generation from geothermal fields, solar panels or for exploiting waste heat for other industrial applications.

Studies have shown that binary cycles can produce more power as sub-cycles than a Rankine cycle is able to. Alexander Kalina studied several commercial variants for combined cycles and concluded that the efficiency of such a cycle can be increased up to 20% if Kalina technology is applied against Rankine. The use of a mixture of ammonia and water as a working medium for power generation had already been proposed by the lagged 50s by Maloney and Robertson [20], however due to the limited range of properties available at that time for the fluid, it was not possible to design cycles of high performance.

The electric power research institute (EPRI, 1986a&b) also studied the combined cycle power on the order of 6MWe. The combined Kalina had 5-14% higher yield and 2-5% lower electricity costs than Rankine. The investment cost per kW produced (€/kWe) for a combined Kalina cycle was about 11% higher than that of a steam combined cycle with superheating and approximately 11% lower than a cycle with two heat regenerations. Kalina and Leibowitz (1987) after studied combined cycles with power output of the secondary cycle up to 200Mwe, concluded that the Kalina cycle can have 16-30% higher power output compared to a secondary steam cycle with three heat regenerations.

Moreover, Kalina et al. and showed a combined cycle of 227MWe with an efficiency reached up to 52.8%, which means that it produces 16% more power than a secondary steam cycle with two heat regenerations. According to the same study, the investment cost of a secondary Kalina cycle is 20% higher and the investment cost per kW produced 2% higher compared to a secondary steam cycle. The cost of the turbine in a Kalina cycle is less than in the steam turbine cycle, since the volume flow in the last stage of the Kalina is less than the one in Rankine, while the cost of the heat exchangers in Kalina cycle is higher. However, the extra power output of the Kalina cycle gives an economic advantage at the end.

Regarding the exploitation of geothermal fields, Desideri and Bidini (1996) compared the flash steam cycles, Rankine cycles with working medium ammonia or ammonia-water

mixture, and Kalina cycles without separator for producing electricity from low or medium temperature geothermal fluid. Result of the study was that the Kalina cycle produced more power than the others. Although the Kalina cycle requires more heat exchangers' surface and therefore the initial capital cost is high, this cost is balanced in the course of the year by the high power output. Lazzeri and Bruzzone (1995) compared flash steam cycles and Kalina cycles for geothermal applications and showed that the Kalina cycles produce at least 10% more power than the rest.

4.2 Kalina cycle investment evaluation and installations

A simple and basic feasibility study of investing in such a technology has been conducted for a 10 MW Kalina Cycle Power Plant and is tabulated below.

Table 1: Pro-forma simplified ROC analysis

Characteristic	Value
Power Plant Capital Cost	11-15 million €
Market Price – Electricity	0.08 cents / kWh
kWh produced per year	78.8 million kW hours @ 90% availability
Operating Costs	0.07 cents / kWh (free waste heat source)
Revenue from Electricity Sales	6.5 million € / year
Gross Profit	5.8 million € / year
Payback	2.5 years
Return on Capital (ROC)	39%
Discount Rate	8%
Inflation over 20 years	2.5%
Net Present Value	48.2 million €

Kalina cycle installations

Kalina technology, as mentioned above, was developed about 25 years ago but it took a few years before the commercial promotion started. Nowadays, globally can be found several commercial applications of the cycle Kalina. The first application was a demonstration unit in Kanoga Park in California (USA), 6.5MW, which served research purposes and put into operation in 1992.

The first purely commercial application cycle is a unit of waste heat in a metal factory in the city of Kashima, Japan, power of 3.5 MW which came into operation in 1999. Plant used as a source hot water, with a supply of 1300 tones / hour and a temperature of 98oC. This installation works until today with an average availability of over 98%.

Of course, since then, many applications of Kalina cycle followed and even more are planned to be constructed in the future. Relative information are tabulated in the table 2 below. It should be noted that each device installed is characterized by a code, depending on the equipment and the procedure followed, e.g. KCS 34, KCS 11 etc.

Table 2: Worldwide distribution of Kalina cycle power plants

Year	Project/ Country	Customer	Power Output	Application	Mode - Statement
1991	Canoga Park / USA	Exergy Inc	6.5 MW	Gas Turb. PP	Demo – In operation
1998	Fukuoka / Japan	MITI	4.5 MW	Incinerator	Demo – In operation
1999	Kashima / Japan	Sumitomo	3.5 MW	Steel Mill	Commercial – In operation
2000	Husavik / Iceland	Municipality	2.0 MW	Geothermal	Commercial – In operation
2006	Fuji Oil / Japan	Fuji Oil Refinery	4.0 MW	Oil Refinery	Commercial – In operation
2009	Unterhaching/Germany	Municipality	3.4 MW	Geothermal	Commercial – In operation
2009	Bruchsal / Germany	EnBW Utility	0.6 MW	Geothermal	Commercial – In operation
2009	Tibet / Tibet	SSNE	50 kW	Geothermal	Commercial – In operation
2010	Shanghai World Expo/ China	SSNE	50 kW	Solar Thermal	Commercial – In operation
2010	Taiwan / Taiwan	SSNE	50 kW	Geothermal	Commercial – In operation
2011	Otari / Japan	GERD	50 kW	Geothermal	Under Construction
2011	Husavik repower / Iceland	Wasabi Energy	2 MW	Geothermal	Under Construction
2011	Khairpur Cement Plant / Pakistan	FLSmidth / DG Khan	8.6 MW	Cement	Under Construction
2012	Ministry of Environment / Japan	GERD	50 kW	Geothermal	Under Construction
2012	Star Cement / UAE	FLSmidth / Aditya Birla	4.75MW	Cement	Under Construction
2013	Taufkirchen / Germany	Geothermie Taufkirchen	4.5 MW	Geothermal	Under Construction - Feasibility
2013	ArcelorMittal South Africa / South Africa	Wasabi Energy	10 MW	Steel	Under Construction - Feasibility
2013	Mogale Alloys (Ruukki) / South Africa	AAP Carbon	5 MW	Ferroalloys	Under Construction - Feasibility
2013	Hernic Ferrochrome (Mirsubishi) / South Africa	AAP Carbon	28 MW	Feroalloys	Under Construction - Feasibility
2013	Tuzla Geothermal Power Plant Refurbishment / Turkey	Imparator Enerji / Enda Enerji	7.5 MW	Geothermal	Under Construction – Pre Feasibility
2013	Tuzla Geothermal Power Plant First Stage build out / Turkey	Imparator Enerji / Enda Enerji	14 – 17.5MW	Geothermal	Under Construction – Pre Feasibility
2014	TATA Steel / South Africa	AAP Carbon	10.5MW	Feroalloys	Under Construction – Pre Feasibility
2014	ArcelorMittal South Africa / South Africa	Wasabi Energy	20 MW	Steel	Under Construction – Pre Feasibility

4.3 Ammonia-water mixture and its phase diagram

The basic features that the ammonia – water mixture presents are very important for the cycle's process and quite different than these that characterize either pure water or pure ammonia separately. Actually, the behavior of this mixture is such different as a totally new fluid. The four main differences are listed below:

1. Ammonia-water mixture has a varying boiling and condensing temperature, while both pure water and pure ammonia have constant boiling and condensing temperatures.

2. Every change in the ammonia concentration can cause alternation in the thermo-physical properties of the mixture. Water's and ammonia's related properties remain always stable.

3. On the one hand the ammonia – water's temperature is able to increase or decrease without any fluctuation in the heat content. On the other hand an energy change is needed in order to influence the temperature of water or ammonia.

4. The freeze temperature for water and ammonia is 0°C and -78°C respectively. An ammonia – water mixture has a very low freezing temperature.

For the two aforementioned differences (1) and (2) the ammonia – water mixture is called non-azeotropic. The phase diagram of such a fluid, as well as of an azeotropic one is shown in figure 12.

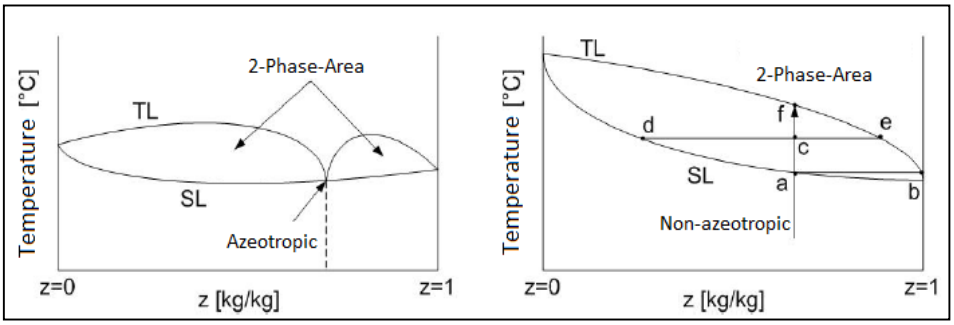

Figure 12: T-z diagram: Azeotropic (left), Non-azeotropic (NH3 -H2O, right)

Phase diagram

The first special feature of the ammonia-water mixture is the most essential for the efficiency of the Kalina cycle, meaning the ability of the mixture, to boil or condense at a "variable" temperature, for any given pressure. The following diagram presents the phase change that takes place in an ammonia-water mixture, at a known pressure and mass concentration, while the temperature is being changed.

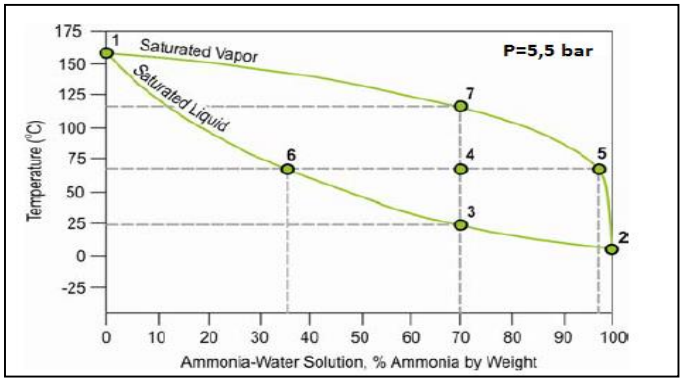

Figure 13: Phase change in ammonia-water mixture (MLCAK 1996)

Although water presents much higher boiling and condensing temperature compared to ammonia, as obvious in table 3, when these two fluids are mixed ammonia seems to be the most volatile substance of them. The meaning of this, on the one hand, is that when an ammonia – water mixture in liquid phase is heated, ammonia will be the first to boil off, i.e. distillation will take place. On the other hand if we try to cool down a vaporized mixture, water will be the first to condense.

Table 3: Ammonia's and Water's data

Feature	Ammonia	Water
Molecular Weight [kg/k mol]	17,0	18,0
Boiling Point @ 1.013bar [°C]	-33,3	100
Critical Temperature [°C]	132,3	374,2
Critical Pressure [bar]	113,5	221,2

As defined, in figure 13 illustrates clearly this special mixture's feature, by plotting a phase diagram with temperature vs. ammonia-water mass fraction, at a given pressure of 5.5 bar. Point 1 corresponds to 156 °C, the temperature where the pure water of 5.5 bar is saturated, meaning that the water boils and the steam condenses. The same happens at point 2 for pure ammonia at 6.9°C. A better look in the curves in between and the liquid-saturation line or the boiling points for several concentrations can be noticed. This is where the mixture begins to vaporize or condenses completely when it is heated or cooled down respectively, while the top curve consists of the dew points where the complete vaporization or the initial condensation take place.

These kind of diagrams are very important in order to identify the processes of vaporization and condensation that occur in such a mixture. An explanation of the example illustrated in figure 14 will confirm this.

A sub-cooled ammonia-water mixture with 70% NH_3 mass fraction is considered and heated. At point 3, 21°C, vaporization starts to occur and the more heat is applied the more it vaporizes, but mainly ammonia at first. The point 7 at 116°C belongs to the boiling point where all of the mixture has reached a saturated vapor state. Even more heat added results

in a superheated ammonia-water vapor. It has to be declared that this process is absolutely reversed if the mixture is cooled down and starts to condense. Therefore, it is also important to examine what happens between the two saturation curves. So, at 66°C and point 4 the solution has actually two discrete components in vapor and liquid phase. The vapor state corresponds to point 5 with a rich solution of 97% NH_3 concentration (meaning 3% water), while the liquid one is point 6 with a lean NH_3 mass fraction of 36%.

In order to calculate the mass fraction of the total mass, the lever-arm principle should be implemented for both points 5 and 6. The results from this relation are the followings:

- 97% NH_3 rich vapor: (Point4 - Point6)/(Point5 – Point6) = (70-36)/(97-36) = 55.7%
- 36% NH_3 lean liquid: (Point5 – Point4)/(Point5 – Point6) = (97-70)/(97-36) = 44.3%

4.4 Variable boiling and condensing temperature

Variable boiling temperature

Several heat sources, as geothermal, characterized as sensible or limited, provide heat energy to the working fluid under many fluctuations.

It has been observed for ammonia – water mixtures that, in a counter-flow heat exchanger for example, the temperature rise follows more closely the straight line temperature drop of a sensible heat source, because of its variation in boiling temperature. This is obvious illustrated in figure 14, where it is heated by a geothermal source and is also compared to a Rankine cycle. It is clearly concluded that the mean temperature of heat applied in an ammonia-water cycle is much higher than a Rankine cycle, as well as the mean temperature of heat rejected is much lower in an ammonia-water cycle than a Rankine cycle. All these facts result in the augmentation of the coefficient of efficiency of Carnot cycle, which depends on the difference between maximum and minimum temperature of the cycle.

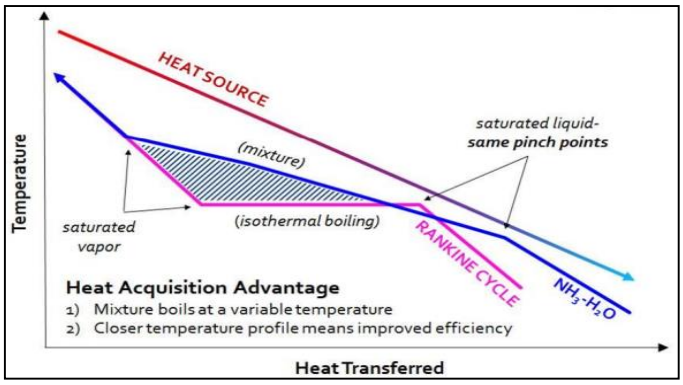

Figure 14: Temperature profile during boiling process (MLCAK 1996)

Variable condensing temperature

After the working fluid in both Rankine and Kalina cycles is vaporized, then it will be expanded into a condensing turbine, at or near its vapor saturation point. Taking into account that at both cycles equal cooling systems for condensing exist, the binary mixture will be distinguished by higher temperature and pressure values than the steam. The higher pressure is due to ammonia's feature of being more volatile than water, while the higher temperature appears as a result of the variable condensing temperature that characterizes the mixture. A simple example described below can give a deeper view on this feature.

Assuming a condenser that is supplied with cooling water at 16°C, it is verified that the steam in a Rankine cycle, expanded in a turbine at approximately its saturated vapor state of 0.04bar and 29°C, will condense at its saturation liquid point at essentially the same pressure and temperature. As the same cooling performance is taken into account, binary mixture will be expanded also at its saturation vapor point of 5.5bar and 116°C. In order to completely condense this fluid it has to be cooled down to its saturation liquid temperature of 21°C, for the given pressure of 5.5bar. It can be easily calculated through first and second thermodynamic law that the existence of such a high temperature in the turbine's exhaustion part would increase the average heat rejection temperature and consequently decrease the cycle's efficiency. This would be the result if the fluid was directed towards to the condenser. Therefore, the Kalina technology doesn't work like this, as this large amount of heat available after the expansion is capable to be used for a high degree of energy recuperation, something that is not possible with the low temperature steam in the Rankine cycle. This great advantage is obvious after a quick view back to the phase diagram on figure 13. Knowing that the temperature at points 7 (turbine exhaustion) and 3 (condenser outlet) is 116°C and 21°C respectively, it is concluded that the working fluid has to affected with a temperature drop of 95°C in order to achieve a complete condensation.

A basic process diagram of Kalina cycle is illustrated in figure 15. After the condenser the working fluid is pumped and goes through a recuparator in order to capitalize this high temperature difference by absorbing heat from the expanded fluid. Simultaneously, this action has a positive impact on the condensation's complete implementation.

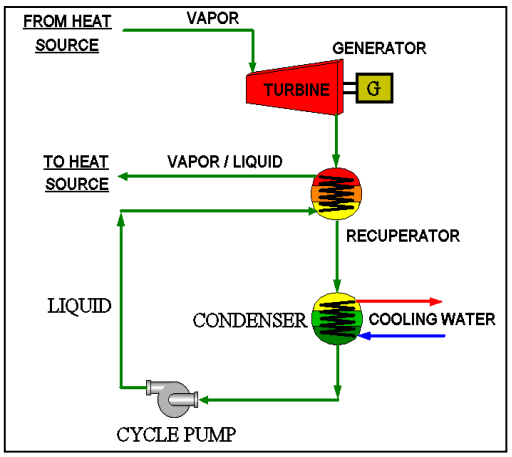

Figure 15: Schematic Recuperation – Condensation

The temperature profile of these processes is shown in , where it is clearly presented how important is Kalina cycle's feature to condense the working fluid in several temperatures,

as a low pressure, high temperature stream is able to transfer heat to another high pressure, low temperature stream.

It has to be noticed that in a Rankine cycle the condensed water's temperature is mainly depended on the outlet cooling water temperature and not the inlet, because of the constant condensing temperature of steam. However, as illustrated in figure 16, while a condensation in a heat exchanger in a Kalina cycle takes place, the final temperature of the binary fluid is influenced by the inlet cooling water conditions, not the outlet, keeping the average heat rejection temperature of the mixture low.

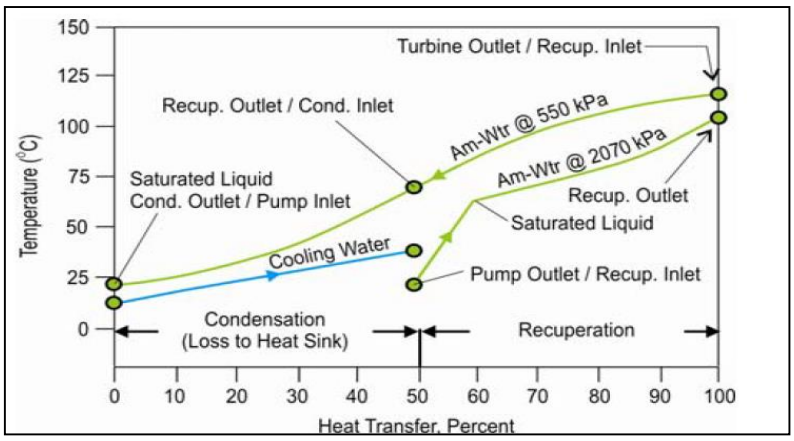

Figure 16: Heat exchange process - recuperation & condensation [Mlcak, 1996]

Another benefit of Kalina cycle process has to be defined. As it was aforementioned the temperature rise of the cooling water can be higher for condensing an ammonia-water mixture than steam. That means that for the same heat rejection in a binary plant, less mass flow rate is required, resulting in a remarkable elimination in capital costs for the cooling system, consisting of cooling towers, fans, pumps, piping, valves and others, but also in an increase in the "net" power production of a Kalina technology power plant.

4.5 Composition change and cycle's efficiency

A great benefit appearing in a Kalina cycle, due to the binary fluid, is the adjustability of its thermo-physical properties in case that any change in the operating parameters occurs. This extra degree of control does not exist in conventional Rankine power cycles. For given heat source conditions there is an optimum ammonia-water concentration that leads to the maximum power output. So, if any temperature variance takes place, the mixture's mass fraction can be adjusted in order to optimize the cycle again.

This feature is very important for the cooling – condensing performance. It is widely known that the cooling temperature has a remarkable variation not only throughout the year, but also during the day. As it is not convenient to change the mixture's composition every hour, it is accepted to regulate it on a seasonal basis. Actually it is normally adjusted in such a

concentration that is able to achieve optimum efficiency for an expected average cooling temperature during a certain period of time. This is quite significant to be decided in cases

where heat sources come from waste heat, geothermal or solar sources. For example a geothermal plant may see its heat source temperature degrade with time as the resource area is developed and more of the geothermal steam or brine is used.

4.6 Operation below freezing temperatures

As it is detailed examined in (Mlcak, 1996), the exergy, i.e. the potential work of a heat source cannot be increased for low heat source temperatures. Especially in Rankine cycles the operation of the plant has to stop in case of a heat sink temperature drop below 5°C, in order to protect the equipment against freeze damage. However, in Kalina cycle plants this can be avoided as it known that ammonia has a very low freezing temperature, so a small amount of ammonia in water can reduce easily the freezing temperature. For example, a lean 25% NH3 – 75%H2O mixture has a low freezing temperature of -51°C.

This why the condensation temperatures of a binary fluid can even be arctic and in many cases air cooled condensers seem to be the best and cost-effective solution to take advantage of it. Therefore, whether water cooled condensers have been selected then exists the obstacle of freezing of the cooling water and there is a limit down at 0°C. It is widely approved that air cooled condensers are a very inappropriate choice for warm climates as they can exploit the mechanism of evaporative cooling that occurs into a cooling tower. That's why power plants with such equipment seem to have very low efficiency during hot periods.

Kalina cycle plant designers are responsible for taking into account all the important factors such as the duration of cold and hot days throughout the year and sometimes implement some new technologies such as a hybrid cooling system that consists of both water and air cooled condensers (figure 17). This kind of solution is possible only for Kalina cycle plants because of the variable condensing temperature and not for the Rankine cycle plants. Depending the ambient condition, the plant is able to adjust its cooling process and spare energy.

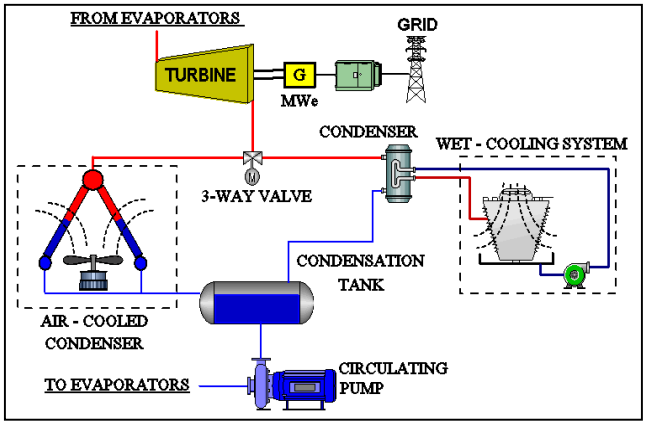

Figure 17: Hybrid Cooling

Another adjustment of this process would be an exceptional solution for seasonal operation as depicted in figures 18 and 19. Then, on the one hand during winter period the "first" condensation occurs through the wet cooling towers and the complete

condensation is finalized by the air cooled condenser (figure 18). In this way, for a given very low dry bulb temperature, i.e. 15°C, a below 0°C final temperature can be reached.

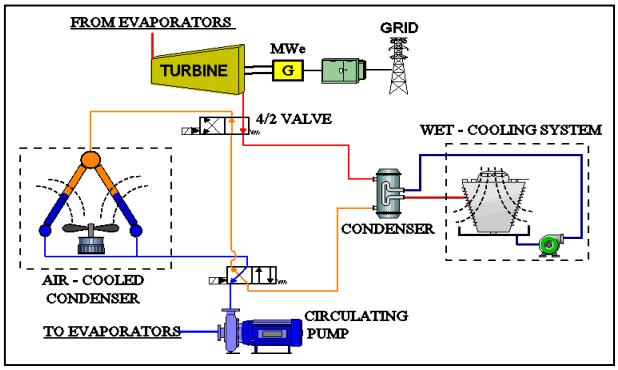

Figure 18: A Schematic - Winter Condenser Series Arrangement

On the other hand during summer season it is preferred to adjust the operation as illustrated in figure 19, so that the “first stage” condenser would be air cooled and the “final stage” condenser would be water cooled.

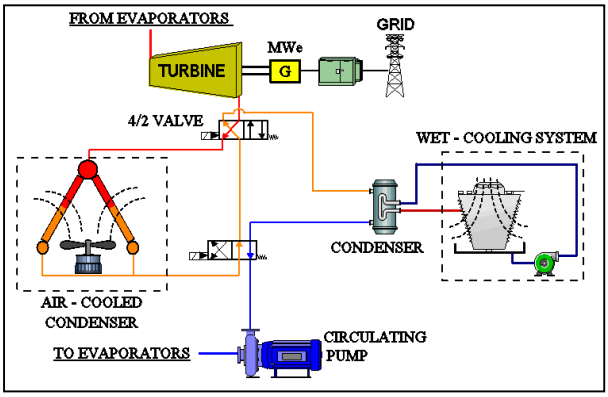

Figure 19: Schematic - Summer Condenser Series Arrangement

5 Unterhaching Kalina Power Plant

5.1 Introduction to Unterhaching Kalina power plant

The Power Plant that is being analysed, for process optimization purposes, is located in South Munich in Germany, in the area of Unterhaching. It was in 2009 when its commercial operation began, after the stage of commissioning, and since then it constitutes the first geothermal power station in south Germany.

Figure 20: The Unterhaching Kalina Power Plant (www.geothermie-unterhaching.de)

It has to be mentioned that since 2007 and until 2009 the geothermal source was being exploited for providing with hot water the large-scale (up to 28km) district heating network in Unterhaching. Every resident is able, upon demand, to install the required pipeline network and compact equipment in order to supply with stable-price heat his household. An example of the install and operation costs is tabulated below in table 4. The existing facilities are capable of transferring annually a large amount of heat that reaches up to 30.5MWth, i.e. approximately 3,000 households, while the plans for the 2015 are to double this capacity, covering at least 50% of the local energy requirements. As it has been announced, after the first 18 months of operation the geothermal energy that has been pumped covered the significant percentage of 25% of the local heating requirements.

Table 4: Pricing example for the Unterhaching district heating

	Single family house	Terraced house
Estimated Consumption Conversion: 1m^3 Gas = 9.18 kWh; 1lt heating oil = 10.08 kWh	25,000 kWh/year	17,500 kWh/year
Annual Consumption Costs	1742,5 €/year	1,219.75 €/year
Capital Connection Costs	5.270,00€	
	Incl. Heat exchanger and 5m of district heating piping on private land	

Notes:

1. The estimated consumption is based on an assumed annual efficiency factor that may vary in individual cases depending on consumer behaviour.
2. Taxes are included in the prices
3. As at 1.10.2013
4. Detailed price list is available at www.geothermie-unterhaching.de

The geothermal source, that exists in a well about 3.5 km below the ground surface, consists of hot water with temperatures ranging from 60 °C to 120 °C. The rock formation at this depth consists of fine porous limestone and dolomite. Another well, where the cold water is being driven after the heat exchanges, is about 3.5 km apart. After chemical testing it has been resulted that the extracted water contains 600 – 1,000 mg/l of salts, mainly hydrogen carbonate, and dissolved gases, e.g. methane and nitrogen. The two wells are connected through the thermal water circuit, which is constructed by fibreglass reinforced plastic to be protected from these corrosive substances.

Through these pipes, the Kalina power plant is fed with the excess of the total 150 l/s hot water that are pumped from the source. On a year basis and at full capacity, it is estimated that approximately 4.7 billion litres of water pass through the plant.

The power generation of the plant is based on a quite new, innovative and adequate for low-temperature applications technology, named Kalina technology. Kalina cycle has been described thoroughly on chapter 5. Shortly, this process uses as working medium a binary mixture that consists of water and ammonia. The great benefit of this binary fluid is that is able to condense and boil at varying temperatures, for a given constant pressure. This fact is of high importance for the plant's efficiency, taking into account the variance of the heat supplied from the geothermal source. After the first years of operations it has be defined that the power generation of the plant is 3.4MWe, with an electrical efficiency factor of approx. 10 – 13%. That means 21.5 Mio. KWh are being produced, able to satisfy the annual energy consumption of approximately 6,000 households. Of course, the produced electricity's provision in the grid is implemented under a specified fee.

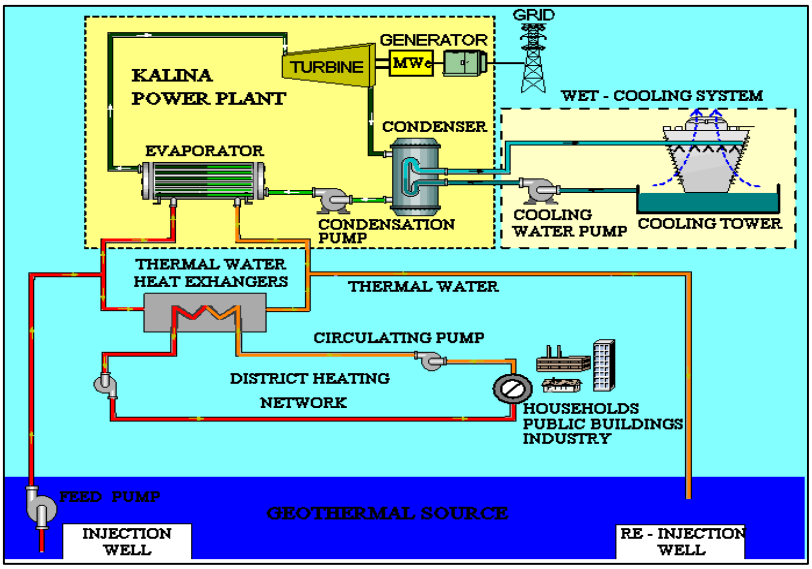

Figure 21: Unterhaching total facilities

Although the environmental conditions change throughout the seasons, the power plant has the capability and the required high technology control systems in order to be adapted flexibly to these changes and maintain a constant power generation of 3.4MW during the year. This is due to the custom-tailored to the local requirements facilities' construction. Furthermore, this mainly friendly-environment way of energy production results in an annual CO_2 savings of about 35,000 tones, as it has been measured on February 2009.

The Kalina Cycle power plant in Unterhaching was funded by the German Federal Ministry for the Environment, Environmental Protection and Reactor Safety, and by the Bavarian State Ministry for Commerce, Infrastructure and Transportation. The route followed till the final step of commercial operation is summarized in the table below.

Table 5: Timetable and milestones of the Unterhaching Power Plant

Time Interval	Milestones
1995 – 1997	Municipal Heating Atlas
2001 - 2002	Preliminary geological investigation and feasibility study. Decision for a geothermal plant. Central condition: Geological risk insurance
2004	Production Well
2006 – 2007	Injection Well
2006 – 2007	Expansion of the heating network, above ground plant and the redundant heat plant
2007	Commencement of the geothermal heating supply
2006 – 2008	Construction and commissioning of the Kalina plant
02.2009	Geothermal electricity generation commence
02.06.2009	Official commercial operation start

The financial evaluation of this geothermal project presents a total investment cost that ranges in 80 million €. Of course, the network's expansion projects, for the heating capacity augmentation, that are consecutively executed have added a significant amount of capital costs in primary calculations. Therefore, as it is estimated, the amortization of these costs is expected in approximately 15 years. More details and information about the Kalina power plant's process are not allowed to be presented in this thesis, except from the interior basic equipment layout depicted in figure 22. The entire turnkey facility was built by Siemens AG (I&S) all the data required for the analysis, the investigation and the calculations conduction constitute intellectual property of the company. Nevertheless, a simple process diagram of the power plant's dual operation is illustrated in figure 21 found above.

Figure 22: Unterhaching Power Plant's interior equipment layout [*www.geothermie-unterhaching.de*]

A general overview of the characteristic values of the Unterhaching facilities' operation are summarized in the following table:

Table 6: Overview of characteristic values of Unterhaching facilities.

Description	Value
Production Well: 1. Well Depth: 2. Temperature:	 3,446 m 122 °C
Injection Well: 1. Well Depth: 2. Temperature:	 3,866 m 133 °C
Well – Output:	Up to 150 l/s
Geothermal thermal output: **Fossil thermal Output:** (peak load, redundancy)	 Up to 38 MW Up to 47 MW
District heating network: **Connected Load:** **Annual Heating Load (2008):**	28 km length, 30.4MW Approx. 3,000 households 47,000 MWh
Geothermal electricity generation: **Electrical output – Annual Electricity Generation**:	3.4MW (average) 21.5 Mio. kWh (i.e. approx.. 6,000 households)
Annual CO2 Saving	Up to 35,000 tonnes
Total Investment (2008)	Approx. 80 million Euros

5.2 Unterhaching power plant's problem definition

After visiting the Kalina Cycle Power Plant in Unterhaching, talking with technical stuff and focusing on the Shankey diagram provided by the company, it was easily concluded that the power plant presents high energy consumption in the condensing process. As a result, the topic of this thesis is focused on the way of optimizing the processes of cooling and condensing the working medium of the cycle, through the development of constructional solutions. In simple words the investigation regards the improvement of the efficiency of the condensation and cooling systems. Detailed analysis on the solutions proposed is done in the following chapters.

A closer view on the Shankey diagram of the plant shows that the Kalina Power Plant consumes the 28.6% (Figure 23) of the total energy required for the Unterhaching facilities for both heating network and power generation operations.

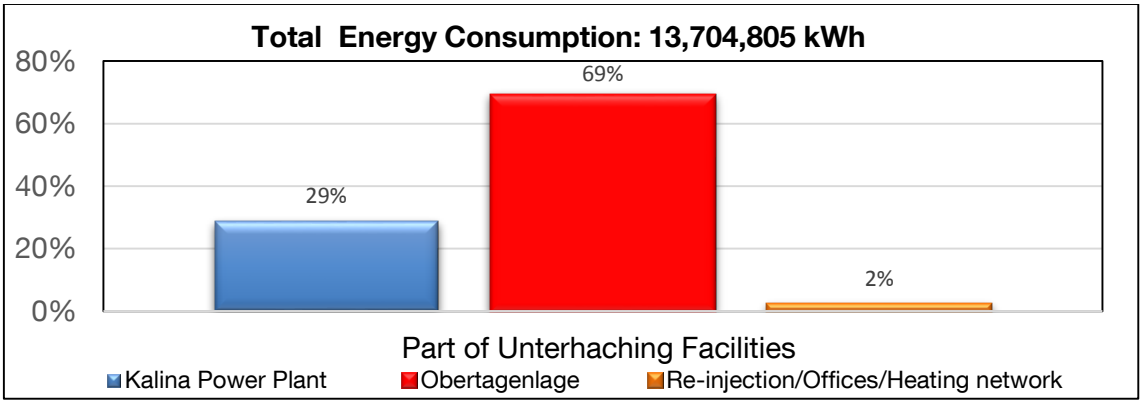

Figure 23: Energy consumption distribution in Unterhaching facilities

From this quantity of electricity used in Power Plant, the 25.9% is consumed by the cooling water circulation pump, while a significant amount that corresponds to 49,7% is needed for the operation of the cooling towers, i.e. for the fans' function, as depicted in Figure 24.

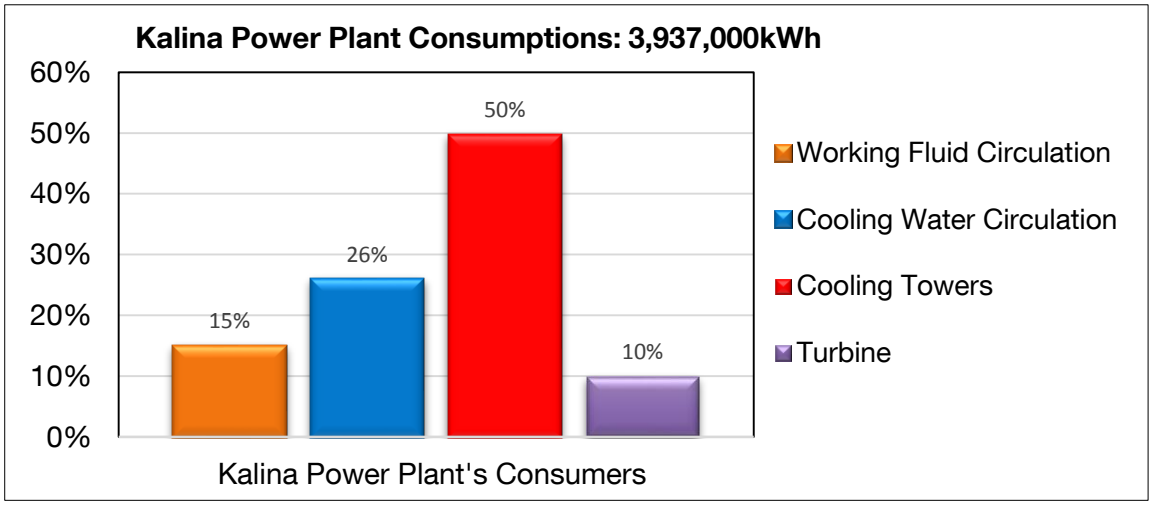

Figure 24: Energy consumption distribution in Kalina Power Plant

These percentages are equal to the 7% und 14.2%, respectively, of the total electricity that is purchased by the grid (Figure 25).

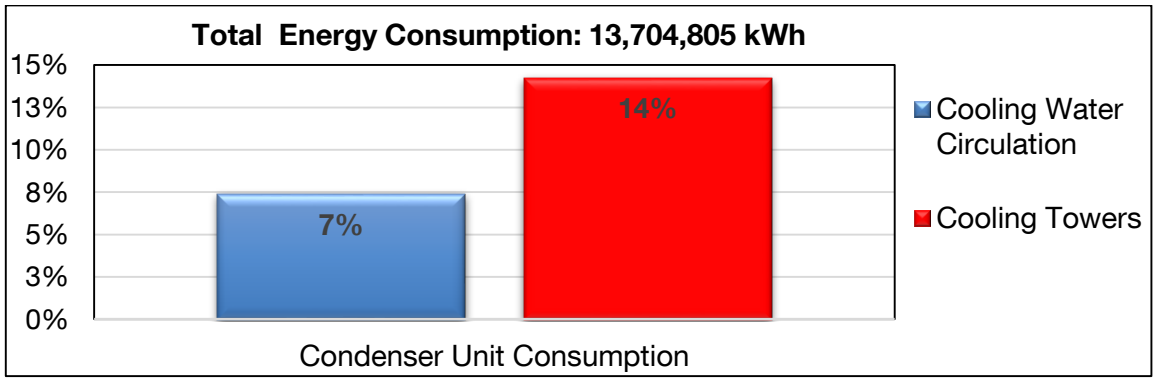

Figure 25: Energy consumption distribution in Condenser Unit as percentage of the total consumption

5.3 Analysis of available signals and corresponding process data

The responsible, for the operation and administration of the Kalina power plant, employees provided the Technical University of Munich (TUM) with the whole sensors' list, accompanied with the Piping and Instrumentation Diagrams. The power plant consists of around 800 sensors in order to ensure the optimum power generation, supervise the process and localize any failures. As aforementioned, the purpose of this thesis was to investigate the cooling system, analyze the current process and check for malfunctions. As a result, the required sensors' values were provided, but only for a specific period, from 13th to 20th of January 2014, on an hour-based time range.

In order to decide the sensors' values needed, simple overviews of the process flow of cooling and condensing systems were designed, as illustrated in Figures 26 and 27.

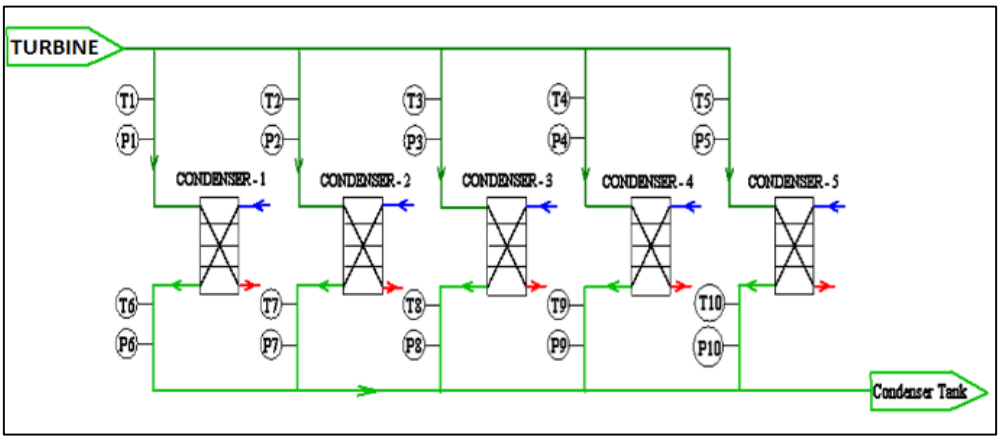

Figure 26: Condensers' unit

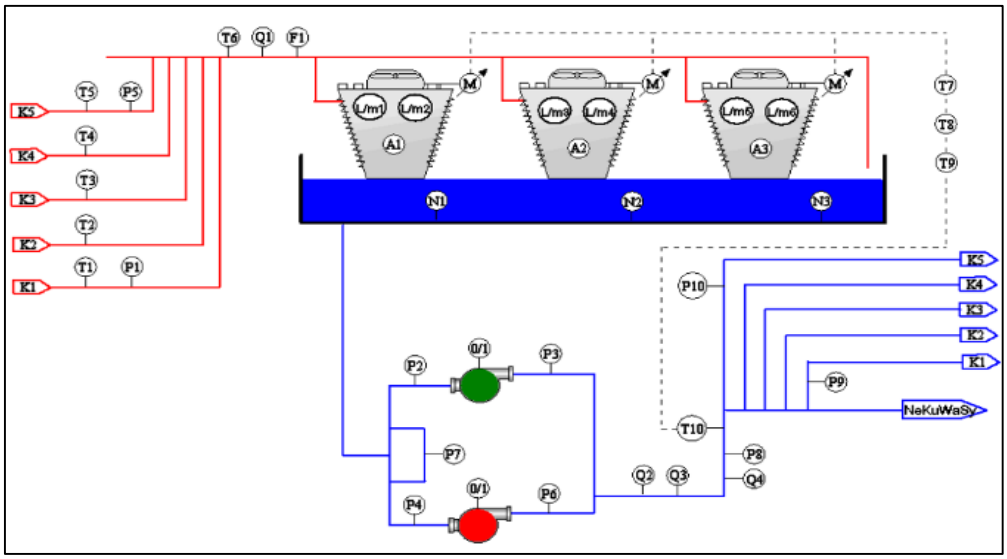

Figure 27: Wet cooling towers

In addition, values about the working fluid's ammonia mass fraction, the mass flow rate of the mixture and the power output have also been taken into account. After collecting the values required, an amount of graphs has been created in order to have an illustrative view and analyze easier their behavior. Firstly, the cooling water towers have been investigated. As shown in charts below, the fluctuation in ambient temperature affects the water temperature that enters the cooling towers, as well as their air volume flow rate and makes them present almost the same way of reaction. This is normal, as the stable power generation requires also a stable cooling range, which is being achieved through these modifications in cooling water unit operation as depicted in figure 28.

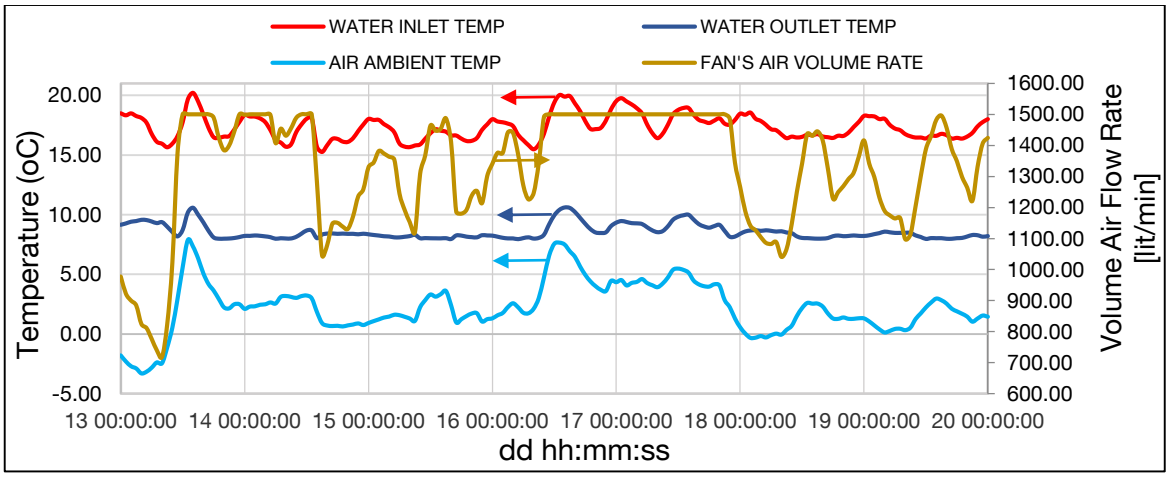

Figure 28: Cooling water tower inlet and outlet temperature, ambient air and air volume flow rate fluctuations during period 13th-20th of January

The achievement of stabilizing the process is obvious from the almost linear increase of the MWh presented below, in figure 29.

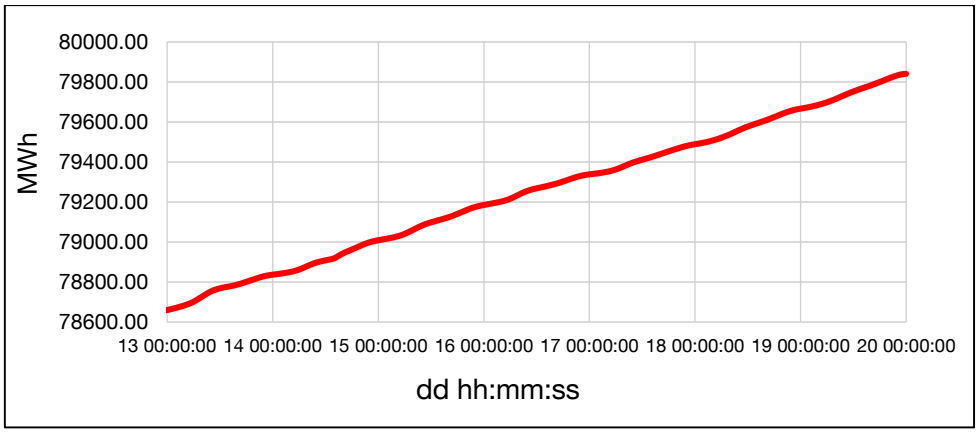

Figure 29: Accumulated overall power output during period 13th-20th of January

As illustrated in figure 30, all three existing cooling towers are working on the same percentage during plant's operation, while the water mass flow rate seems to remain constant, independently of the changes in cooling process that mentioned above.

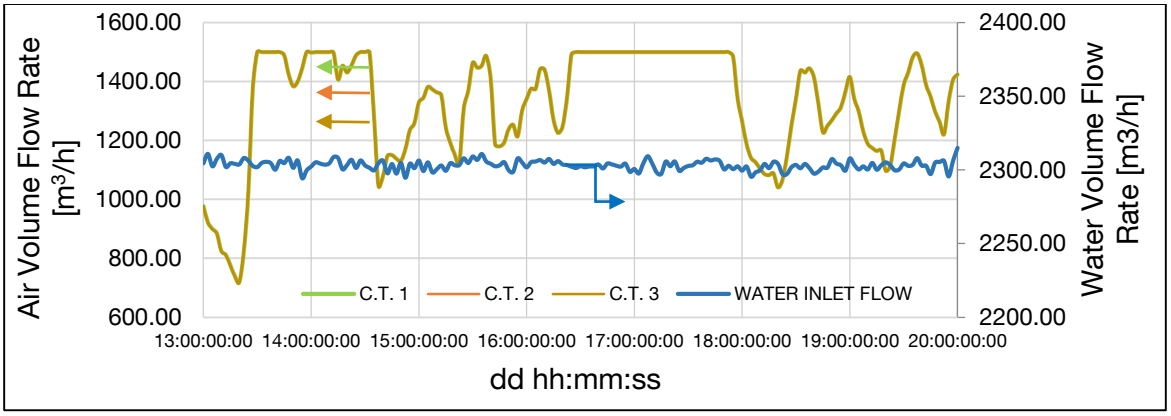

Figure 30: Cooling towers' air volume flow rate and water mass flow rate fluctuations during period 13th-20th of January

Analyzing further the condensing unit's signals, a remarkable abnormality has been found. As depicted in figures 31, condensers 2 and 3 seem to operate differently from condensers 1, 4 and 5 at their inlet of ammonia mixture. This remark is also obvious in the correlation coefficient analysis that is presented in following paragraph.

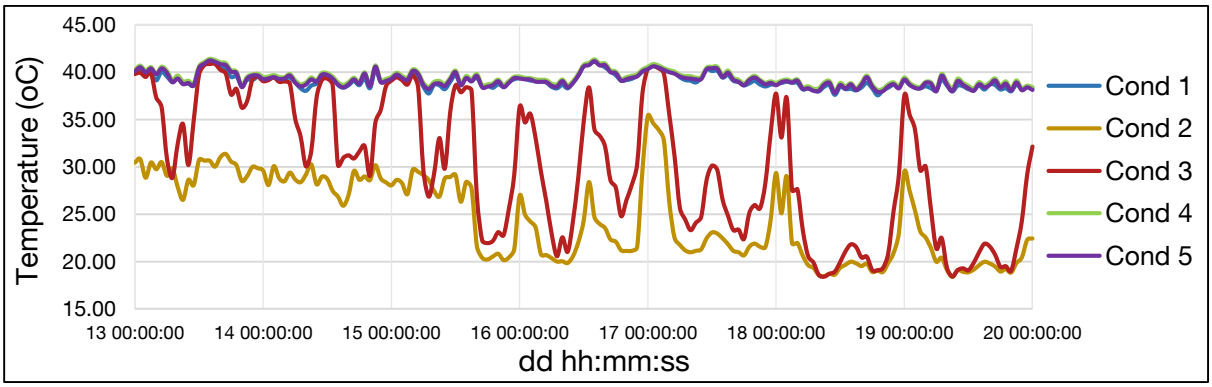

Figure 31: Condensers 1, 2, 3, 4, 5 inlet temperature values of the ammonia mixture during period 13th-20th of January

After discussing with responsible, for the technical part of the power plant, staff about this malfunction and checking more their process through the annual data, it was concluded that the sensors of working fluid inlet temperature in condensers 2 and 3 are defective and they are scheduled to be substituted during the arranged stop, for maintenance purposes, of the power plant. So, their values will not be under consideration in further studies.

It has to be referred that although the inlet temperature of the binary medium is the same for condensers 1, 4, 5, this does not happen for their outlet temperature, which present small difference. Taking into account that the inlet cooling water temperature and the mass flow rate of both streams are equal for each unit, this difference may stem from the different coefficient of efficiency that characterizes each condenser.

The total condensation mass flow rate appears a remarkable fluctuation behavior through this week, and as illustrated in figure 6.6 and is obviously concluded from the figures below, it follows the power production line and is reflected on the heat rejection variance. As a

result these three variables seem to have strong correlation, as expected, considering, on the one hand, that the turbine's power output is directly influenced by the proliferation $\dot{m}_{mixture}\Delta h$ and the input and output condition of the mixture seems to be stable through this period. More precisely, the pressure and temperature of the working medium at the turbine's inlet are stable at around 19bar and 120°C respectively, while the same values at the outlet are approximately 6bar and 85°C respectively. On the other hand, the heat rejection in condensers is given by the equation $Q_{rej} = \dot{m}_{mixture}\Delta h_{cond}$, and that justifies this strong correlation.

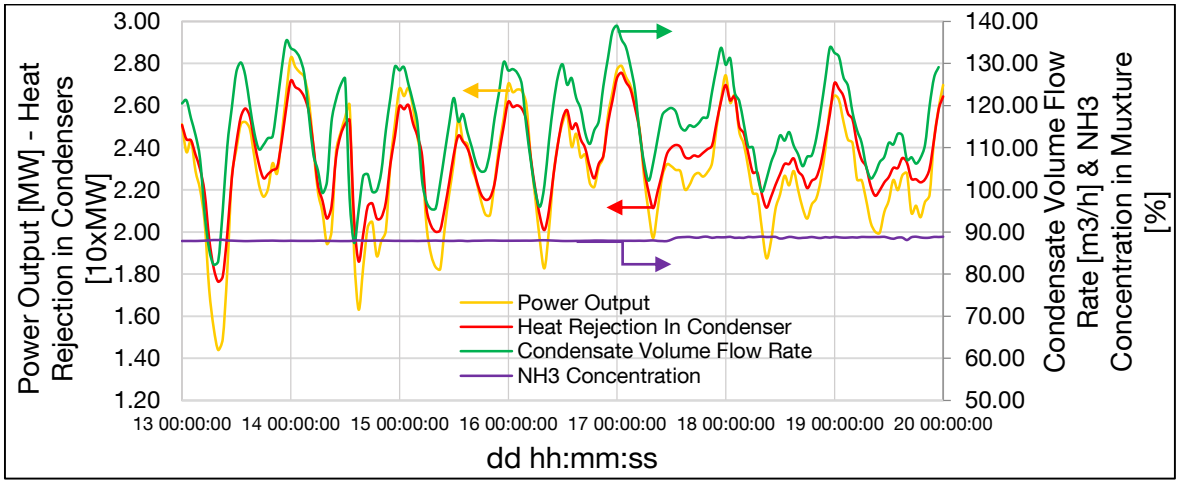

Figure 32: Working medium volume flow rate, output power and ammonia mass concentration in condensate during period 13th-20th of January

During the design of the Kalina cycle process, it is very important to determine the optimum ammonia concentration in the mixture, so that the phenomena of evaporation and condensation are taking place under the best heat exchange performance. In the case of Unterhaching, the optimum ammonia mass percentage seems to be around 88% and as depicted in figure 6.6 this remains almost stable. As presented in previous chapter, concerning the Kalina technology, the condensation is more efficient with a lean ammonia mixture. Consequently, more liquid medium is added just before the condensation unit, so that the cycle takes advantage of this special feature of the mixture.

Another remark that came up after the signals' analysis concerns the pressure drop that occurs in the condensers. The registered values showed that the input and output pressure is almost the same for each condenser, with a pressure drop values ranging at approx. 0.05bar.

5.4 Condenser Parameters

Take into account all the above signal analysis, the condenser's operation and performance is highly influenced by several parameters. The definition of them is of great importance, so that it is decided which of them can be affected in order to achieve the required improvement. The graphical presentation that follows gives a clear and overview.

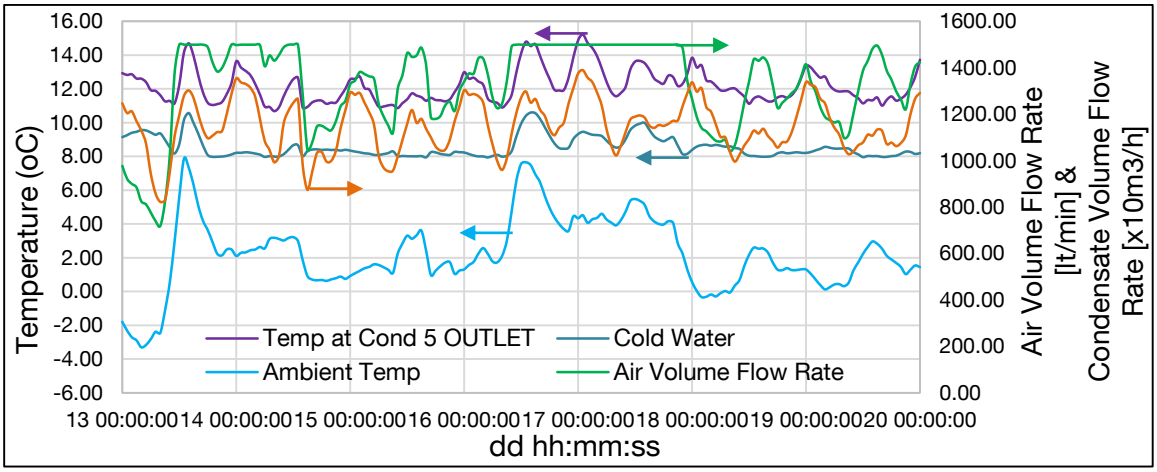

Figure 33: Working medium and air volume flow rate, temperature of cold water, condensate at condenser 5 outlet and ambient during period 13th-20th of January

After observation of figure 33, it is clear that the condenser's outlet temperature on the mixture's side follows almost exactly the fluctuations of the condensate volume flow rate and the tower's cooling range. The peaks and troughs of the ambient temperature seem also to affect the values of the condenser's outlet temperature, the cooling range, the fan's operation and even the amount of heat rejection in the condenser (see figure 32). It happens several days that although the ambient temperature becomes lower, the fan keep on operating without any change in the air volume flow rate. This happens in order to achieve a higher cooling range, as the inlet water temperature in the C.T. increase (see Figure 34)
In order to influence the condenser unit, by changing in the existing process, primarily it is important to verify that this change can increase the power generation of the cycle. For this purpose, an effort to correlate the inlet and outlet temperatures of the condenser with the electricity production has been undertaken. The results are presented graphically in figures 34 and 35. The correlation coefficient between working fluid's temperature at condenser 5 outlet and power generation has also been calculated and is equal to 0.68, showing the remarkable correlation between their values.

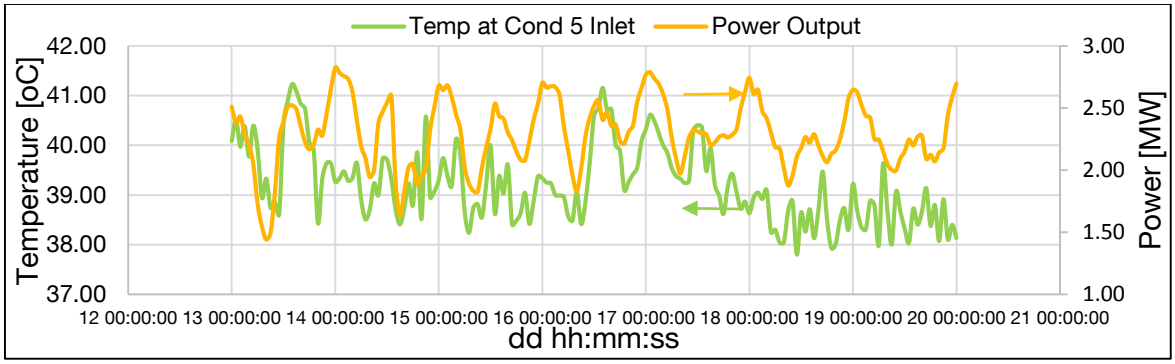

Figure 34: Condensate temperature at condenser 5 inlet and power production during period 13th-20th of January

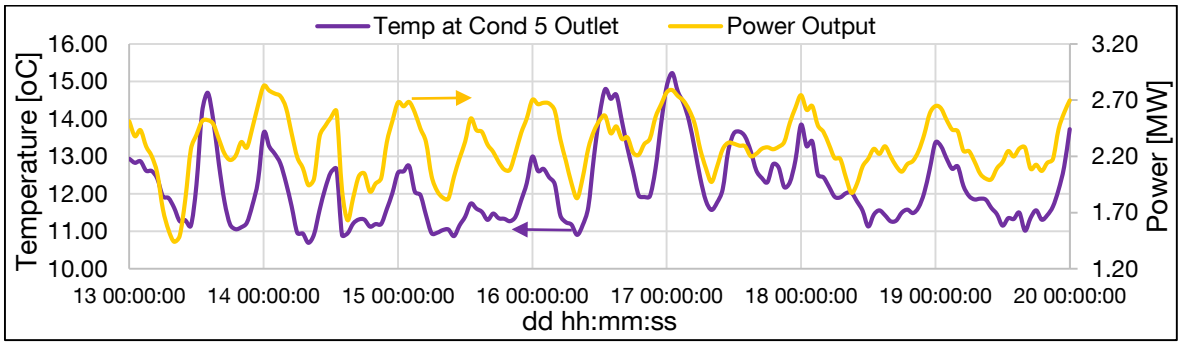

Figure 35: Condensate temperature at condenser 5 outlet and power production during period 13th-20th of January

6 Cooling Towers

6.1 Introduction to cooling towers

Cooling towers are constructions that remove heat from water, by transferring it to air. They can be mainly counter-flow or cross-flow, depending on the angle that the inlet air meets the water. Of course there are several configurations of them, but the less energy consuming are the induced – draft cooling towers. Larger towers and lowers ambient wet-bulb temperatures are able to decrease the temperature of the water at the collection basin of the tower.

The majority of the cooling towers are designed for a cooling range up to 10°C, 0.23m^3/h per ton of cooling, with a fan motor 0.1hp/ton and air volume flow rates about 1.7m^3/h/hp. The water outlet temperature can be calculated when data such as water flow rate, cooling load, and the ambient wet-bulb temperature are known. A relative software that automates the process has been developed, called CoolSim (Kissock, 1997), which evaluates also the fraction of time that a cooling tower can deliver water at a target temperature, based on inlet water temperature and ambient conditions.

Sensible and latent cooling

By the time that air meets the water droplets, there are two mechanisms that can make the water cool down, based on the inlet air and water condition. These are the sensible and latent cooling of the air, or simply the latent, or evaporative, cooling of the air that is quite more dominant. In case that the air enters the tower at a lower temperature that the inlet water, then through part sensible and part latent cooling it will exit the tower completely saturated. On the one hand, the sensible cooling effect takes place while the air temperature augments by absorbing heat from the water. On the other hand, the latent cooling occurs while the water loses energy and evaporates. In case that the dry-bulb temperature increases at a higher value that the water, for a given wet-bulb temperature, then the air cools while it saturates and the whole cooling is done due to evaporative cooling. As long as the air enthalpy constitutes a function only of the wet-bulb temperature, the cooling performance of the tower is the same for each phenomenon. Therefore, the dry-bulb temperate plays a more significant role regarding the evaporation rate and a positive correlation coefficient presents between their values.

Cooling tower simulation introduction

A program in Matlab environment has been developed in order to simulate the cooling performance of an induced draft counter-flow wet-cooling tower, same type as one of the towers installed in Unterhaching Kalina Cycle Power Plant. The cooling tower is divided into three zones, which are shown in figure below, the rain, the fill packing and the spray zone, in which heat and mass transfer between air and water occur. A model for each zone has been developed, but actually the models for rain and spray zones are the same,

except from some basic input variables that are changing. These models are described in the following paragraphs and a parameters' variation analysis take place.

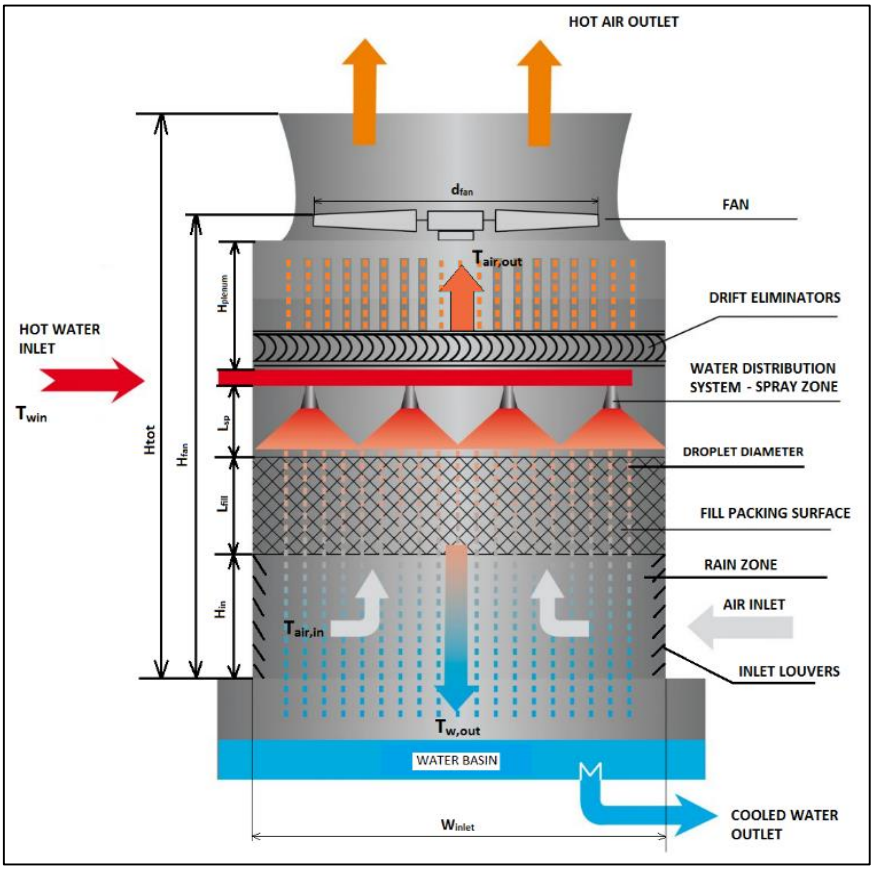

Figure 36: Induced draft counter-flow cooling tower (www.hamon.com)

6.2 Rain and spray zone model

Principles

In rain and spray zone, air comes directly in contact with water droplets. This phenomenon is characterized by simultaneous heat, mass and momentum transfers between the air and the droplets. By the time a unique droplet meets the air, a film of saturated air-vapour is formed on the droplet surface and heat is transferred by convection and radiation. As the radiation has a very small value, it will be neglected from the energy balance. The heat and mass transfer occurs at the interface of the droplets and the surrounding air as depicted in figure 37.The temperature difference between the water and the air constitutes the reason for the heat transfer, while the mass transfer is based on the existence of a vapour concentration gradient among the vapour layer and the ambient air, which means that latent heat is transferred to the air from the droplet and evaporation takes place.

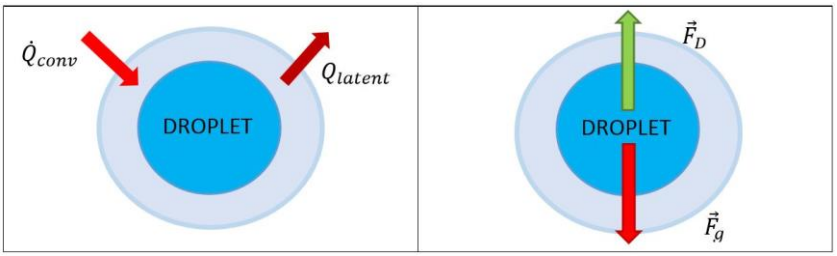

Figure 37: Droplet Heat, Mass and Momentum mechanism

Energy balance equation

Based on the previous figure, and the heat and mass transfer basic equations the rate of energy absorbed by each droplet can be expressed as:

$$\dot{m}_w \cdot c_{p,w} \cdot \Delta T_d = a_{c,d} \cdot S_d \cdot (T_{air} - T_d) + \frac{dm_d}{dt} h_{fg} \tag{6.1}$$

What should be taken into account is the number of droplets per unit volume on the moist air. This can be estimated by (S.P. Fisenko, 2002):

$$N_v = \frac{G_w}{V_d \rho_w u_d} \tag{6.2}$$

So, for the droplets on a discrete volume inside the rain zone (dz) the above equation is formed as:

$$N_v = \frac{G_w}{V_d \rho_w u_d} = \frac{\frac{\dot{m}_w}{A_{fr}}}{V_d \rho_w u_d} => N_v \cdot dz \cdot A_{fr} = \frac{3\frac{\dot{m}_w}{A_{fr}} \cdot dz \cdot A_{fr}}{S_d \, \rho_w u_d R_d} => N_{v,tot} S_d = \frac{3\dot{m}_w dz}{S_d \, \rho_w u_d R_d} =>$$

$$\frac{\dot{m}_w}{S_{d,tot}} = \frac{\rho_w u_d R_d}{3dz} \tag{6.3}$$

The mass flux transferred to the air by evaporation $\left(\frac{\mathrm{dm_d}}{\mathrm{dt}}\right)$ is evaluated by the difference between humidity ratio of saturated moist air at water temperature and the humidity ratio of moist air (w), as below:

$$\frac{dm_d}{dt} = S_d a_D \{w_{sw}(T_d) - w_{air}\} \tag{6.4}$$

Based on equations from (6.1) to (6.4), the energy balance for a number of droplets in discrete volume of the rain zone can be expressed as:

$$\frac{dT_d}{dz} = \frac{3\{a_{c,d} \cdot (T_{air}(z) - T_d(z)) - a_{D,d} \cdot [w_{sw} \cdot (T_d(z)) - w_{air}(z)] \cdot h_{fg}\}}{c_{p,w} \cdot \rho_w \cdot u_d(z) \cdot R_d(z)} \tag{6.5}$$

From equations (6.3) and (6.4) it can also be derived that the change in the radius of the droplets through the discrete volume of the rain zone comes from (S.P. Fisenko, 2002):

$$\frac{dR_d(z)}{dz} = -a_{D,d}\frac{[w_{sw}\cdot(T_d(z))-w_{air}(z)]}{\rho_w \cdot u_d(z)} \quad (6.6)$$

As for the various parameters that are being used in equations (6.5) and (6.6), they constitute:

- The convection heat transfer coefficient $(a_{c,d})$, which is given based on Nusselt number by (W.E. Ranz,1952):

$$Nu = \frac{a_{c,d}D_d}{\lambda_{air}} = 2 + 0.6 \cdot Re_d^{0.5} \cdot Pr^{0.33} => a_{c,d} = \frac{\lambda_{air}}{D_d}\left(2 + 0.6 \cdot Re_d^{0.5} \cdot Pr^{0.33}\right) \quad (6.7)$$

- The droplet surface area (S_d):

$$S_d = 4 \cdot \pi \cdot R_d^2 \quad (6.8)$$

- The latent heat of water vaporization (h_{fg}):

- $h_{fg} = 3.4831814 \times 10^6 - 5.8627703 \times 10^3 \times T + 12.139568 \times T^2 - 1.40290431 \times 10^{-2} \times T^3$ (6.9)

- The Reynolds number (Re_d):

$$Re_d = \frac{2\rho_{air}R_d|u_d(z)-u_{air}(z)|}{\mu_{air}} \quad (6.10)$$

- The Prandtl number (Pr):

$$\mathrm{Pr} = \frac{c_{p,air}v_{air}}{\lambda_{air}} \quad (6.11)$$

- The mass transfer coefficient for a falling droplet that meets an ascending air flow (S.P. Fisenko, 2004), based on the Sherwood Number, defined by formula:

$$Sh = \frac{a_{D,d}D_d}{D_f} = 2 + 0.6 \cdot Re_d^{0.5} \cdot Sc^{0.33} => a_{D,d} = \frac{D_f}{D_d}\left(2 + 0.6 \cdot Re_d^{0.5} \cdot Sc^{0.33}\right) \quad (6.12)$$

Where:

- Sc is the Schmidt number given by:

$$\mathrm{Sc} = \frac{v_{air}}{D_f} \quad (6.13)$$

- D_f is the diffusion coefficient [m²/s] given by an empirical equation (Kloppers, 2003):

$$D_f = 0.04357(T_{air} + 273)^{1.5} \frac{(1/M_a + 1/M_v)^{0.5}}{p(V_a^{0.33} + V_v^{0.33})^2} \quad (6.14)$$

With $M_a = 28.97 kg/mole$ and $V_a = 29.9$ for air, while $M_w = 18.016 kg/mole$ and $V_w = 18.8$ for water.

- The humidity ratio for moist air $\left(w_{air}\ [\frac{\text{kg}}{\text{kg}}\text{dry air}]\right)$ (Kloppers, 2003):

$$w = \left(\frac{2501.6 - 2.3263(T_{wb} - 273.15)}{2501.6 + 1.8577(T - 273.15) - 4.184(T_{wb} - 273.15)}\right) \times \left(\frac{0.62509 p_{vwb}}{p_{abs} - 1.005 p_{vwb}}\right) - \left(\frac{1.00416(T_{air} - T_{wb})}{2501.6 + 1.8577(T - 273.15) - 4.184(T_{wb} - 273.15)}\right) \quad (6.15)$$

Where p_{vwb} is the water-vapor-pressure [Pa], at water temperature and can be derived from air and steam tables that are inserted as separate programs in Matlab and T_{wb} [°C] is the wet-bulb air tempearture, which is determined by (Stull, 2011):

$$T_{wb} = T_{air,db} \cdot atan\left[0.151977 \cdot (RH + 8.313659)^{\frac{1}{2}}\right] + \text{atan}(T_{air,db} + RH) - \text{atan}(RH - 1.676331) + 0.00391838 \cdot RH^{\frac{3}{2}} \cdot \text{atan}(0.023101 \cdot RH) - 4.686035 \quad (6.16)$$

Attention should be paid in the units. RH is the relative humidity in [%] and $T_{air,db}$ the air dry-bulb temperature in [°C].

- The humidity ratio of saturated moist air at water temperature $\left(w_{sw}\ [\frac{\text{kg}}{\text{kg}}\text{dry air}]\right)$ (Kloppers, 2003):

$$w_{sw} = \left(\frac{0.62509 p_{vwb}}{p_{abs} - 1.005 p_{vwb}}\right) \quad (6.17)$$

The differential equations regarding the variance in air temperature and humidity ratio, through the finite discrete volume of the rain zone, are derived after combining the above equations and have the following form (S.P. Fisenko, 2002):

$$\frac{dT_{air}(z)}{dz} = \frac{4\pi R_d(z)^2 N_v}{C_{p,air}\rho_{air}(u_d(z) - u_{air})}\{a_{c,d}[T_{air}(z) - T_d(z)]\} \quad (6.18)$$

$$\frac{dw_{air}(z)}{dz} = \frac{4\pi R_d(z)^2 N_v}{\rho_{air}(u_d(z) - u_{air})}\{a_{D,d}[T_{air}(z) - T_d(z)]\} \quad (6.19)$$

Droplet motion

Droplet trajectories are described by the Lagrangian framework. As depicted in figure 37 the forces that affect a droplet derive from the Newton's second law and the relevant drag force from the air. Of course, other forces such as buoyancy forces or forces due to pressure gradient are present, but based on previous studies and the assumption that all droplets are isolated and have spherical shapes, these forces can be neglected, because they do not seem to have any effect on the droplet's flow. Considering this, the motion of a single droplet can be described by the following equation:

$$\frac{d(m\vec{u}_d)}{dt} = \vec{F}_D + \vec{F}_g \tag{6.20}$$

Where $\vec{F}_g$ constitutes the gravitational force given by:

$$\vec{F}_g = mg \tag{6.21}$$

While $\vec{F}_d$ constitutes the drag force and for a spherical droplet can be expressed regarding the drag coefficient:

$$\vec{F}_D = \frac{1}{2} C_D \rho_{air} S_d (u_d(z) - u_{air})^2 \tag{6.22}$$

The drag coefficient for an isolated solid spherical droplet can be defined, for Reynolds numbers up to 800, by the following empirical equation (L. Schiller, 1933)

$$C_D = \frac{24}{Re_d}\left(1 + 0.15 Re_d^{0.687}\right) \tag{6.23}$$

The equation (1.21), based on equations (1.22) to (1.24) and the (1.3), can be expressed in the following differential form:

$$\frac{du_d(z)}{dz} = \frac{g}{u_d(z)} - C_D \frac{\rho_{air}(u_d(z) - u_{air})^2}{2u_d(z)} \cdot \frac{\pi R_d(z)^2}{m_d} \tag{6.24}$$

To sum up, the differential equations that simulate the heat and mass transfer phenomenon when upcoming air meets falling droplet and the motion effects as well, through a discrete volume of the spray zone are the followings:

$$\frac{dR_d(z)}{dz} = -a_{D,d} \frac{[w_{sw} \cdot (T_d(z)) - w_{air}(z)]}{\rho_w \cdot u_d(z)} \tag{6.25}$$

$$\frac{du_d(z)}{dz} = \frac{g}{u_d(z)} - C_D \frac{\rho_{air}(u_d(z) - u_{air})^2}{2u_d(z)} \cdot \frac{\pi R_d(z)^2}{m_d} \tag{6.26}$$

$$\frac{dT_d}{dz} = \frac{3\{a_{c,d} \cdot (T_{air}(z) - T_d(z)) - a_{D,d} \cdot [w_{sw} \cdot (T_d(z)) - w_{air}(z)] \cdot h_{fg}\}}{c_{p,w} \cdot \rho_w \cdot u_d(z) \cdot R_d(z)} \tag{6.27}$$

$$\frac{dT_{air}(z)}{dz} = \frac{4\pi R_d(z)^2 N_v}{C_{p,air} \rho_{air}(u_d(z) - u_{air})} \{a_{c,d}[T_{air}(z) - T_d(z)]\} \tag{6.28}$$

$$\frac{dw_{air}(z)}{dz} = \frac{4\pi R_d(z)^2 N_v}{\rho_{air}(u_d(z) - u_{air})} \{a_{D,d}[T_{air}(z) - T_d(z)]\} \tag{6.29}$$

In order to solve the equations presented above, five boundary conditions are required. These are: at the point where the water starts to be sprayed, the initial values of droplet diameter, water temperature, water velocity and the temperature and humidity ratio of air that exits the fill packing.

Parameters influence, simulation and conclusions

A program in Matlab environment has been developed in order to solve the above equations. It has to be declared that these differential equations can be used either for the spray or for the rain zone. Several tests have been conducted, varying the main variables, in order to understand how they affect the final values of temperatures and evaluate the cooling performance of the tower.

First of all, as it is proved in previous studies (B.A. Qureshi, 2006), the radius of the droplets in the spray zone is high correlated with the water flow rate. Particularly, the higher the water flow rate, the smaller the droplet, because of the larger pressure loss on sprinklers. The maximum radius of a droplet can be derived from the balance of the forces on the droplet. In case that the drag force is higher than gravity, something that occurs for very small droplets, the droplets are carried away by the upcoming air.

It has to be mentioned, concerning the variation of parameters, that in case that they are not varied they take the following values:

$T_{air,in} = 10^oC, RH_{air,in} = 80\%, T_{droplet,in} = 20^oC, \dot{V}_{air,in} = \frac{20m^3}{sec}, u_{droplet,in} = 1\frac{m}{sec}$, $D_{droplet,in} = 0.001m$

The investigation of the parametes will mainly focus on the rain zone, as the ambient temperature will be the main input variable given in the final calculations. Same content of calculations are implemeted, also, for the spray zone, where the droplet's diameter, temperature and velocity, the zone's height and the air temperature take different initial values, depending on the results of the fill packing simulation, which is presented in following paragraph, and the spray sprinklers specifications.

Based on the the initial parameters' values given above, it was possible to extract from the simulation model the temperature profiles along the a rain zone with 4m height.

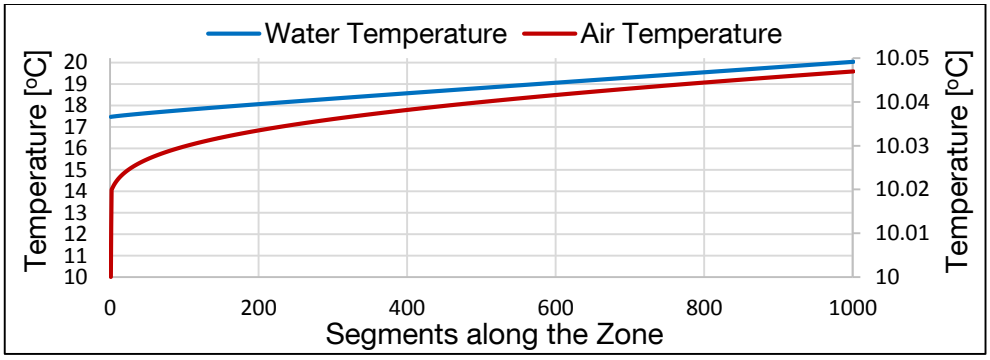

Figure 38: Air and water temperature profiles along the length of the zone

Varying, now, the radius of the inlet droplet in the area, it is obvious that as it increases, the possible temperature drop in the water droplet is reducing.

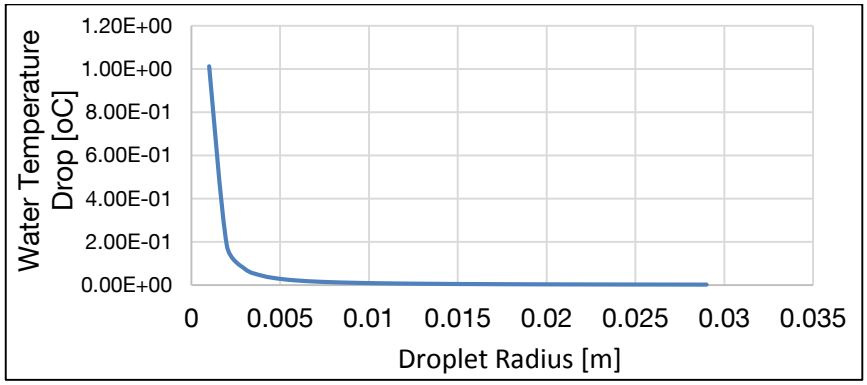

Figure 39: Droplet effective radius

The significant role of the ambient temperature, for the final temperature of the water and reduction of the droplet's radius is depicted in figure 40. As expected, the cold days the cooling performance can be quite effective without requiring, of course, additional fan power to enhance the cooling process.

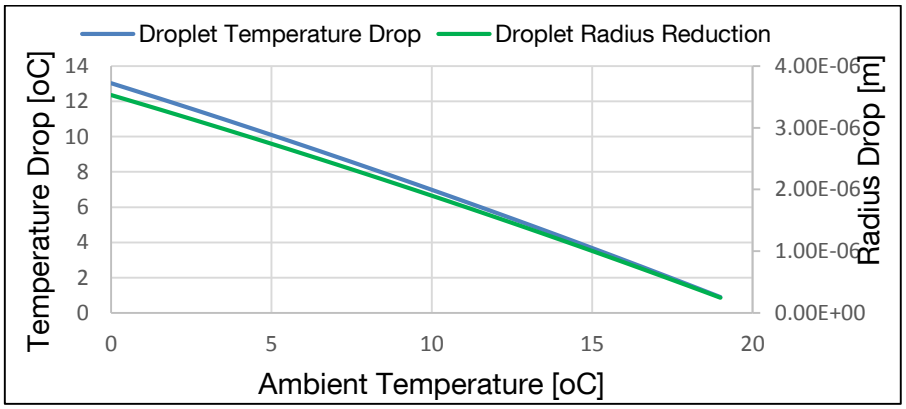

Figure 40: Influence of ambient temperature on the droplet temperature drop and radius reduction

Keeping constant the ambient temperature and varying the initial temperature of the droplet, it is feasible to confirm that the higher the inlet temperature of the water the more the droplet temperature drop and radius decrease. The air temperature is, also, increasing but with a slower pace as the water temperature.

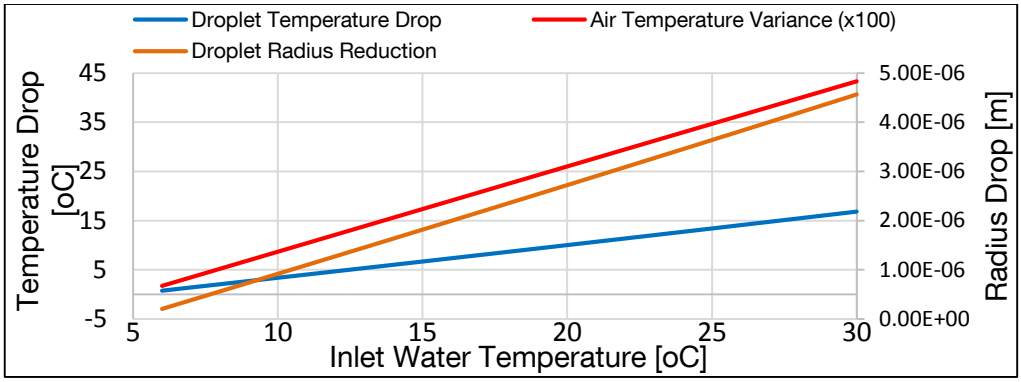

Figure 41: Influence of inlet water temperature on droplet temperature, droplet radius and air temperature

The variance of the droplet initial velocity seems to influence slightly the drop on the air and water temperature. As depicted in figure 42, the effect of the droplet velocity on the radius is really small and it is easily observed that after a specific value, the velocity of the droplet does not have any more impact on the temperature and radius reductions.

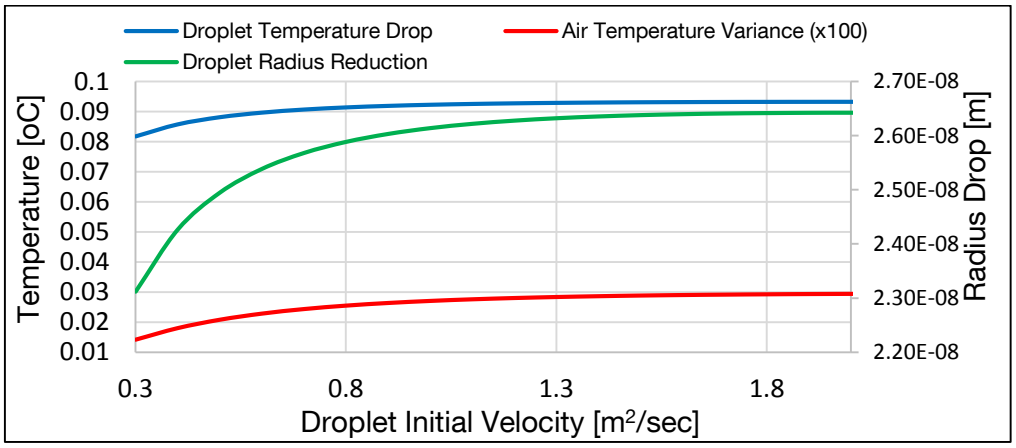

Figure 42: Influence of droplet initial velocity on droplet temperature, droplet radius and air temperature

Finally, the simulation program was used to investigate how the length of the zone, where the droplets come in contact with the air, influence the several parameters as previously. The results are illustrated in figure 43 and it is clear that as the zone's length is increasing the air temperature difference is increasing, as well as the droplet temperature drop and the radius reduction. These results are plausible, taking into account the differential equations (6.25), (6.27), (6.28) and the fact that the time period of contact is increasing by increasing the zone length and the heat and mass phenomena take place for longer.

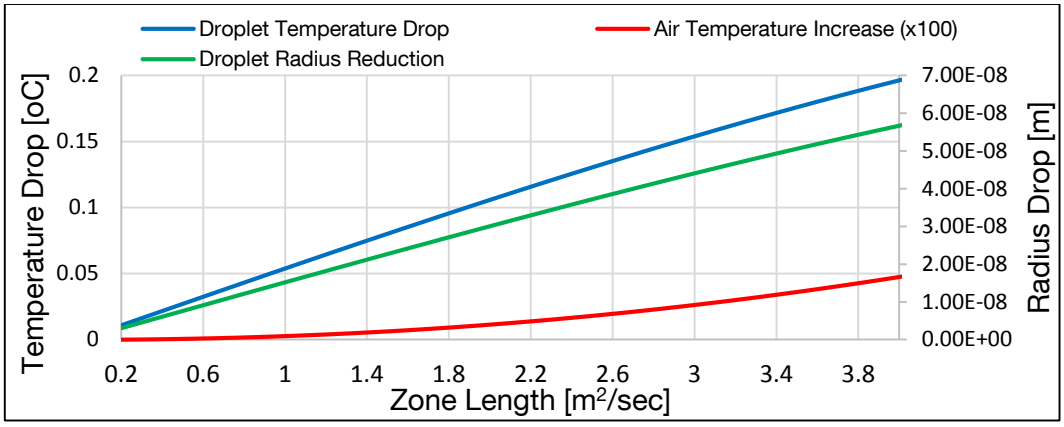

Figure 43: Influence of zone length on droplet temperature, droplet radius and air temperature

6.3 Fill Packing Zone Model

After the first direct contact of the air with the water falling droplets in the rain zone and before entering the spray zone, the air meets the water in the fill packing zone (figure 36), where heat and mass transfer occur. This paragraph describes a model that developed, based on the Poppe Approach, for the evaluation of the fill packing's cooling performance, as well as the investigation of the influence of the several parameters on it.

Poppe Approach

The Poppe Approach is widely believed to be the most accurate method for simulating the cooling performance of a counter-flow wet-cooling tower. The governing equations for heat and mass transfer in the fill packing of a counter-flow cooling tower are implemented, after dividing the fill zone into as many as required finite elements, at each one of these intervals. The following figure present one of these intervals, characterized as control volume "dz", where the air comes in contact with the water drops.

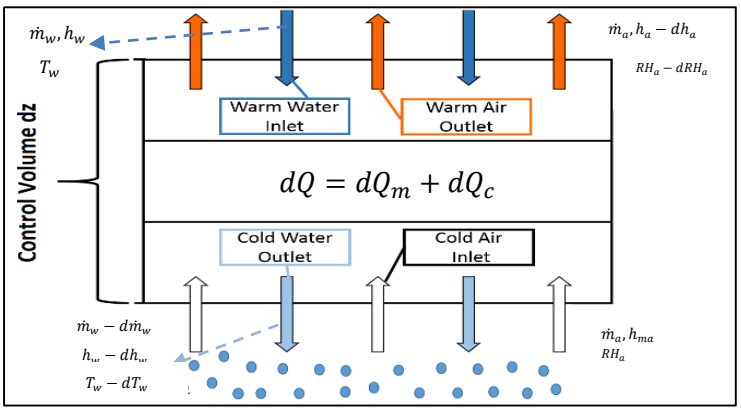

Figure 44: Control volume "dz", where air interacts with water

It has to be clearly defined that the following equations are suitable for unsaturated air. Therefore, the relative final equations for the occasion of supersaturated air will also by presented. The mass balance for a specific control volume is given by:

$$dh_w = \dot{m}_a dw \tag{6.30}$$

The energy balance for the same volume yields:

$$\dot{m}_a dh_{ma} - \dot{m}_w dh_w - h_w d\dot{m}_w = 0 \tag{6.31}$$

Substituting equation (6.30) into (6.31) the following equations is formed:

$$dT_w = \frac{\dot{m}_a}{\dot{m}_w}\left(\frac{1}{c_{pw}} dh_{ma} - T_w dw\right) \tag{6.32}$$

A mass balance at the interface between water and air concludes in:

$$d\dot{m}_w = U_d(w_{sw} - w)dA \tag{6.33}$$

And an energy balance at the interface between water and air results in:

$$dQ = dQ_m + dQ_c \tag{6.34}$$

Where dQ_m constitutes the enthalpy transfer due to difference in vapour concentration between the saturated air at the interface and the mean stream air given by:

$$dQ_m = h_v d\dot{m}_w = h_v U_d(w_{sw} - w)dA \tag{6.35}$$

Variable h_v is the water vapour enthalpy at the bulk water temperature T_w, given by:

$$h_v = h_{fgwo} + c_{pv}T_w \tag{6.36}$$

As for dQ_c, the sensible heat transfer due to the temperature difference, is evaluated by:

$$dQ_c = U(T_w - T_a)dA \tag{6.37}$$

The enthalpy of saturated air evaluated at the local bulk water temperature is defined by:

$$h_{masw} = c_{pa}T_w + w_{sw}\left(h_{fgwo} + c_{pv}T_w\right) = c_{pa}T_w + wh_v + (w_{sw} - w)h_v \tag{6.38}$$

The enthalpy of the air-water vapor mixture per unit mass of dry air is determined by:

$$h_{ma} = c_{pa}T_a + w\left(h_{fgwo} + c_{pv}T_a\right) \tag{6.39}$$

The specific heat of the air-water vapor mixture for unsaturated air is expressed by:

$$c_{pma} = c_{pa} + wc_{pv} \tag{6.40}$$

From equations (6.38) and (6.39) and by ignoring the small differences in specific heats, the following formula can be extracted:

$$T_w - T_a = \frac{(h_{masw} - h_{ma}) - (w_{sw} - w)h_v}{c_{pma}} \tag{6.41}$$

While substituting (6.40) into (B6.37), the resultant equation is:

$$dQ = U_d \left[\frac{h}{c_{pma} h_d} (h_{masw} - h_{ma}) + \left(1 - \frac{U}{c_{pma} U_d}\right) h_v (w_{sw} - w) \right] dA \tag{6.42}$$

The order $\frac{U}{c_{pma} U_d}$, also called as Lewis factor, indicates the relative rates of heat and mass transfer in an evaporative process.

According to literature (Bosnjakovic, 1965), an empirical relation for the Lewis factor for unsaturated air is:

$$Le_f = 0.865^{0.667} \frac{\left(\frac{w_{sw} + 0.622}{w + 0.622} - 1\right)}{ln\left(\frac{w_{sw} + 0.622}{w + 0.622}\right)} \tag{6.43}$$

From equation (6.42) the enthalpy transfer of the air stream can be derived as below:

$$dh_{ma} = \frac{1}{\dot{m}_a} dQ = \frac{U_d dA}{\dot{m}_a} \left[Le_f (h_{masw} - h_{ma}) + \left(1 - Le_f\right) h_v (w_{sw} - w) \right] \tag{6.44}$$

The transfer area for a dz element can be defined as:

$$dA = A_{fill} A_{fr} dz \tag{6.45}$$

By assuming a 1D model of the cooling tower fill, where the available area for heat and mass transfer is equal at any horizontal section through the fill.

In the equation (6.45), A_{fill} is the wetted area divided by the corresponding volume of the fill and A_{fr} is the corresponding frontal area or face area.

Combining equations (6.44) and (6.45), the resultant relation is:

$$\frac{dh_{ma}}{dz} = \frac{U_d A_{fill} A_{fr}}{m_a} \left[Le_f (h_{masw} - h_{ma}) + \left(1 - Le_f\right) h_v (w_{sw} - w) \right] \tag{6.46}$$

Bourillot (1983) presented the Poppe Approach equations as a system of three equations that describe the change of water temperature (dT_w), air enthalpy (dh_{ma}), and humidity ratio (dw) to the change of air travel distance(dz).

By integrating equations (6.33) and (6.44) into equation (6.31) the formula below is extracted.

$$\dot{m}_w dh_w = U_d dA \left[h_{masw} - h_{ma} + \left(Le_f - 1\right) \{ h_{masw} - h_{ma} - (w_{sw} - w) h_v \} - (w_{sw} - w) c_{pw} T_w \right] \tag{6.47}$$

Equation (6.32) can also be written as:

$$\frac{dw}{dT_w} = \frac{1}{c_{pw} T_w} \frac{dh_{ma}}{dT_w} - \frac{1}{T_w} \frac{\dot{m}_w}{\dot{m}_a} = \frac{dh_{ma}}{T_w dh_w} - \frac{1}{T_w} \frac{\dot{m}_w}{\dot{m}_a} \tag{6.48}$$

And by integrating in this formula the equations (6.46) and (6.47), the result is:

$$\frac{dw}{dT_w} = \frac{c_{pw}\frac{\dot{m}_w}{\dot{m}_a}(w_{sw}-w)}{h_{masw}-h_{ma}+(Le_f-1)\{h_{masw}-h_{ma}-(w_{sw}-w)h_v\}-(w_{sw}-w)c_{pw}T_w} \quad (6.49)$$

Substituting, also, equation (6.49) into (6.48), the following expression is defined:

$$\frac{dh_{ma}}{dT_w} = \frac{\dot{m}_w c_{pw}}{\dot{m}_a}\left(1+\frac{c_{pw}T_w\,(w_{sw}-w)}{h_{masw}-h_{ma}+(Le_f-1)\{h_{masw}-h_{ma}-(w_{sw}-w)h_v\}-(w_{sw}-w)c_{pw}T_w}\right) \quad (6.50)$$

In order to find the third equation of the Poppe method it has, firstly, to be determined from (6.30) and (6.34) the expression:

$$U_d dA = \frac{\dot{m}_a dw}{w_{sw}-w} \quad (6.51)$$

Which after divided by m_w and some rearrangements can be transformed into:

$$\int \frac{U_d}{\dot{m}_w}dA = \int \frac{\dot{m}_a}{\dot{m}_w}\frac{\frac{dw}{dT_w}}{(w_{sw}-w)}dT_w \Rightarrow \frac{U_d A}{\dot{m}_w} = \int \frac{\dot{m}_a}{\dot{m}_w}\frac{\frac{dw}{dT_w}}{(w_{sw}-w)}dT_w \quad (6.52)$$

The last equation, called as Merkel number defined by Poppe approach, is written as:

$$Me_P = \int \frac{m_a}{m_w}\frac{\frac{dw}{dT_w}}{(w_{sw}-w)}dT_w \quad (6.53)$$

After substitution of the (6.49) into (6.53) and differentiation of the latter with respect to the water temperature it is found that:

$$\frac{dMe_P}{dT_w} = \frac{c_{pw}}{h_{masw}-h_{ma}+(Le_f-1)\{h_{masw}-h_{ma}-(w_{sw}-w)h_v\}-(w_{sw}-w)c_{pw}T_w} \quad (6.54)$$

It has to be defined that the ratio of the mass flow rates, $\frac{m_w}{m_a}$, changes as the air moves through the fill. The variable value of water mass flow rate can be determined as the inlet water mass flow rate is known. In order to be able to calculate the variable mass flow rate, a control volume is selected, as illustrated in figure 44, upon which the mass balance implemented gives:

$$\dot{m}_{win} = \dot{m}_w + \dot{m}_a(w_{out}-w) \quad (6.55)$$

Equation, which can also be written as:

$$\frac{\dot{m}_w}{\dot{m}_a} = \frac{\dot{m}_{win}}{\dot{m}_a}\left(1-\frac{\dot{m}_a}{\dot{m}_{win}}(w_{out}-w)\right) \quad (6.56)$$

The equations (6.43), (6.49), (6.50) and (6.56) are the required equations in order to evaluate the air outlet enthalpy and humidity.

In case of supersaturated air the procedure for extracting the equations required is the same as for the unsaturated air. One important difference is that the enthalpy of supersaturated air, given that the excess water vapor will condense as a mist, is evaluated by the expression:

$$h_{ss} = c_{pa}T_w + w_{sa}\left(h_{fgwo} + c_{pv}T_a\right) + (w - w_{sa})c_{pw}T_a \tag{6.57}$$

Where w_{sa} constitutes the humidity ratio of saturated air at temperature T_a.

Generally, the equation that has to be used in this occasion are the same as above for the unsaturated air, with substituting the w with w_{sa} and the h_{ma} with h_{ss}.

To summarize, the following system of governing equations is determined for implementing Poppe Approach:

A. *For unsaturated air:*

$$\frac{dw}{dT_w} = \frac{c_{pw}\frac{\dot{m}_w}{\dot{m}_a}(w_{sw}-w)}{h_{masw}-h_{ma}+(Le_f-1)\{h_{masw}-h_{ma}-(w_{sw}-w)h_v\}-(w_{sw}-w)c_{pw}T_w} \tag{6.58}$$

$$\frac{dh_{ma}}{dT_w} = \frac{\dot{m}_w c_{pw}}{\dot{m}_a}\left(1 + \frac{c_{pw}T_w\,(w_{sw}-w)}{h_{masw}-h_{ma}+(Le_f-1)\{h_{masw}-h_{ma}-(w_{sw}-w)h_v\}-(w_{sw}-w)c_{pw}T_w}\right) \tag{6.59}$$

$$\frac{dMe_P}{dT_w} = \frac{c_{pw}}{h_{masw}-h_{ma}+(Le_f-1)\{h_{masw}-h_{ma}-(w_{sw}-w)h_v\}-(w_{sw}-w)c_{pw}T_w} \tag{6.60}$$

B. *For supersaturated air:*

$$\frac{dw}{dT_w} = \frac{c_{pw}\frac{\dot{m}_w}{\dot{m}_a}(w_{sw}-w_{sa})}{h_{masw}-h_{ss}+(Le_f-1)\{h_{masw}-h_{ss}-(w_{sw}-w_{sa})h_v+(w-w_{sa})c_{pw}T_w\}+(w-w_{sw})c_{pw}T_w} \tag{6.61}$$

$$\frac{dh_{ma}}{dT_w} = \frac{\dot{m}_w c_{pw}}{\dot{m}_a}\left(1 + \frac{c_{pw}T_w\,(w_{sw}-w)}{h_{masw}-h_{ss}+(Le_f-1)\{h_{masw}-h_{ss}-(w_{sw}-w_{sa})h_v+(w-w_{sa})c_{pw}T_w\}+(w-w_{sw})c_{pw}T_w}\right) \tag{6.62}$$

$$\frac{dMe_P}{dT_w} = \frac{c_{pw}}{h_{masw}-h_{ss}+(Le_f-1)\{h_{masw}-h_{ss}-(w_{sw}-w_{sa})h_v+(w-w_{sa})c_{pw}T_w\}+(w-w_{sw})c_{pw}T_w} \tag{6.63}$$

System Solving Methodology – 4th Order Runge Kutta

In order to solve the system presented above the numerical method Runge-Kutta of fourth order has to be implemented. A basic form of the equations for both unsaturated and supersaturated air is the following:

$$\frac{dw}{dT_w} = f(w, h_{ma}, T_w) \tag{6.64}$$

$$\frac{di_{ma}}{dT_w} = g(w, h_{ma}, T_w) \tag{6.65}$$

$$\frac{dMe_P}{dT_w} = h(w, h_{ma}, T_w) \tag{6.66}$$

It has to be mentioned that In case of supersaturated air the enthalpy h_{ma} is substituted by h_{ss}.

The use of fourth order Runge-Kutta premises the division of the fill packing in one or more intervals, which are characterized by the same temperature increase through each of them. Furthermore, the fill packing of the cooling tower is also divided in levels, which constitute horizontal planes across the fill intervals. A better view of levels and intervals is illustrated in figure 45.

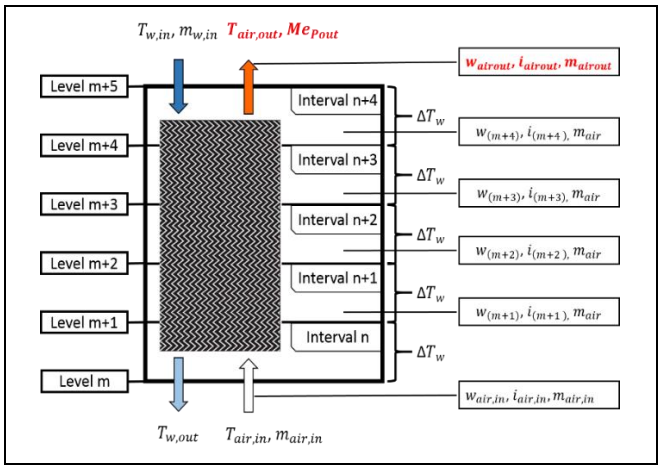

Figure 45: Fill packing of a counter-flow cooling tower divided into five intervals

As a result, in between two levels, a fill interval exists, which in its turn consists of four more division elements at each of which the four orders of Runge-Kutta numerical method are evaluated. Starting from a level where the variables' values are known, for example if the inlet conditions of air and water in the fill are given, it is possible to determine the values of humidity, enthalpy and Merkel number of the next level, based on the equations presented above and by using the following formulas derived from Runge-Kutta:

$$w_{(n+1)} = w_{(n)} + \left(j_{(n+1,1)} + 2j_{(n+1,2)} + 2j_{(n+1,3)} + j_{(n+1,4)}\right)/6 \tag{6.67}$$

$$h_{ma(n+1)} = h_{ma(n)} + \left(k_{(n+1,1)} + 2k_{(n+1,2)} + 2k_{(n+1,3)} + k_{(n+1,4)}\right)/6 \tag{6.68}$$

$$Me_{p(n+1)} = Me_{p(n)} + \left(l_{(n+1,1)} + 2l_{(n+1,2)} + 2l_{(n+1,3)} + l_{(n+1,4)}\right)/6 \tag{6.69}$$

Where:

$$j_{(n+1,1)} = \Delta T_w \cdot f\left(w_{(n)}, h_{ma(n)}, T_{w(n)}\right) \tag{6.70}$$

$$k_{(n+1,1)} = \Delta T_w \cdot g\left(w_{(n)}, h_{ma(n)}, T_{w(n)}\right) \tag{6.71}$$

$$l_{(n+1,1)} = \Delta T_w \cdot h\left(w_{(n)}, h_{ma(n)}, T_{w(n)}\right) \tag{6.72}$$

And with $m = 2, 3, 4$:

$$j_{(n+1,\mathrm{m})} = \Delta T_w \cdot f\left(w_{(n)} + \frac{j_{(n+1,\mathrm{m}-1)}}{2}, h_{ma(n)} + \frac{k_{(n+1,\mathrm{m}-1)}}{2}, T_{w(n)} + \frac{\Delta T_w}{2}\right) \quad (6.73)$$

$$k_{(n+1,\mathrm{m})} = \Delta T_w \cdot g\left(w_{(n)} + \frac{j_{(n+1,\mathrm{m}-1)}}{2}, h_{ma(n)} + \frac{k_{(n+1,\mathrm{m}-1)}}{2}, T_{w(n)} + \frac{\Delta T_w}{2}\right) \quad (6.74)$$

$$l_{(n+1,\mathrm{m})} = \Delta T_w \cdot h\left(w_{(n)} + \frac{j_{(n+1,\mathrm{m}-1)}}{2}, h_{ma(n)} + \frac{k_{(n+1,\mathrm{m}-1)}}{2}, T_{w(n)} + \frac{\Delta T_w}{2}\right) \quad (6.75)$$

Where $\Delta T_w = T_{w,n+1} - T_{w,n}$ (6.76)

With n being the number of level that the calculations take place and m the order of Runge-Kutta.

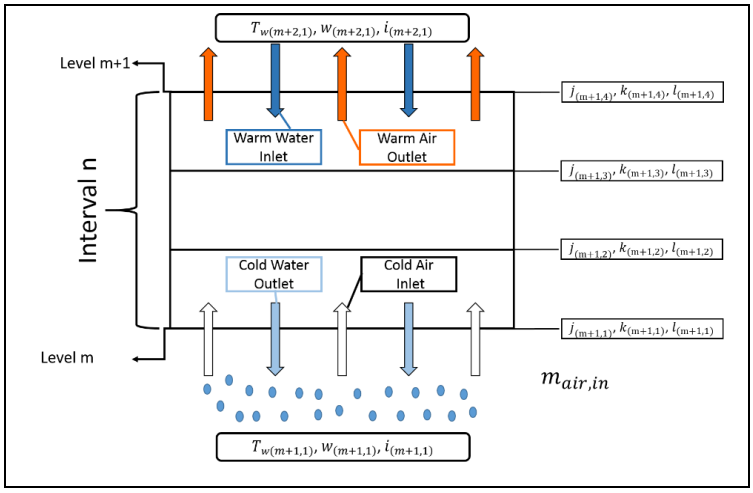

Figure 46: Fill's Interval n Divided by Runge-Kutta Method

Analysis of a wet-counter-flow C.T. fill according to Poppe Approach

The process for analyzing a counter-flow fill of a wet-cooling tower according to Poppe Approach and Runge-Kutta numerical method presented above will be detailed described in this section. A code in Matlab environment has been developed based on this process in order to evaluate the cooling towers' performance, as is referred in following sections.

First of all, it is important to have some initial variables' values in order to begin with calculations. These values are the atmospheric pressure P_{air}, the air inlet temperature $T_{air,in}$, the inlet air relative humidity $RH_{air,in}$, the dry air mass flow rate $\dot{m}_{air,in}$, the inlet water temperature T_{win}, i.e. the water that returns from the condenser in the cooling tower, the inlet water mass flow rate $\dot{m}_w$ and the height of the fil packing L_{fill}

The water temperature difference at each interval constitutes, as derived from equations (6.70) to (6.76), a significant parameter for the evaluations of the Runge-Kutta orders. A way of estimating its value is described in this paragraph, based on the possible heat and mass transfer between air and water. Firstly, the heat transfer coefficient is assumed, for forced convection and according to (Incropera, 2007) to be $\alpha = 30\ W/m^2K$, while the total heat transfer area in the fill zone, based on Unterhaching Power Plant Cooling Towers'

dimensions is estimated to be $10{,}000m^2$. The user is able to define the number of intervals (N_{int}) along the fill packing and as a result the heat transfer area at each interval can be calculated by:

$$A_{int} = A_{tot}/(N_{int} - 1) \tag{6.77}$$

Given the above and after estimating a value for the water temperature at the outlet of the fill packing a bit greater that the ambient temperature it is possible to define the heat transfer at the first interval (n=1) by:

$$Q_{tr} = \alpha \cdot A_{int} \cdot \left(T_w^{n=1} - T_{air}^{n=1}\right) \tag{6.78}$$

The evaluation of the mass transfer that occurs requires the estimation of the diffusion mass flow by the equation based on the first Fick's law:

$$J = \frac{D_f \cdot \varphi}{L_{diff} \cdot A_{int} \cdot M_{H_2O}} \tag{6.79}$$

Where for simplifying the calculations, the diffusion distance, i.e. the distance between two films of the fill packing, is assumed to be $L_{diff} = 0.05\,m$ and the diffusion coefficient according to Wikipedia for air and water $Diff = 0.2 \cdot 10^{-4}\,m^2/sec$. The variable M_{H_2O} is the molar mass of water equal to $18\,g/mole$ and the concentration gradient between water surface and air [mol/m^3] is defined by:

$$D_{con} = \frac{dV_x}{R_g \cdot T_{air}} \tag{6.80}$$

Where dV_x constitutes the difference between the partial pressure at water surface and saturation and the partial pressure in air, at the given relative humidity, each of them extracted from air tables in Matlab, R_g the gas constant and the T_{air} the air temperature at each interval.

Now, it is feasible to determine the heat flow after the heat and mass transfer by formula:

$$\dot{Q}_{n+1} = \dot{Q}_n + Q_{tr} + h_{ev} \cdot J_n \tag{6.81}$$

The variable h_{ev} corresponds to the evaporation enthalpy and is equal to the difference between the saturation vapour enthalpy and the saturation liquid enthalpy, both calculated at the water temperature by steam tables given in Matlab. Based on calculations till this point, the water temperature at the outlet of the interval can be calculated depending on whether saturation has occurred or not. Finally, the value of the water temperature difference at a specific interval can be defined, in order to start the Poppe Approach algorithm.

The final value of water temperature at the outlet of the fill packing or the first interval will be evaluated through an iterative procedure. As aforementioned, a value slightly greater than the ambient is given as input in the algorithm. At the end of the Poppe Approach algorithm a value for the inlet water temperature has been calculated. This values is compared with the real value of inlet water temperature and their difference constitute the convergence criteria of the whole program. A value of 0.05 is proven to fulfill this purpose, depending computational time required and result's accuracy.

The rest flow of the Poppe Approach algorithm will be described in the next paragraphs. Based on the input aforementioned data it is possible to evaluate the humidity ratio of air at the inlet level w_{in} according to equation (6.15) as referred in previous paragraph, as well as the enthalpy of inlet air given by equation (6.39).

Then an assumption should be made for the air temperature leaving the fill T_{aout} , in order to evaluate the humidity ratio at this elevation. Moreover the outlet air wet-bulb temperature is equal to T_{aout} approximated, as it is assumed that the air is going to be supersaturated at this point. An iteration procedure is also followed here, so that the calculated humidity ratio at the outlet approaches the initial estimation.

The iterations start with the definition of the values of the variables for the first fill interval, i.e.: $T_{w(1,1)} = T_{wout,}\, w_{(1,1)} = w_{in}, h_{ma(1,1)} = h_{main}$.

Then the humidity ratio of saturated air is evaluated at $T_{w(1,1)}$ according to:

$$w_{de} = \left(\frac{0.62509 p_{vwb}}{p_{abs} - 1.005 p_{vwb}}\right) \tag{6.82}$$

The enthalpy of water vapor and of saturated air from equations (6.36) and (6.38) respectively, both calculated at local bulk water temperature. Furthermore, the values of Lewis factor from (6.43) and mass balance from (6.56) are required in order to proceed with the calculation of orders $j_{(1,1)}$, $k_{(1,1)}$, $l_{(1,1)}$, which based on the governing equations are expressed by:

(6.83):

$$j_{(1,1)} = \frac{\Delta T_w c_{pw(1,1)} \left(\frac{\dot{m}_w}{m_a}\right)_{(1,1)} \left(w_{sw(1,1)} - w_{(1,1)}\right)}{h_{masw(1,1)} - h_{ma(1,1)} + \left(Le_{f(1,1)} - 1\right)\left\{h_{masw(1,1)} - h_{ma(1,1)} - \left(w_{sw(1,1)} - w_{(1,1)}\right) h_{v(1,1)}\right\} - \left(w_{sw(1,1)} - w_{(1,1)}\right) c_{pw(1,1)} T_{w(1,1)}}$$

(6.84):

$$k_{(1,1)} = \Delta T_w c_{pw(1,1)} \left(\frac{\dot{m}_w}{\dot{m}_a}\right)_{(1,1)} \times \left(1 + \left(\frac{c_{pw(1,1)} T_{w(1,1)} \left(w_{sw(1,1)} - w_{(1,1)}\right)}{h_{masw(1,1)} - h_{ma(1,1)} + \left(Le_{f(1,1)} - 1\right)\left\{h_{masw(1,1)} - h_{ma(1,1)} - \left(w_{sw(1,1)} - w_{(1,1)}\right) h_{v(1,1)}\right\} - \left(w_{sw(1,1)} - w_{(1,1)}\right) c_{pw(1,1)} T_{w(1,1)}}\right)\right)$$

(6.85)

$$l_{(1,1)} = \frac{\Delta T_w c_{pw(1,1)}}{h_{masw(1,1)} - h_{ma(1,1)} + \left(Le_{f(1,1)} - 1\right)\left\{h_{masw(1,1)} - h_{ma(1,1)} - \left(w_{sw(1,1)} - w_{(1,1)}\right) h_{v(1,1)}\right\} - \left(w_{sw(1,1)} - w_{(1,1)}\right) c_{pw(1,1)} T_{w(1,1)}}$$

Before continuing with the second intermediate step of Runge-Kutta for the first interval the new starting values have to be determined. For this reason:

$$T_{w(1,2)} = T_{wout} + \Delta T_w/2, w_{(1,2)} = w_{in} + j_{(1,1)}/2, h_{ma(1,2)} = h_{main} + k_{(1,1)}/2 \tag{6.86}$$

The same calculations take place in order to find the rest orders of Runge-Kutta method: $j_{(1,2)}$, $k_{(1,2)}$, $l_{(1,2)}$, $j_{(1,3)}$, $k_{(1,3)}$, $l_{(1,3)}$, $j_{(1,4)}$, $k_{(1,4)}$, $l_{(1,4)}$.

Having defined all the orders it is possible to evaluate the Poppe method's design variables by the equations 6.67 to 6.69 for n=0 (Level 0):

$$w_{(1)} = w_{(0)} + \left(j_{(1,1)} + 2j_{(1,2)} + 2j_{(1,3)} + j_{(1,4)}\right)/6 \tag{6.87}$$

$$h_{ma(1)} = h_{ma(0)} + \left(k_{(1,1)} + 2k_{(1,2)} + 2k_{(1,3)} + k_{(1,4)}\right)/6 \tag{6.88}$$

At this stage it is important to check whether the air has become supersaturated or remains still unsaturated. For this purpose the following set of calculations has to be followed.

A first assumption is being made that the air remains unsaturated after the first interval for example. According to this, the wet and dry-bulb temperatures are calculated and if wet-bulb temperature at level 1, $T_{wb(1)}$ is greater than air temperature at the same level, $T_{air(1)}$, then the assumption was wrong and the air has turned to supersaturated, meaning that $T_{wb(1)} = T_{air(1)}$.

- *Dry-bulb Temperature Evaluation at Level n*

Given the four Runge-Kutta orders, the air enthalpy at level n is already known. Following the first assumption for unsaturated air, a value for the dry-bulb temperature, $T_{db(n)}$, is also assumed. After evaluating the required specific heats at $\left(T_{db(n)} + 273.15\right)/2$ for the equation (6.39), the enthalpy of an air vapor mixture per unit mass of dry air can be determined and compared with the air enthalpy at level n. If these values are within close tolerance, then the value of $T_{air(n)}$ is correct. While the value of $T_{db(n)}$ is not given, an iterative procedure has to be implemented, through the optimization algorithms of Matlab, i.e. "fminsearch".

- *Wet-bulb Temperature Evaluation at Level n*

The steps for the determination of the wet-bulb temperature is somehow the same as for the dry-bulb temperature. Given the humidity ratio at level n by the Runge-Kutta method a wet-bulb temperature $T_{wb(n)}$ is assumed. Then the vapor pressure at $T_{wb(n)}$ from air-steam tables given in Matlab and the humidity ratio from (6.15) are evaluated, with the last to be compared with the already determined humidity ratio at level n. If these values are in close tolerance, then the assumption is correct. Of course, in this case, also, an iterative procedure has to be implemented through the optimization algorithms of Matlab, i.e. "fminsearch".

- *Wet and Dry-bulb Temperature Evaluation at Level n for Supersaturated Air*

The steps defined above are, as declared, for the case that the air remains unsaturated. If the air becomes supersaturated, then the dry-bulb temperature is equal to wet-bulb temperature at level n, $T_{wb(n)} = T_{db(n)}$, and a value for them is assumed. As a result, the vapor pressure at $T_{wb(n)}$ as aforementioned and the humidity ratio $w_{sa(n)}$ from (6.15) are evaluated, as well as the supersaturated air enthalpy according to (6.57). This value is checked to be within close tolerance with air enthalpy given at level n in order to confirm that the value assumed is correct. Finally, in this case, also, an optimization algorithm of Matlab has been implemented to find the required value for the minimum tolerance.
To make it clearer, the algorithmic procedure described above is depicted below in the form of a simple flow chart.

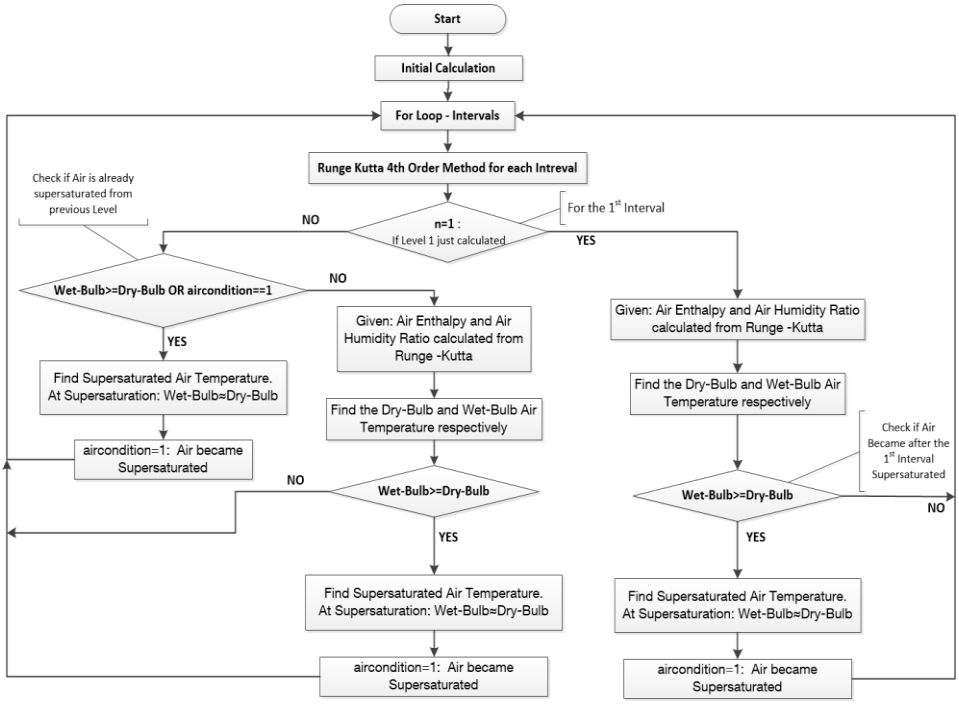

Figure 47: Flow chart for supersaturation control and relative wet- and dry-bulb temperatures

Until this phase all required calculations for the interval n have been completed. In order to continue with interval n+1, the new initial variables' values have to be defined. Consequently:

i. Water Temperature: $T_{w(n+1)} = T_{w(n)} + \Delta T_w$ (6.89)

ii. Air Enthalpy and Humidity Ratio:

a. If air still unsaturated: $h_{ma(n+1,1)} = h_{ma(n)}$ and $w_{(n+1,1)} = w_{(n)}$ (6.90)
b. If air supersaturated: $h_{ss(n+1,1)} = h_{ss(n)}$ and $w_{\mathrm{sa}(n+1,1)} = w_{\mathrm{sa}(n)}$ (6.91)

After these calculations, the iterations' procedure continues with the next intervals' calculations that are the same as presented above for interval n. When the governing equations have been solved for all the intervals, it is feasible to know the required values of: $\boldsymbol{T_{air,out}}$, $\boldsymbol{w_{airout}}$, $\boldsymbol{h_{airout}}$.

Of course, these values have come from a first assumption about the $\boldsymbol{T_{air,out}}$ and consequently about the humidity ratio $\boldsymbol{w_{airout}}$. Into the code that has been developed, a proper condition has been selected in order to confirm that the calculated humidity is within close tolerance with the assumed, meaning that the first assumption is correct or adjusting the estimation so that convergence is speed up.

Fill Packing Algorithm Result

The program that has been developed to implement the calculations presented above is able to evaluate the temperature profiles of air and water along a specific fill packing, for given inlet conditions. Such a program is significant before the pressure losses and the fan power consumption, which are described in next paragraphs of the thesis, are calculated and an optimum operation point of the cooling tower is defined. An example of a specific case is presented here. Particularly, the values of the basic input parameters are the followings. Atmospheric pressure $P_{air} = 10^5 Pa$, air inlet temperature $T_{air,in} = 10^o C$, inlet air relative humidity $RH_{air,in} = 80\%$, dry air volume flow rate $\dot{V}_{air,in} = 30 m^3/s$, the inlet water temperature $T_{win} = 20^o C$, the inlet water mass flow rate $\dot{m}_w = 210 kg/s$ and the height of the fil packing $L_{fill} = 1.5m$. The profiles are depicted in the following graph.

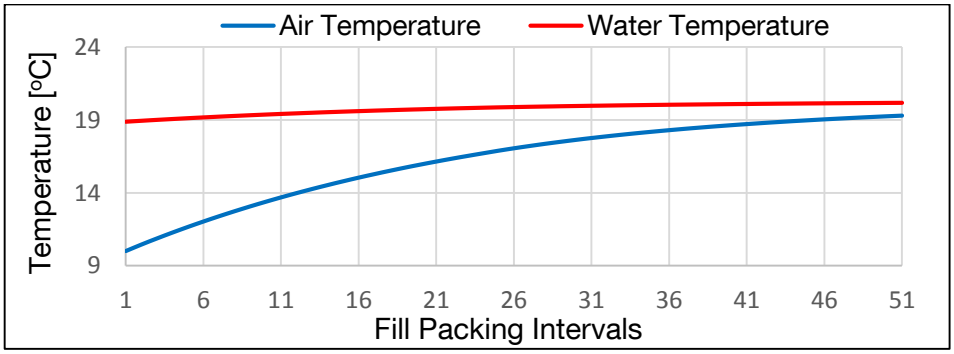

Figure 48: Air and water temperature profiles along the fill packing for a specific cooling case

The fill packing was divided in 50 intervals and the convergence criteria set 0.1. The algorithm converged after 4 iterations, i.e. five initializations of water outlet temperature, and 3.7 sec were required. The convergence evolution is illustrated below:

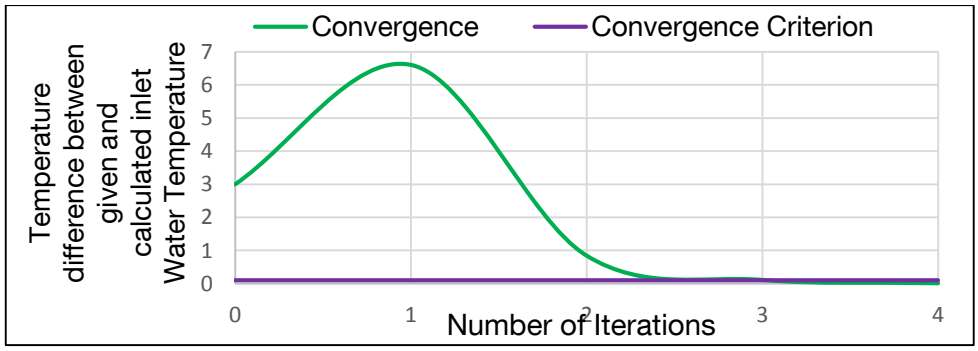

Figure 49: Fill packing algorithm convergence

Based on the dimensions of the cooling towers that exist in Unterhaching Power Plant, the algorithm described here concerning the cooling performance of the fill packing will be implemented for several cases to show its utility. A variation of the various main parameters aims to create a “cooling tower map” that depicted the cooling performance for various conditions. The variables that will range among reasonable for Unterhaching Power Plant’s case values are the ambient temperature and relative humidity, the air mass flow rate, the

inlet water mass flow rate and the inlet water temperature. For each case, one of these variables will vary, while the rest will remain constant and the outlet water temperature will be evaluated.

- Case 1: $\dot{m}_{water} = 200\,\frac{kg}{sec}$, $\dot{V}_{air} = 100\,m^3/sec$, vary $T_{air,in}, RH_{air}$

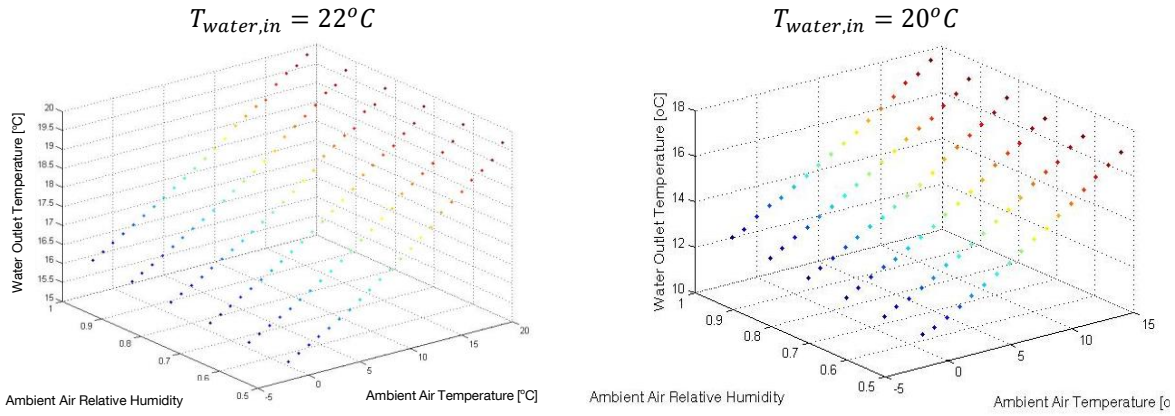

Figure 50: Outlet water temperature for various ambient air conditions and inlet water temperature

From the figure above it is concluded that the lower the humidity, the more moisture the air can accept, the more heat can be rejected in the fill packing and consequently the outlet water is slightly lower. Between the two graphs there is a difference in the cooling performance, as the higher the temperature of the water that enters the tower, the higher water temperature that exits the fill packing.

- Case 2: $T_{water,in} = 20^oC$, $\dot{V}_{air} = 100\,\frac{m^3}{sec}$, $RH_{air} = 80\%$, vary $T_{air,in}$, $\dot{m}_{water}$

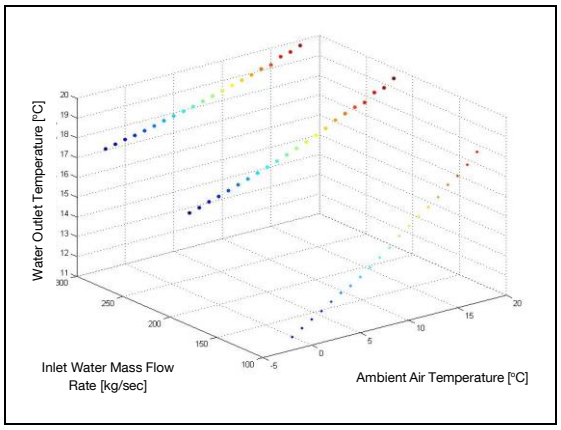

Figure 51: Outlet water temperature for various ambient air temperatures and inlet water mass flow rates

It seems that with a low water mass flow rate, a better cooling performance can be achieved for specific ambient conditions as the water remains more time in contact with

the air. Of course, the sufficient circulation of the whole cooling system should be taken into account.

- Case 4: $\dot{m}_{water} = 200\frac{kg}{sec}$, $RH_{air} = 80\%$ vary $T_{water,in}$, $\dot{V}_{air}$, $T_{air,in}$

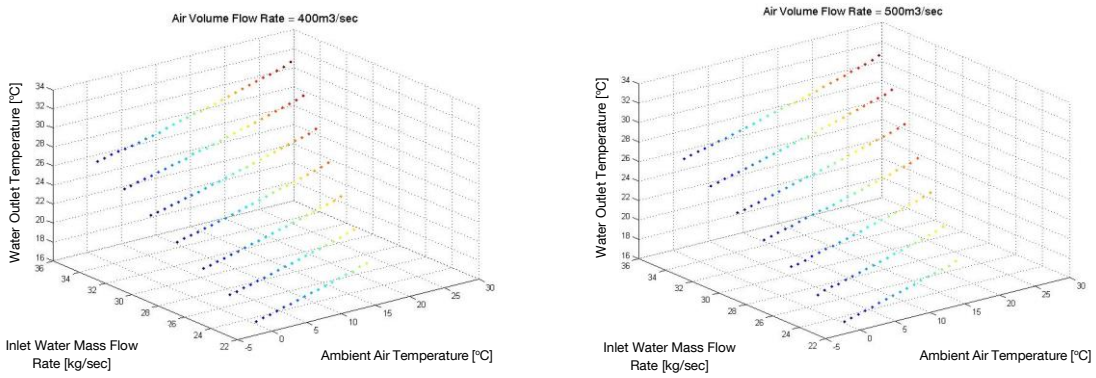

Figure 52: Outlet water temperature for various ambient air temperatures and inlet water temperatures and different air volume flow rates

It is obvious from figures presented above that even if the air volume flow rate changes, this does not inluence the cooling result for the several water and air inlet temperatures and a constant water mass flow rate that have been tested. Moreove, as expected, lower inlet water temperature results in lower outlet water temperature, with their relationship to seem to be almost linear.

- Case 4: $T_{water,in} = 20^oC$, $\dot{m}_{water} = 200\frac{kg}{sec}$, $RH_{air} = 80\%$, vary $T_{air,in}$, $\dot{V}_{air}$

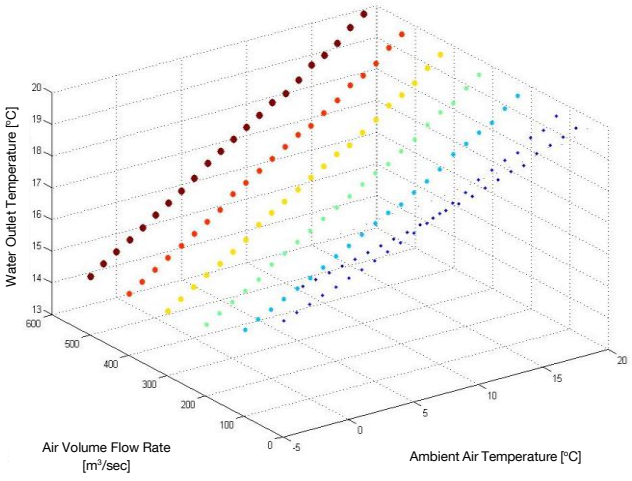

Figure 53: Outlet water temperature for various ambient air temperatures and air volume flow rates

As expected, a higher air volume flow rate enhances the evaporation effect and the evaporation cooling as well, resulting in a cooler outlet water temperature. Therefore, it is

remarkable that when the ambient air temperature is in close tolerance with the inlet water temperature, the cooling performance is not influenced by changes of the air volume flow rate. Furthermore, there is also a low limit for the air volume flow rate, after which the cooling performance seems to have a much worser efficiency.

From the data collected above it is also possible to evaluate the heat rejection that occurs and the amount of water that is lost due to evaporation. The heat rejected by the cooling tower is given by:

$$Q = \dot{m}_{air}(h_{made} - h_{main}) \tag{6.92}$$

While the evaporation water losses can be evaluated by:

$$\dot{m}_{w,evap} = \dot{m}_{air}\left(w_{de,out} - w_{\text{in}}\right) \tag{6.93}$$

The relative figures are presented below for: $T_{water,in} = 20^{o}C$, $\dot{m}_{water} = 200\frac{kg}{sec}$, $RH_{air} = 80\%$, $\dot{V}_{air} = 100$, various $T_{air,in}$.

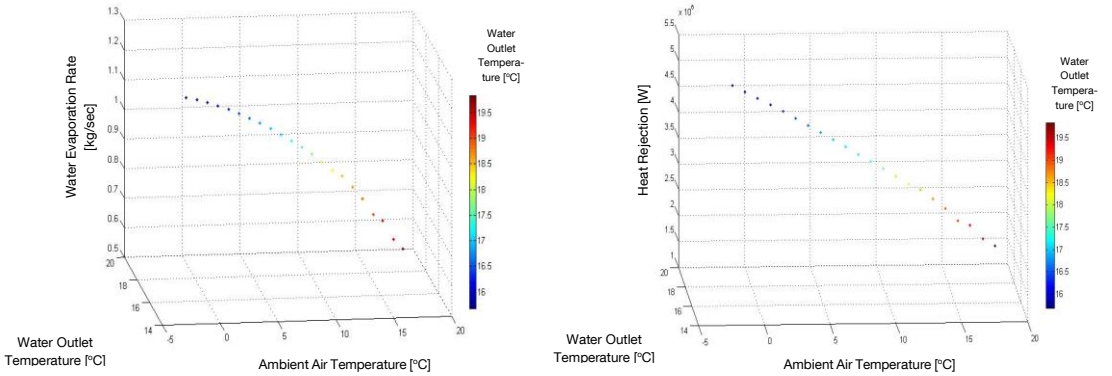

Figure 54: Water evaporation rate (left) and Heat rejection (right) for variable ambient air tem-peratures and water outlet temperatures

Figure on the left shows that lower temperatures tend to achieve better evaporative cooling and consequently more water is lost due to evaporation. Therefore, this amount, which will be balanced from the make-up water, seems to be really small, i.e. around 0.5% of the water that enters the tower. As for the heat rejection, de-picted on the right, is higher when the cooling performance is better, which corre-spond to low inlet air temperatures and as a result low outlet water temperatures.

The main goal of all the figures created was to show the important utility of the algorithm developed, for the evaluation of the cooling performance of the fill

packing zone. Any change in a variable has a specific influence in the final water temperature and these figures, whose combination is able to create an entire map of performance, can easily depict it. Of course, this algorithm has to be extented with the already described algorithm (paragraph 6.2) about rain and spray zone, as well as with the relative equations regarding the fan power consumption. All these follow on the next paragraphs.

6.4 Pressure Losses through the Cooling Tower & Fan Power Consumption

➢ Loss coefficients' calculation

The pressure loss coefficients are required in order to determine the total pressure drop that occurs from the inlet of the air until the inlet of the fan. This calculation is significant as this value of pressure drop has to be overcome by the fan, meaning that it influences directly the fan power consumption. The equations for the pressure loss coefficients are based on empirical equations that have been extracted from experiments (Kloppers, 2003). The relative formulas for each part of the cooling tower are presented below.

❖ Louvers

The specified loss coefficient due to the louvers is determined by the following equation:

$$K_{iLfi} = K_{iL}\left(\frac{\rho_{av\_in-\mathrm{de}}}{\rho_{av\_in}}\right)\left(\frac{W_{in}B_{in}}{2H_{in}W_{in}}\right)\left(\frac{\mathrm{m}_{av\_in}}{\mathrm{m}_{av\_in-\mathrm{de}}}\right)^2 \tag{6.94}$$

Where K_{iL} is defined as the loss coefficient for inlet louvers

❖ Rain zone

The loss coefficient for the rain zone is given by (Kloppers, 2003):

$$K_{rz} = 1.5a_v v_w(\tfrac{H_{in}}{D_d}) \cdot \left[0.219164 - 0.30487\alpha_\rho\rho_a + 8278.7\alpha_\mu\mu_a + 0.954153\{0.328467\exp(135.7638\alpha_L d_d) + 0.47\} \cdot \{26.28482(\alpha_L H_{in})^{-2.95729} + 0.56\} \cdot \exp\{\ln(0.204814\exp(0.066518\alpha_L W_{in}) + 0.21 \cdot (3.9186\exp(-0.3\alpha_L H_{in})) \cdot (0.31095\ln(\alpha_L d_d) + 2.63745)\} \cdot \{2.177546(a_v v_{azo})^{-1.46541} + 0.21\}\right] \tag{6.95}$$

With $v_w = G_w/\rho_{wout}$ and where the range of applicability is the same as for the rain zone Merkel number in a rectangular cooling tower. Referred to fill conditions the final value of the rain zone loss coefficient will be (Kloppers, 2003):

$$K_{rzfill} = K_{rz}\left(\frac{\rho_{av\_in-\mathrm{de}}}{\rho_{av\_in}}\right)\left(\frac{\mathrm{m}_{av\_in}}{\mathrm{m}_{av\_in-\mathrm{de}}}\right)^2 \tag{6.96}$$

❖ Support structure

Referred to the mean conditions through the fill, the specified loss coefficient due to the support structure of the fill can be calculated by the equation:

$$K_{ssfill} = K_{fs}\left(\frac{\rho_{av\_in-\mathrm{de}}}{\rho_{av\_in}}\right)\left(\frac{\mathrm{m}_{av\_in}}{\mathrm{m}_{av\_in-\mathrm{de}}}\right)^2 \quad (6.97)$$

Where K_{fs} corresponds to the loss coefficient for fill support system.

❖ Actual fill

First, the specified fill loss coefficient has to be defined by (Kloppers, 2003):

$$K_{fdm} = \left(a_{p1}{G_w}^{b_{p1}}{G_a}^{c_{p1}} + a_{p2}{G_w}^{b_{p2}}{G_a}^{c_{p2}}\right){L_{fi}}^{d_p} \quad (6.98)$$

Where a_p, b_p, c_p, d_p constitute coefficients specified for each fill and can be selected after experimental studies by the following table, based on the fill type.

Table 7: Coefficients specified by each fill

Type of Fill	Coefficients						
	a_{p1}	b_{p1}	c_{p1}	a_{p2}	b_{p2}	c_{p2}	d_p
Trickle	4.547	1.376	-1.770	5.058	0.381	0.673	-0.207
Splash	10.05	1.297	-1.992	7.761	0.595	0.251	-1.542
Film	5.151	0.877	-1.462	10.806	0.226	0.293	-0.236

In case of splash fills the value of K_{fdm} has also to be multiplied by the value of ${\Delta_{fi}}^{-0.042869}$, where Δ_{fi} the fill spacing. Now, the actual fill loss coefficient applicable to the cooling tower can be defined by:

$$K_{fi} = K_{fdm} + \left(\frac{{G_{av\_\mathrm{de}}}^2}{\rho_{av\_\mathrm{de}}} - \frac{{G_{av\_in}}^2}{\rho_{av\_in}}\right) / \left(\frac{{G_{av\_in-\mathrm{de}}}^2}{\rho_{av\_in-\mathrm{de}}}\right) \quad (6.99)$$

❖ Spray zone

In the spray zone above the fill, the loss coefficient that is referred to the mean conditions through the fill can be determined by (Kloppers, 2003):

$$K_{spfill} = L_{sp}\left[0.4\left(\frac{G_w}{G_a}\right) + 1\right]\left(\frac{\rho_{av\_in-\mathrm{de}}}{\rho_{av\_\mathrm{de}}}\right)\left(\frac{\mathrm{m}_{av\_\mathrm{de}}}{\mathrm{m}_{av\_in-\mathrm{de}}}\right)^2 \quad (6.100)$$

❖ Water distribution system

The, referred to the mean conditions through the fill, loss coefficient is specified according to:

$$K_{wdfill} = K_{wd}\left(\frac{\rho_{av\_in-\mathrm{de}}}{\rho_{av\_\mathrm{de}}}\right)\left(\frac{\mathrm{m}_{av\mathrm{de}}}{\mathrm{m}_{av\_in-\mathrm{de}}}\right)^2 \quad (6.101)$$

Where $K_{wd} = 0.5$ is characterized as an approximation for a water distribution system loss coefficient (Kloppers, 2003).

❖ Drift eliminator

Generally, each eliminator is investigated separately and through experiments the loss coefficient of a drift eliminator can be determined. A typical empirical relation for a drift eliminator loss coefficient is given (Kloppers, 2003), referred to the mean conditions through the fill:

$$K_{de} = a_{de}Ry_{de}^{b_{de}}\left(\frac{\rho_{av\_in-\mathrm{de}}}{\rho_{av\_\mathrm{de}}}\right)\left(\frac{\mathrm{m}_{av\_\mathrm{de}}}{\mathrm{m}_{av\_in-\mathrm{de}}}\right)^2 \quad (6.102)$$

Where for example type c: $a_{de} = 27.4892$ and $Ry_{de}^{b_{de}}$ a characteristic flow parameter at drift eliminator outlet given by:

$$Ry_{de}^{b_{de}} = \left(\frac{\rho_{airde}u_{airde}}{\mu_{airde}}\right)^{-0.14247} \quad (6.103)$$

❖ Sum in the vicinity of the fill

The sum of loss coefficients in the vicinity of the fill is:

$$K_{vcfi} = K_{ssfill} + K_{fi} + K_{spfill} + K_{wdfill} + K_{de} \quad (6.104)$$

❖ Inlet loss coefficient

Assuming an isentropic fill packing for an induced draft rectangular cooling tower, the inlet loss coefficient can be determined, in the absence of a rain zone (De Villiers,E., 1999):

$$K_{ct(norz)} = 0.2339 + \left(3.919\cdot 10^{-3}{K_{vcfi}}^2 - 6.840\cdot 10^{-2}K_{vcfi} + 2.5267\right)\cdot exp\left\{\frac{W_{in}}{H_{in}}\left(0.5143 - 0.1803\cdot exp\{0.0163K_{vcfi}\}\right)\right\} - \sinh^{-1}\left[2.77\cdot \exp\left\{0.958\frac{W_{in}}{H_{in}}\right\}\cdot exp\left\{K_{vcfi}\left(2.457 - 1.015\frac{W_{in}}{H_{in}}\right)\cdot 10^{-2}\right\}\cdot\left(\frac{r_{in}}{W_{in}} - 0.013028\right)\right] \quad (6.105)$$

As De Villiers and Kroger have declared the inlet loss coefficient factor presented below can be ignored in rain zones where $W_{in}/H_{in} \leq 3$, so $C_{rz} = 1$. When this factor in a rectangular cooling tower is needed, it can be calculated through the following empirical equation (Bourillot, 1983):

$$C_{rz} = 1 - G_w \left[0.123 - 12.1d_d - 272.26{d_d}^2 + 5.04 \cdot 10^{-4} \cdot exp\left\{0.466\frac{W_{in}}{H_{in}}\right\}\right] \cdot (1 - 1.16 \cdot 10^{-3} \cdot exp\{G_a\}) \quad (6.106)$$

Which is valid for $3 \leq W_{in}/H_{in} \leq 7.5m, 3 \leq d_d \leq 6mm, 1 \leq G_w \leq 3kg/m^2s, 2 \leq G_a \leq 6\ kg/m^2s$.

Finally, the tower inlet loss coefficient in the presence of a rain zone is determined by:

$$K_{ct} = C_{rz} \cdot K_{ct(norz)} \quad (6.107)$$

And the referred to the mean conditions through the fill, loss coefficient is specified according to:

$$K_{ctfill} = K_{ct}\left(\frac{\rho_{av\_in-\mathrm{de}}}{\rho_{av\_in}}\right)\left(\frac{\mathrm{m}_{av\_in}}{\mathrm{m}_{av\_in-\mathrm{de}}}\right)^2 \quad (6.108)$$

❖ Fan upstream

The fan upstream loss coefficient referred to the mean conditions through the fill is specified by:

$$K_{upfi} = K_{up}\left(\frac{\rho_{av\_in-\mathrm{de}}}{\rho_{av\_\mathrm{de}}}\right)\left(\frac{\mathrm{m}_{av\_\mathrm{de}}}{\mathrm{m}_{av\_in-\mathrm{de}}}\right)^2\left(\frac{\mathrm{A}_{fr}}{A_{fan}}\right)^2 \quad (6.109)$$

Where: $A_{fan} = 4\pi/{d_{fan}}^2$ (6.110)

❖ Total loss coefficient

The total loss coefficient in finally possible to be evaluated by adding all the loss coefficients calculated above:

$$K_{total} = K_{vcfi} + K_{fi} + K_{wdfill} + K_{de} \quad (6.111)$$

➢ Calculation of value of pressure after drift eliminators

Given the simplest form for the draft equation of a cooling tower:

$$\Delta p_{out} - \Delta p_{in} = \Sigma K {\rho u^2}/_2 \quad (6.112)$$

Where Δp_{out} and Δp_{in} correspond to the pressure difference outside and inside the cooling tower respectively, it is clear that the effect of the ambient conditions on the draft equation integrates into the pressure difference external to the tower by $\Delta p_{out} = p_{in} - p_{top,out}$.

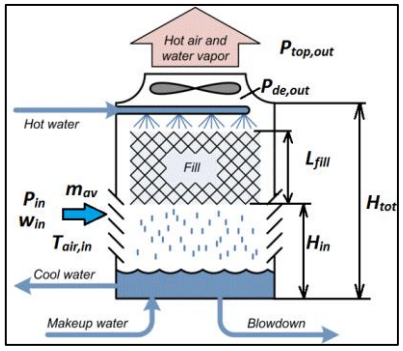

Figure 55: Dimensions and other information about a forced wet counter-flow cooling tower

According to Bourillot (1983) it has been defined that the pressure between ground level and an arbitrary elevation h can be calculated by:

$$p_{top,out} = p_{in}\left(1 - 0.00975\, H_{tot}/T_{air,in}\right)^{3.5(1+w_{in})\left(1-\frac{w_{in}}{w_{in}+0.62198}\right)} \tag{6.113}$$

Based on equation (6.112) the pressure after the drift eliminator can be determined (Bourillot, 1983) by the following equation:

$$p_{de,out} = p_{in}\left[1 - 0.00975\left(H_{in} + L_{fill}/2\right)/T_{air,in}\right]^{3.5(1+w_{in})\left(1-\frac{w_{in}}{w_{in}+0.62198}\right)} - \left(K_{iLfi} + K_{rzfill} + K_{vcfi} + K_{ctfill}\right)\frac{\left(\frac{\mathrm{m}_{av}}{\mathrm{A}_{fr}}\right)^2}{2\rho_{av}} \tag{6.114}$$

➢ Calculation of Air Conditions at Fan Inlet

Assuming that the conditions at the inlet of the fan are equal to those at the outlet of the fill it can be concluded that:

- ✓ $T_{fan,in} = T_{de,out}$
- ✓ $\rho_{fan,in} = \rho_{de,out}$
- ✓ $p_{fan,in} = p_{de,out}$

In case that the distance between the drift eliminator and the fan is of such a value that provokes pressure and temperature drop, then the following calculations have to be made.

First of all, the temperature lapse rate inside the cooling tower is known (Kloppers, 2003) by the equation:

$$\xi_{T_{de,out}} = -(1 + w_{sa,de,out}) \cdot g \cdot \left[1 + 0.42216 \cdot 10^{-11} {w_{sa,de,out}}^2 p_{de,out} \exp\left(\frac{5406.1915}{T_{de,out}}\right) \cdot \frac{\{h_{fgw} - (c_{pw} - c_{pv})(T_{de,out} - 273.15)\}}{\{(w_{sa,de,out} + 0.622) R_g T_{de,out}\}}\right] / \left[c_{pma} + 3.6696 \cdot 10^{-8} {w_{sa,de,out}}^2 p_{de,out} \exp\left(\frac{5406.1915}{T_{de,out}}\right) \cdot \frac{\{h_{fgw} - (c_{pw} - c_{pv})(T_{de,out} - 273.15)\}}{{T_{de,out}}^2}\right] \tag{6.115}$$

Where the water specific heat is calculated at $(T_{de,out} + 273.15)/2$ and the specific heats of dry air and water vapor by tables given in Matlab. So, it can be evaluated the:

$$c_{pma} = c_{pa} + w_{sa,de,out} \cdot c_{pv} \tag{6.116}$$

Now assuming that the temperature lapse rate is essentially constant through the distance between the drift eliminator outlet and the inlet fan, the air temperature at the fan inlet can be defined as:

$$T_{fan,in} = T_{de,out} + \xi_{T_{de,out}} \cdot H_{plenum} \tag{6.117}$$

At which temperature the corresponding density of the air-vapor mixture [kg air-vapor/m^3] is given by:

$$\rho_{fan,in} = \left(1 + w_{sa,de,out}\right)\left[1 - \frac{w_{sa,de,out}}{w_{sa,de,out}+0.62198}\right] p_{fan,in}/(RT_{fan,in}), \tag{6.118}$$

➢ Fan Calculations

The actual air volume flow rate [m^3/s] through the fan is:

$$\dot{V}_{fan} = m_{av\_\mathrm{de}}/\rho_{av\_\mathrm{de}} \tag{6.119}$$

Every fan has its own performance curves that are varying depending on mainly the rotational speed and the blade angle as well. An example of such curves that contain the fan power consumption, the fan static pressure and the fan static efficiency is depicted on figure 51.

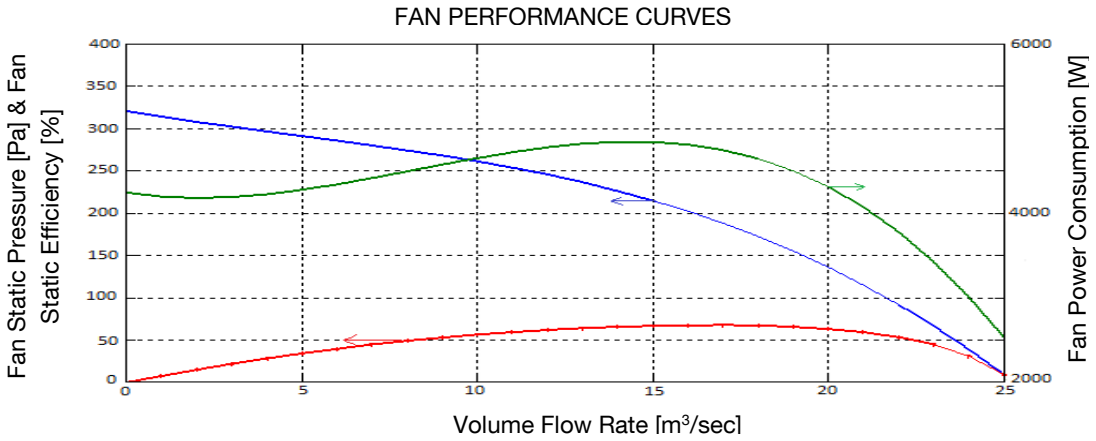

Figure 56: Fan Performance Curves at Specific Rotational Speed

It is vital to define about fans that the total pressure that an axial fan works against is made up of the static pressure which is the sum of the system resistances and velocity pressure which is a loss associated with accelerating the surrounding air from zero to the design velocity. The only useful work done is by the static pressure component. Positive static pressure is created as a fan moves air through a system, while negative static pressure is

what all other components in the airflow path create as they resist air movement. Velocity pressure does not contribute to a fans ability to remove system heat energy; therefore it's not normally included in fan efficiency calculations. It constitutes a common practice in industrial applications to use the fans with an efficiency varying from 55% to 75%.

Given the above curves for different rotational speeds of the fan, as long as the fan has a variable frequency drive, it is possible to extract their relative equations for the specified air volume flow rate.

As presented in ISO 12759 ("Fans – Efficiency classification for fans") and in AMCA 205 ("Energy Efficiency Classification for fans") the fan power consumption can be evaluated by:

$$P_{fan} = \Delta p_{fan,st} \cdot \dot{V}_{air} \tag{6.118}$$

According to Bourillot (1983) the fan static pressure rise coefficient is defined by:

$$K_{F/difst} = (2 \cdot \Delta p_{fan,st} \cdot \rho_{av\_fan,in}) / (\frac{4 \cdot m_{av\_de}}{\pi \cdot d_{fan}^2})^2 \tag{6.119}$$

The value of this coefficient is derived from the final draft equation, which is described below, and constitutes a significant parameter in order to calculate at least the required fan power consumption.

➢ Draft Equation

The draft equation describes the relation between the flow resistances presented above, the ambient conditions, the cooling tower dimensions and the fill packing performance characteristics at a given flow rate. Taking into account the pressure differences due to gravity field, meaning the pressure difference between the inside and outside of the tower, the draft equation takes the following form:

$$\left(K_{ssfill} + K_{fi} + K_{spfill} + K_{wdfill} + K_{de} + K_{fi} + K_{wdfill} + K_{de} + K_{upfi}\right) \times \frac{\left(m_{av,in-de}/A_{fr}\right)^2}{\left(2\rho_{av,in-de}\right)} - K_{\frac{F}{difst}} \times \frac{\left(m_{av\_de}/A_c\right)^2}{\left(2\rho_{av\_fan,in}\right)} = \left(p_{in} - p_{amb,H_{tot}}\right) - \left(p_{in} - p_{fill}\right) - \left(p_{fill} - p_{fan,in}\right) - \left(p_{fan,out} - p_{tower,top}\right) \tag{6.120}$$

Whether this equation is verified, then the values selected for the design variables $m_{av,in-de}$,$T_{de,out}$, T_{wout} are correct.

If the pressure differences due to gravity field has been ignored, then the above equation has the following form:

$$\left(K_{ssfill} + K_{fi} + K_{spfill} + K_{wdfill} + K_{de} + K_{fi} + K_{wdfill} + K_{de} + K_{upfi}\right) \times \frac{\left(m_{av,in-de}/A_{fr}\right)^2}{\left(2\rho_{av,in-de}\right)} - K_{\frac{F}{difst}} \times \frac{\left(m_{av,de}/A_c\right)^2}{\left(2\rho_{av,fan,in}\right)} = 0 \tag{6.121}$$

If the left-hand side is equal to zero or very close to zero, then the values approximated for $m_{av,in-de}$, $T_{de,out}$, T_{wout} are correct for the specific cooling tower, with the given fan specifications.

As it has been declared (Bourillot 1983) there is only a very small difference between the two draft equations (6.120) & (6.121). It is concluded, therefore, that the pressure differentials due to the pressure gradient field can be ignored, when an induced draft cooling tower is under investigation. This happens because the pressure differential generated by the fan constitutes the dominant term in first draft equation.

An algorithm to calculate the pressure losses through the cooling tower and the fan power consumption has been developed in Matlab. A correlation between these two parameters is presented in figure 52 below, for various air mass flow rates. The values of the main variables that have been selected are the followings:

$$T_{air,in} = 25^o C,\ RH_{air} = 80\%,\ T_{water,out} = 9^o C, L_{sp} = 0.5m, L_{rz} = 4m, L_{fill} = 1.5m$$

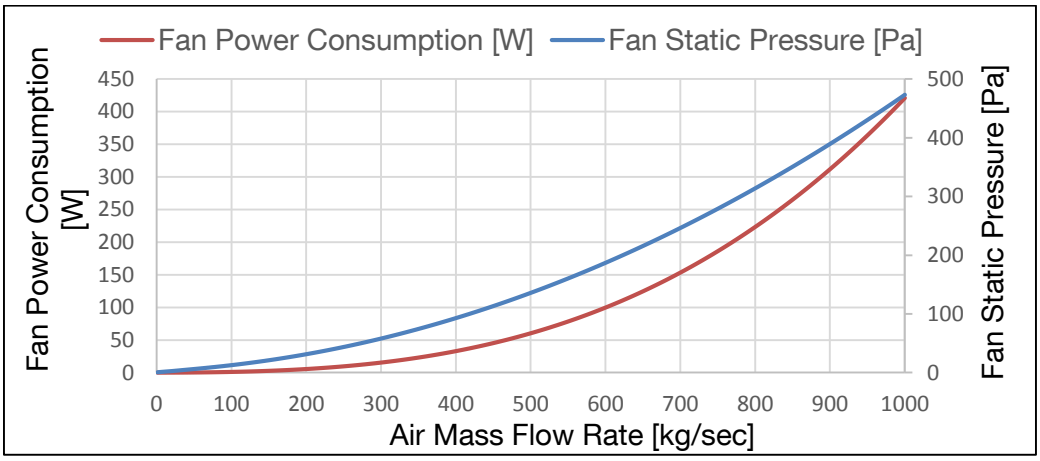

Figure 57: Correlation between pressure losses through the cooling tower and fan power consumption for various air mass flow rates

From such a graph, it is possible to decide whether the cooling performance that is achieved with a specific air mass flow rate is acceptable, taking into account the fan power required. It is obvious that the higher the air mass flow rate the more fan power is consumed, as also the pressure losses to be overcome are increasing. In figure 58, the fan power consumption based on the cooling performance is illustrated, for a given inlet air temperature. Of course, the better cooling performance requires also more energy consumption. Depending the pump power consumed for the water circulation, which influence also the final cooling of the water, its correlatation with the water mass flow rate is presented in the next paragraph.

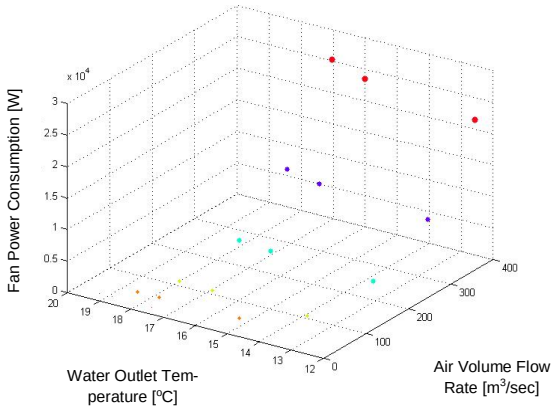

Figure 58: Fan power consumption for different air volume flow rates and water outlet temperatures

Each colour of the figure 58 corresponds to an air volume flow rate, while dots with different colours that spread along the water outlet temperature axes correspond to three different water mass flow rates (from right to left: 100, 200 and 300 kg/s). It is obvious that the best result in matter of cooling performance and power consumption prerequisites much air volume flow rate and few water mass flow rate.

6.5 Cooling water pump variable speed operation and pressure losses

In chapter 5 it has been illustrated that the water mass flow rate remains almost constant in case of Unterhaching, even though other important variables as the ambient temperature or the power output seem to fluctuate. A change in the water mass flow rate will affect the cooling water pump power consumption, which consumes annually around 1million kWh, as well as the heat rejection in the condensers. Of course, in case that the heat rejection must be constant, water temperature has to change, and that will result in changing the cooling towers' operation. Taken all into account, the optimum point of pump's and cooling towers' operation, regarding their energy consumption should be possible to be defined.

As a first step, the pump's operation is being investigated. In order to correlate its water mass flow rate with its power consumption, a formula that calculates the corresponding pressure losses is important to be extracted.

In Unterhaching power plant's Shankey diagram that is provided, the total power consumption of the water circulation pump ($P_{pump,y}$) is given, while from the data acquisition system the current water volume flow rate ($\dot{Q}_{cw}$) is known. Consequently, the total pressures losses in the cooling system that the pump has to overcome for the current operation are able to be defined. Furthermore, the relative values for the pressure upstream and downstream of the condenser's cold side are registered by pressure sensors and the height from the pump's level up to the spray zone (H_{sp}) can be extracted from the cooling towers' drawings that have been provided. From these data it is feasible now to determine

the current pressure losses through the condenser unit $(\Delta p_{phe,c})$ and the pumping head required for the spray zone from equation:

$$\Delta p_{head,sp} = \rho_w \cdot g \cdot (H_{inlet} + L_{fill} + L_{sp}) \tag{6.124}$$

The pressure drop through a plate heat exchanger for a single phase flow is:

$$\Delta p_{phe} = \frac{1}{2} \cdot \zeta \cdot \rho_w \cdot \frac{u_w^2}{d_p} \cdot L_{phe} \tag{6.125}$$

Where ζ is the friction factor, ρ_w the water density, u_w is the water velocity, d_p is corresponding pipe's inlet diameter and L_{phe} the length of the plate heat exchanger. As proposed by Heat Atlas 2010, the friction factor required for the calculation of the pressure drop can be evaluated from:

$$\frac{1}{\sqrt{\zeta}} = \frac{\cos\theta}{\sqrt{a_2 tan\theta + a_3 sin\theta + {\zeta_0}/{\cos\theta}}} + \frac{1-cos\theta}{\sqrt{\zeta_1}} \tag{6.126}$$

The parameters ζ_1 and ζ_0 can be calculated after defining whether the flow is laminar or turbulent. Consequently, the value of the Reynolds number is a main prerequisite and can be evaluated by:

$$Re = \frac{u_w \cdot d_p}{v} \tag{6.127}$$

Where v the kinematic viscosity at the specific water temperature. In case that Reynolds number is less than 2300, i.e. laminar flow, the relative values for ζ_1 and ζ_0 are:

$$\zeta_0 = \frac{64}{Re} \tag{6.128}$$

$$\zeta_1 = \frac{597}{Re} + 3.85 \tag{6.129}$$

While for turbulent flow the above equations have the following form:

$$\zeta_0 = \frac{1}{(1.8\ln(Re) - 1.5)^2} \tag{6.130}$$

$$\zeta_1 = a_1 \zeta_0 \tag{6.131}$$

The values for the coefficients α are given (Heat Atlas 2010) as below:

$a_1 = 3.8,\ a_2 = 0.18,\ a_3 = 0.36$

The variable θ in equation (6.126) constitutes the plate inclination angle. In order to define its value for further calculations, the above equations are solved for the current pressure drop on the plate heat exchanger.

Except the aforementioned pressure losses, there exist also pressure drop due to the flow of the water through the rest of the pipes. These can defined also as per equation X.2, where the friction factors are given (Heat Atlas 2010) as below:

If Reynolds number is below 2300 then:

$$\zeta = \frac{64}{Re} \tag{6.132}$$

If Reynolds number is greater than 2,300 and less than 100,000 then:

$$\zeta = \frac{0.3164}{\sqrt[4]{Re}} \tag{6.133}$$

If Reynolds number is greater than 100,000 and less than 2x10^6 then:

$$\zeta = 0.0054 + \frac{0.3964}{Re^{0.3}} \tag{6.134}$$

While for higher Reynolds numbers is:

$$\frac{1}{\sqrt{\zeta}} = -0.8 + 2log\left(Re\sqrt{\zeta}\right) \tag{6.135}$$

The specifications (length, diameter) for the piping where not available. As the pressure drop in the plate heat exchanger, the pumping head and the total pressure losses of the cooling system for the current operation were possible to be calculated, the total losses through the piping, valves and fittings that exist among the connection of the pump with the condenser and the condenser with the cooling tower could be evaluated. Then, for the given water mass flow rate, values for the length and the diameter of the piping could be assumed, so that all equipment losses are included, and confirm them after using the above equations for pressure drop along circular pipes.

The pump power consumption ($P_{pump,i}$) for a given water volume flow rate ($\dot{Q}_{cw,i}$) and the relative calculated total pressure drop (Δp_{tot}) can be easily calculated from the following formula:

$$P_{pump,i} = \Delta p_{tot} \cdot \dot{Q}_{cw,i} \tag{6.136}$$

The equations presented above were used in order to create, through iterations, a graphic that illustrates the pump's power consumption increase in correlation with water mass flow rate's increase. The relative graph is presented below and the red dot corresponds to the current operation point. The selected values are accepted, as the pump power consumption fits with its average value that can be extracted from the total water circulation power consumption, given in power plant's Shankey diagram.

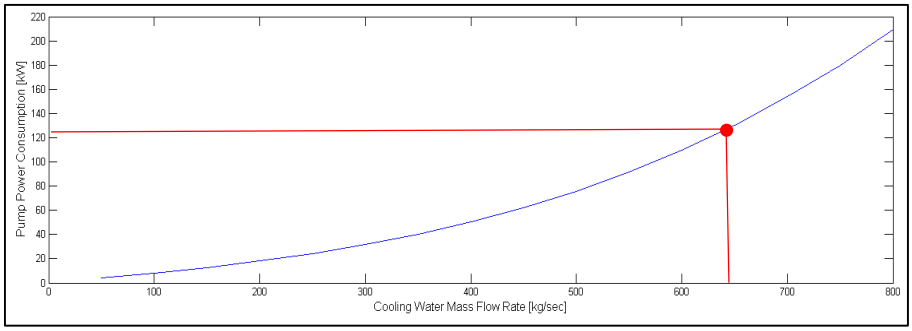

Figure 59: Pump Power Consumption as a function of Cooling Water Mass Flow Rate

It is feasible now, by taking everything into account, to see how the two main energy consumers of the cooling system behave in correlation to each other and specify the optimum operation point, depending on cooling performance and power consumption. A complete model that simulates the cooling tower performance and evaluates the fan power consumption for given inlet conditions and various inlet water mass flow rates, based on paragraphs 6.2-6.4, is combined with the pump operational cost in paragraph 6.5. Inlet conditions: $T_{air,in} = 5^oC,\ RH_{air} = 80\%$,

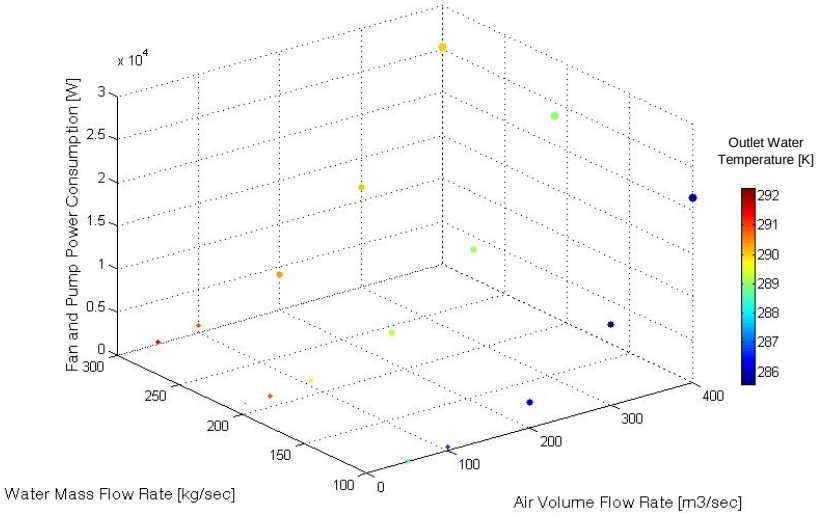

Figure 60: Total power consumption of cooling system for various air and water flow rates

6.6 Models‘ validation

All the already described models can be used for simulating the whole cooling system and calculating its power consumptions. Their implementation can be used from any indirect cooling system, after the proper adjustment of the main variables. In order to validate the models separately but mainly their combination, a comparison with the given from Unterhaching power plant’s data acquisition system values for the towers’ cooling performance

and the relative power consumption from its Shankey diagram takes place in this paragraph. The results depicted below.

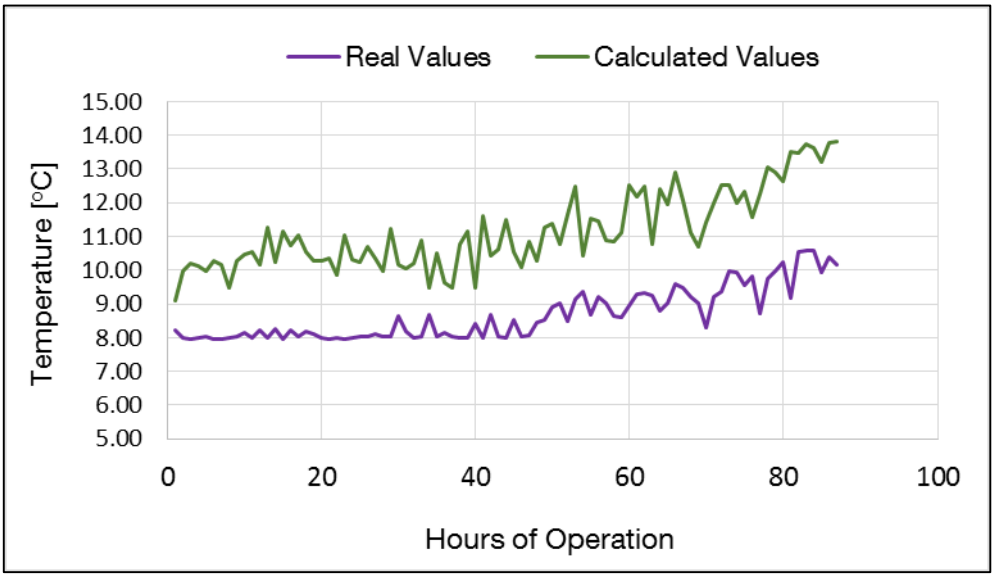

Figure 61: Comparison between measured values and values calculated from the models for the cold water temperature for a given period of time

It has to be mentioned that both water and air mass flow rates kept constant for all calculations, while in Unterhaching a variable speed drive is used for the fan's operation. This could be a reason for the divergence that is obvious, as well as the influence that may the several assumptions, that have been made, have on models, such as the droplet radius and velocity.

6.7 Condensing unit operational optimization

Except from the fan power consumption that is required in cooling towers to cool down the cooling water, the pump power consumption constitutes also a significant energy consumer in the cooling unit. In this paragraph, a focus on the condenser's operation is undertaken and an algorithm is presented that will be able to evaluate the optimal temperature of the cooling water that exits the condensers and enters the cooling towers. This algorithm is mainly based on all the aforementioned equations in this paragraph that calculate the fan and pump power consumptions for a given water temperature at the outlet of the cooling tower. As a result, the optimal water mass flow rate will, also, be possible to be selected in order to eliminate the cooling system's operational costs.

First of all it is important to define the parameters that are known and will remain constant through the calculations. Starting from the water or cold side, the collection water basin of the towers (T_{wout}) has a given temperature, which constitutes the temperature of the water that exits the cooling towers and enters the condenser. In addition, the specific heat of the water at constant pressure (c_{pw}) is equal to 4.2x10^3 J/kg K.

From the data that are registered from the Unterhaching Power Plant it is feasible to know the temperature of the working medium upstream $(T_{wfin})$and downstream (T_{wfout}) of the condensers and the mass flow rate (m_{wf}) that passes through each of them, for the given operating conditions of course. The ammonia concentration of the fluid $(NH3per_{mix})$ and the pressure difference on the hot side (ΔP_{hs}) can also be derived from the plant's data acquisition system. Consequently, the required inlet (hin_{wf}) and outlet $(hout_{wf})$ enthalpies can be evaluated. For this purpose the software "REFPROP" and its functions in "Matlab" environment have been used. Then, the heat that has to be rejected in each condenser (Q_{rej}) can be determined from the equation:

$$Q_{rej} = m_{wf} \times \left(h_{in,wf} - h_{out,wf}\right) \tag{6.137}$$

Unterhaching Power Plant stuff has provided us with all the necessary technical specifications of the condensers and consequently the heat transfer area (A [m²]) can be defined. As for the overall heat transfer coefficient, it can approximated based on given data from Unterhaching power plant and in compliance with literature $(U = 3000\ [W/m2\ K])$. The water mass flow rate $\left(m_{cw}\ [\frac{kg}{s}]\right)$ can also be defined as a function of the water temperature by the following formula:

$$m_{cw}(T_{wout}) = Q_{rej} / \left(c_{pw}(T_{win} - T_{wout})\right) \tag{6.138}$$

Based on the LMDT theory, the mean logarithmic temperature for the counter-flow plate heat exchangers installed in the condensing unit of Unterhaching is also used in the algorithm as a function of the water temperature at condenser's outlet and its equation is the following:

$$\Delta T_m(T_{wout}) = \frac{(T_{wfout} - T_{win}) - (T_{wfin} - T_{wout})}{ln((T_{wfout} - T_{win})/(T_{wfin} - T_{wout}))} \tag{6.139}$$

Additional data that are required are the efficiency of the cooling water $(Pcon_{eff})$ and condensate (Pcw_{eff}) pumps, the height of the spray zone of the cooling tower $(H_{sp}\ [m])$ that is given in the technical drawings of the towers, the gravity acceleration $(g\ [m/s^2])$, the annual operating hours of the condenser $(OpHours\ [hours])$ and the cost of electricity consumption as Euros per Kilowatt-hours $(Celec\ [€/kWh])$. Given the above it is possible to evaluate the total operational cost of the condenser as a sum of the operational cost of the hot side (€) per hour from equation:

$$OC_{hs} = \left(\left(10 \times \Delta P_{hs} \times g \times m_{wf}(T_{wout})\right)/\left(Pcon_{eff} \times 1000\right)\right) \times 3600 \times C_{elec} \tag{6.140}$$

And the operational cost of the cold side (€) per hour from equation:

$$OC_{cs} = \left(\left(H_{sp} \times g \times m_{cw}(T_{wout})\right)/\left(Pcw_{eff} \times 1000\right)\right) \times 3600 \times C_{elec} \tag{6.141}$$

Consequently the total cost (€) would be:

$$OC\_con_{tot}(T_{wout}) = OC_{hs}(T_{wout}) + OC_{cs}(T_{wout}) \quad (6.142)$$

Another significant value for the algorithm is the unit cost for the heat exchanger per installed unit of heat transfer area. As a result, the condensers' capital cost is primarily required. Looking on their drawings, it is concluded that they constitute flat plate heat exchangers and in order to approximately evaluate their capital cost, formulas and values from (Turton, 1998) are used. Particularly, according to same literature source, the purchased cost of several equipment $\left(C_p^0\ [€]\right)$ can be estimated by the following equation:

$$log_{10}C_p^0 = K_1 + K_2 log_{10}(A) + K_3[log_{10}(A)]^2 \quad (6.143)$$

Where regarding plate heat exchangers the values of K are given in (Turton, 1998) as $K_1 = 4.6656$, $K_2 = -0.1557$, $K_3 = 0.1547$ and A is the heat transfer area given by Plant's data. Consequently, the unit cost for the condenser per installed unit of heat transfer area in €/m² can be determined by:

$$ConPerArea = C_p^0/A \quad (6.144)$$

Furthermore it is required to know the annual cost of heat exchanger operation as a percentage of the cost of installed heat exchanger area (1/year). Given the above, this can be evaluated by:

$$AC_{HE} = OC_{con_{tot}}(T_{wout})/C_p^0 \quad (6.145)$$

Prior to the determination of the final cost function, the formula that calculates the cost of the cooling water $\left(C_w\ [\frac{€}{kg}]\right)$ has to be extracted. This equation derives from the simulation algorithm for the cooling towers that has been presented in paragraphs 6.2 – 6.4. Through this code it is feasible to evaluate the fan power consumption $\left(P_{fan}\ [W]\right)$ required to cool the water down to specific temperature for different inlet water temperatures and inlet water mass flow rates. Given these values, it is possible to define the cost of cooling water as below:

$$C_w = P_{fan} \times \frac{3600}{1000} \times C_{elec}/m_{cw}(T_{win,con}) \quad (6.146)$$

Taking all the above into consideration it is possible to extract the final equation that calculates the total operational cost of the condenser unit. This equation that sums the cost of the total amount of the cooling water and the fixed cost of the heat exchanger installed takes the following form:

(6.147)

$$C_{tot}(T_{win,con}) = \mathrm{OpHours} \times C_w \times m_{cw}(T_{wout}) \times 3600 + AC_{HE} \times ConPerArea \times \frac{Q_{rej}}{U\Delta \mathrm{T_m}(T_{wout})}$$

All the equations presented above and the relative process have been implemented through Matlab software. The results that have been extracted for this specific case are presented below.

As a first example, it is assumed that the cost of cooling for each kg of water that is pumped is given (from known fan average power consumption and average water mass flow). The heat rejection that is desired, based on the inlet and outlet temperatures of the ammonia mixture, corresponds to $22MW_{th}$, while the water temperature at the inlet of cooling tower is 18^oC and the cost of electricity consumption as Euros per Kilowatt-hours is $Celec = 0.03\ [€/kWh]$. Based on these values and the technical specification given for cooling towers and condensers, a figure that relates the total operational cost per hour with the temperature of the cooling water that enters the condenser is created and presented below.

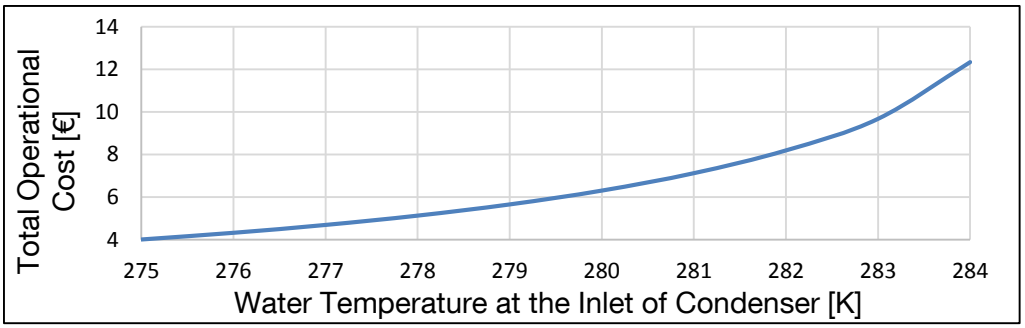

Figure 62: Relationship between water temperature at condenser's inlet and condenser unit operational cost, for a given case

It is obvious from figure 61 that a colder water will reduce the water mass flow rate that is required for a specific heat transfer in the condenser, and the water pumping cost as well. Therefore, in these calculations it has not been taken into account that a colder water, for given water temperature at cooling tower's inlet, is achieved by increasing the fan power consumption. In conclusion, it's a trade-off situation and a relative algorithm that is based on all the models already described and shows the correlation between the two main consumers has been developed and the results are depicted in figure 63.

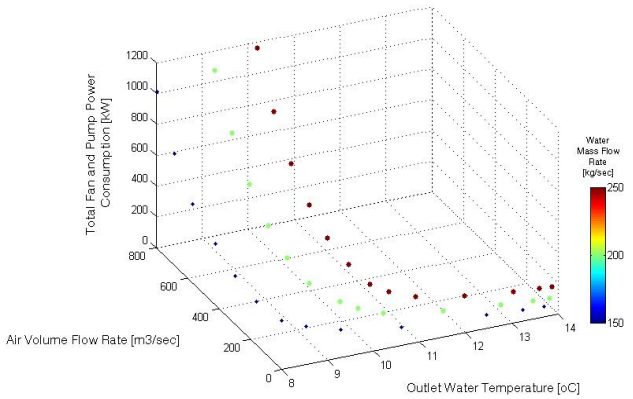

Figure 63: Total fan and pump power consumption for various air and water flow rates and corresponding cooling performance

Each color corresponds to a different water mass flow rate. It is concluded from figure 63 that after a specific desired cooling performance, for given ambient conditions, a lot of power consumption would be required. Furthermore, based on the same calculations, the mixture temperature at the outlet of the condenser has been evaluated, as it is directly affected by the cooling performance. Its values for various air volume flow rates and water mass flow rates, in conjunction with the cold water achieved and the relative total power consumption required are illustrated in figures 64 and 65.

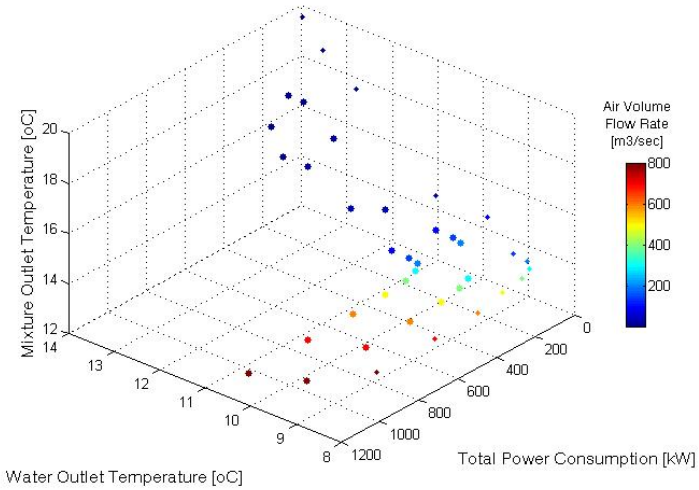

Figure 64: Mixture temperature at condenser outlet for various air volume flow rates and cold water temperatures, with required total power consumption

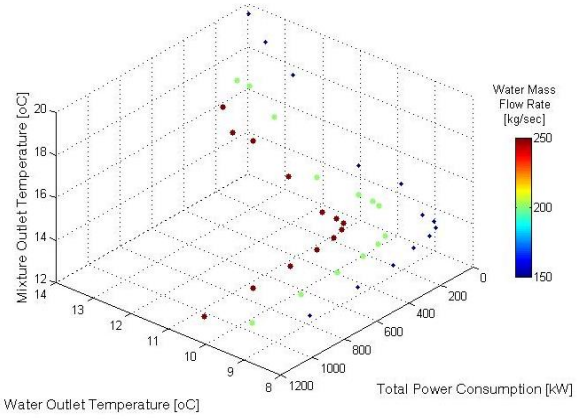

Figure 65: Mixture temperature at condenser outlet for various water mass flow rates and cold water temperatures, with required total power consumption

Trying to identify the utility of such graphics for the operation of a power plant, it is concluded from figure 64 and the brown dots that for a desired mixture outlet temperature, for example 12ºC, there are several combinations to be achieved, that are characterized by the outlet water temperature, the air volume flow rate and the water mass flow rate. Brown dots correspond to the same air volume flow rate. In figure 64, it is depicted that the same

result can be achieved for various water mass flow rates. The blue dot corresponds to the minimum operational cost, so this is the one that has to be selected.

In order to define which cold water temperature or mixture outlet temperature is more beneficial for the power plant's operation, it an important prerequisite to investigate their values' influence on the power output. For this reason, a simulation of the whole Kalina cycle was required and has been conducted, for a constant water mass flow rate, by the colleague of the project (Mr. Lukas Schwan) through the Aspen software. The relative results are presented below.

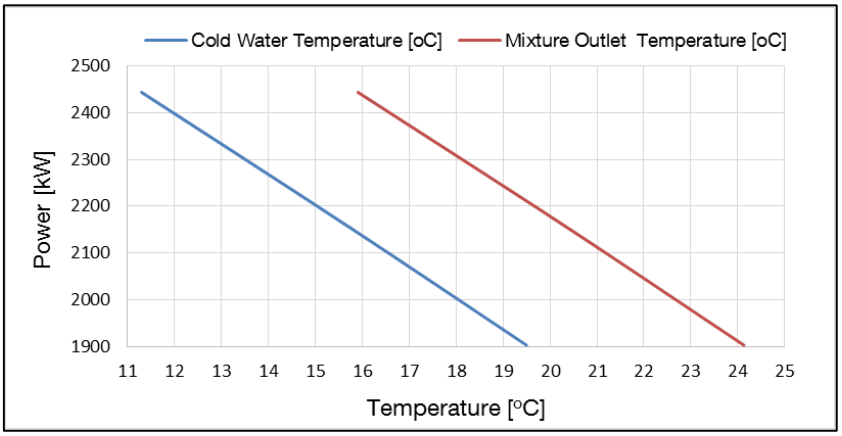

Figure 66: Power output relatioship with cold water mixture outlet temperatures

It is clearly concluded that the lower the temperatures the higher the electricity production.

7 Earth – to – air heat exchanger

7.1 Introduction to EAHE idea

According to previous chapters, it is justified that the ambient temperature constitutes an important factor for the cooling performance of the cooling towers and the internal energy consumption of the Kalina Power Plant. The cooling result in turn influences the condenser's operation and consequently the power output. Taking all the above into consideration it seems that if there is a way to affect the inlet air condition, that would maybe improve the total operation of the power plant.

Using an additional energy to reduce the ambient temperature would probably drive in an unprofitable financially result. For this reason, the idea of underground cooling came up and is presented below. The advantage of this idea is that after the installation costs, there is no extra need for operational costs, except of course the additional static pressure that the fan should create in order to overcome the total pressure drop through the earth to air heat exchanger.

The natural phenomenon of the earth's cooling ability, the mathematical background for the simulation of the idea and the regarding results are presented below.

Working principle

As it is widely known, the earth is characterized by constant temperature at a specific depth, which happens to be less than ambient air temperature in summer and higher than ambient air temperature in winter. By blowing air into the buried pipe, heat exchange between the earth around buried pipe and air passing along the pipe takes place.

This phenomenon has been taken into consideration in order to cool down the air entering the cooling towers of the power plant, during the hot periods of the year. Using such an earth-air heat exchanger, it is possible to provide air at lower temperature than ambient air temperature and as result a reduction in fan's consumption can be achieved or even a better cooling of the circulating water of the plant's cooling unit.

Taking into account that the earth's temperature is higher than ambient air temperature in winter, this heat exchanger can be used during cold periods of the year in order to provide with heat the building facilities. Such an operational concept helps in exploiting the buried pipe throughout the year.

The following paragraphs present a procedure through which the air temperature at buried pipe outlet can be evaluated.

For given values of sub-soil temperature, pipe technical specifications (length, radius, thickness) and ambient conditions, the air temperature at the pipe's outlet can be defined

by the algorithm described below. Therefore, firstly a model for estimating the sub-soil temperature has to be developed.

7.2 EAHE System Model

Generally there are different models that simulate an EAHE system, either analytical or numerical, which are differentiated each other by the way of calculating the outlet temperature, knowing the inlet temperature and the surface temperature of the pipe. As it is proved through publications all of these models seem to base on the same approach and have approximately the same results. The only differentiation constitutes the way of writing down the problem.

It has to be mentioned that modelling and simulation of an earth-to-air tube system constitutes a quite complex procedure, due to the several mechanisms that take place around the earth tube. For the purpose of analysing the heat transfer phenomena, the following assumptions have to be made about the soil and the pipe:

1. The soil surrounding the pipe is isotropic and homogenous, with constant thermal conductivity in all ground layers.
2. Soil temperature in the pipe vicinity can be calculated using the soil model discussed below beyond a particular distance from the centre of the pipe (thickness of the annulus
3. Convection flow inside the pipe is hydro-dynamically and thermally developed.
4. Pipe has a uniform cross sectional area in the axial direction.
5. The temperature profile in the pipe vicinity is not affected by the presence of the pipe. As a result, the pipe surface temperature is uniform in the axial direction.

Soil Temperature Calculations

Assuming that the soil is homogenous and its thermal diffusivity is constant, the temperature at any depth z and time t can be calculated, according to (Labs, 1989) by equation:

$$T(z,t) = T_m - A_s e^{-z\left(\frac{\pi}{365 a_s}\right)^{1/2}} cos\left\{\frac{2\pi}{365}\left[t - t_0 - \frac{z}{2}\left(\frac{365}{\pi a_s}\right)^{1/2}\right]\right\} \quad (7.1)$$

This equation has been verified, according to (Al-Ajmi, 2006), in comparison with measured soil temperature values (Allison TR, 1979) and it is concluded that the difference between measured and predicted values range within $\pm\, 1^o C$.

Attention should be taken on the units in equation 7.1. If the variables are expressed per hour for example the constant of 365 days is substituted by the relative hours, i.e. 8760 hours.

In order to define the T_m, i.e. the mean ground surface temperature, the following procedure is required. First of all, (Derradji, 2014), the ground surface temperature is evaluated by:

$$T_{sur} = T(0,t) = T_m + A_s Re(e^{-iwt}) \quad (7.2)$$

Where T_m and A_s are the annual mean value and amplitude of the ground surface temperature variation respectively. They should be evaluated after taking into account (Krarti, 1995):

a. The convective heat transfer between the air and ground:

$$Q_{conv} = h_s(T_a - T_{sur}) \quad (7.3)$$

Where:

- h_s is the convective heat transfer coefficient at the soil surface (W/m^2 °C), given approximately according to McAdams book "Heat Transmission" (1954) by

$$h_s = 5.7 + 3.8u \quad (7.4)$$

Where u corresponds to the annual average value of wind velocity (m/s) and

- Ta is the air temperature above the ground surface (°C) and can be estimated by

$$T_a(t) = T_{ma} + T_{va} Re\left[e^{(iwt+\varphi_s)}\right] \quad (7.5)$$

where T_{ma} the average air temperature (°C), T_{va} is the amplitude of the air temperature as defined above, w is the annual angular frequency that is equal to 1,992x10^{-7}rad/sec and φ_s the phase angle difference between the air and soil surface temperature (rad) by the equation presented below.

- T_{sur} constitutes the ground surface temperature (°C)

b. The solar radiation absorption by the ground, according to (Krarti, 1995):

$$Q_{solrad} = \beta S \quad (7.6)$$

Where:

- β is the absorption coefficient that depends on the soil absorptance and shading condition, being equal to 1 – soil albedo (i.e. the reflection coefficient, equals to the ratio of reflected radiation from the surface to incident radiation upon it)

- S is the horizontal solar radiation that can be approximated by

$$S(t) = S_m + S_v Re\left[e^{(iwt+\varphi_s+\varphi_I)}\right] \quad (7.7)$$

Where:

  - S_v corresponds to the amplitude of solar radiation (W/m^2) and can be evaluated by dividing the difference between the maximum and the minimum annual solar radiation value by two:

$$S_v = (S_{max} - S_{min})/2 \quad (7.8)$$

- S_m is the average solar radiation (W/m^2)
- w is annual angular frequency equals to 1.992 x 10^{-7} rad/sec
- φ_I is the phase angle between the insolation and the air temperature (rad), calculated by subtracting the insolation phase angle from air temperature phase
- φ_s is defined below

c. The long-wave radiation emitted from the soil, approximated according to (Krarti, 1995):

$$Q_{longrad} = \varepsilon \Delta R \quad (7.9)$$

Where:

- ε is the hemispherical emittance of the ground surface, ranging from 0.93 to 0.96
- ΔR is a radiation constant that depends on soil radiative properties, air relative humidity, effective sky temperature and is well assumed to be $63 W/m^2$

d. The latent heat loss due to the evaporation, given by:

$$Q_{latent} = 0.0168 f h_s[(aT_{sur} + b) - RH_a(aT_a + b)] \quad (7.10)$$

Where:

- a and b are constants equal to $103 Pa/oC$ and 609Pa respectively
- f is the fraction of evaporation rate, depending on soil's cover and moisture level
- RH_α the relative humidity

Taking into consideration all four phenomena described above, it is possible to extract the heat transfer rate on the ground surface:

$$-k_s \frac{\partial T}{\partial x}(x = 0) = E_{conv} - E_{longrad} + E_{solrad} - E_{latent} =>$$

$$h_s(T_{ma} - T_m) - \varepsilon \Delta R + \beta S_m - 0.0168 f h_s(aT_m + b - ar_a T_{ma} - RH_a b) = 0 \quad (7.11)$$

And if this equation is solved for T_m, the result is:

$$T_m = \frac{1}{h_e}[h_r T_{ma} - \varepsilon \Delta R + \beta S_m - 0.0168 h_s f b(1 - RH_a)] \quad (7.12)$$

Where the rest variables required to be defined are:

- $h_r = h_s(1 + 0.0168 a RH_a f)$ (7.13)

with h_s the convective heat transfer coefficient at the soil surface ($\frac{W}{m^2}°C$), α a constant equal to $103Pa/oC$, RH the relative humidity and f the fraction of evaporation rate depending on the soil's cover and moisture level,

- h_e is given by $h_e = h_s(1 + 0.0168af)$ (7.14)

δ value is calculated by $\delta = \frac{1+i}{D_{pen}}$ (7.15)

D_{pen} constitutes the penetration depth (m) evaluated from equation:

$$D_{pen} = \sqrt{\frac{2a_s}{w}} \quad (7.16)$$

As for the rest variables required, A_s is the amplitude of the soil surface temperature variation given by:

$$A_s = \left\| \frac{h_r T_{va} - \beta S_v e^{i\varphi_I}}{h_e + \delta\lambda_s} \right\| \quad (7.17)$$

Where:

- T_{va} is the amplitude of the air temperature, equal to:

$$T_{va} = (T_{max} - T_{min})/2 \quad (7.18)$$

- β the soil absorption coefficient that is equal to 1 – soil albedo,
- S_v is the amplitude of the solar radiation (W/m^2)as defined above,
- λ_s the soil thermal conductivity $(W/m^{2\circ}C)$.

The variable t_0 $[sec]$ constitutes the phase constant of the soil surface and it can be calculated by formula:

$$t_0 = t_{0a} + \frac{\varphi_s}{w} \quad (7.19)$$

Where:

- t_{0a} is the phase constant of the air $[sec]$, i.e. the time elapsed from the beginning of the year at which the air temperature reaches the minimum value in the year and
- φ_s is evaluated by

$$\varphi_s = -Arg\left[\frac{h_r T_{va} - \beta S_v e^{i\varphi_I}}{h_e + \delta\lambda_s}\right] = -Arg[A_s] \quad (7.20)$$

And is characterized as the phase angle difference between the air and soil surface temperature (rad).

Variable a_s used in basic function of $T(z,t)$ corresponds to the soil thermal diffusivity (m^2/s) and can be expressed by:

$$a_s = \lambda_s/(\rho_s C_{p,s}) \quad (7.21)$$

Where ρ_s is the soil density (kg/m^3) and $C_{p,s}$ the specific heat of soil $(J/kg\ K)$.

As long as these values are known, then the temperature at any depth z and time t can be calculated. An example is the following in figure 67 for Kuwaiti site at depth varying from 1m to 4m in with values for the annual mean ground temperature (T_m), annual surface temperature amplitude (A_s), soil thermal diffusivity (a), and phase constant (t_0) to be 27 oC, 13.3 oC, 0.0038 m^2/h and 552 h, respectively.

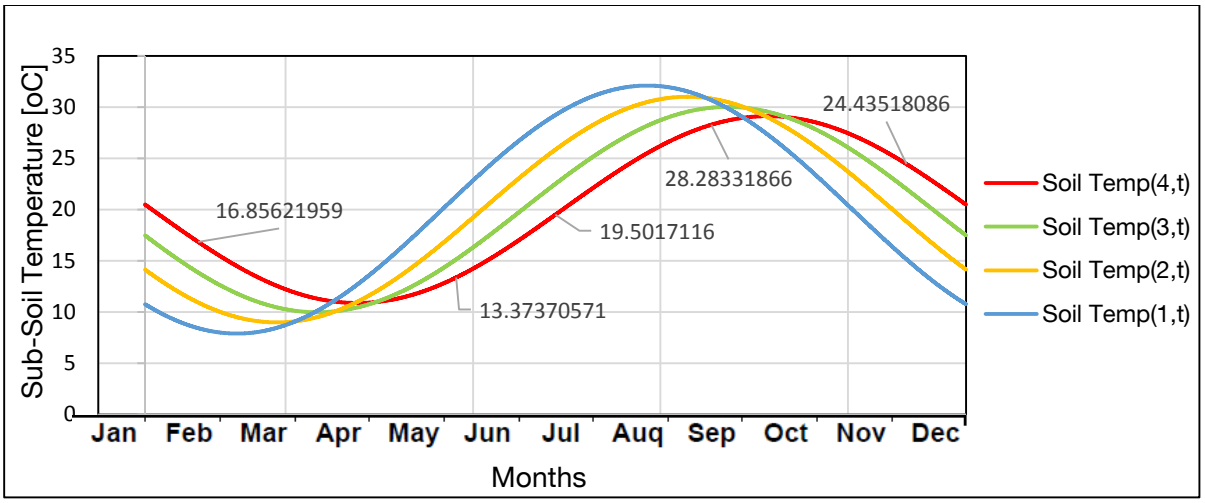

Figure 67: Predicted Soil Temperature at depths 1-4 meters

In case that all the values presented above are not able to be defined for the determination of 7.1, another simpler equation can be used, as proposed (Bansal et al., 2009). After experimental studies that took place, it has been concluded (Givonni, 1991) that a good estimation about soil's temperature at a certain depth at day t, based on the weather conditions of the location, is given by:

$$T_{(z,t)} = T_m + A_0 \cdot e^{-Fz} \cdot sin(0.986t - T_{sur,max} - Lz) \quad (7.22)$$

Where:

- T_m is the annual mean ground surface temperature
- A_0 is the annual amplitude of the soil's surface temperature and equals to the annual range divided by two $((T_{max} - T_{min})/2)$
- 0.986 the days of the year expressed in degrees (360/365)
- t the day number (t=1 for the first of January)
- $T_{sur,max}$ the day in which the maximum soil's temperature has been observed
- F and L the range damping factor and the time lag per meter depth, both of which depend on the climate and soil type and their value is selected by the following table.

Table 8: Values for F and L factors according to different climates

	Loam/clay		Intermediate		Sandy	
Climate	**F**	**L**	**F**	**L**	**F**	**L**
Desert	0.45	24	0.50	25	0.55	26
Arid	0.40	22.5	0.45	23.5	0.50	24.5
Intermediary	0.35	21	0.40	22	0.45	23
Humid	0.25	19.5	0.35	20.5	0.40	21.5
Wet	0.20	18	0.30	19	0.35	20

Heat transfer along the pipe

As a first step, the overall heat transfer coefficient has to be defined. For this purpose the three thermal resistance values are required, based on the figure 68.

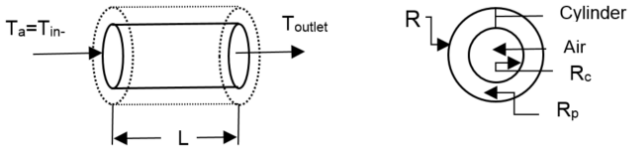

Figure 68: Earth-air heat exchanger with its layers

Thermal Resistance due to convection heat transfer between the air in the pipe and the pipe inner surface $(°C/W)$:

$$R_c = \frac{1}{2\pi r_{pipe,in} L h_c} \tag{7.23}$$

Thermal Resistance due to conduction heat transfer between the pipe inner and outer surface (oC/W):

$$R_p = \frac{1}{2\pi L \lambda_p} ln\left(\frac{r_{pipe,out}}{r_{pipe,in}}\right) \tag{7.24}$$

Where the extra parameters required are:

- The convective heat transfer coefficient at the inner pipe surface $(W/m^{2\circ}C)$,

$$h_c = \frac{Nu\lambda_{air}}{2r_{pipe,in}} \tag{7.25}$$

Where:

- λ_{air} is the thermal conductivity of the air [W/m2°C] (Hanby, 1994):

$$\lambda_{air} = 0.02442 + (10^{-4}(0.6992T_{am}) \tag{7.26}$$

With T_{am} being the ambient temperature (°C).

- Nu is the Nusselt number and (Incropera et al., 1996), if Re < 2300 is given as Nu = 4.36, while as proposed by (Gnielinski, 1976) for fully developed laminar and turbulent flow in a circular pipe for ranges $Pr \in [0.5,\ 2000]$ and $Re \in (2300,\ 5x10^6)$ it can be evaluated by:

$$Nu = \frac{(fr/8)(Re-1000)Pr}{1+12.7(fr/8)^{1/2}\left(Pr^{2/3}-1\right)} \quad (7.27)$$

The Reynolds number that characterizes the mode flow is given by equation:

$$Re = \frac{\rho_{air} \cdot \dot{m}_{air} \cdot D}{\mu_{air}} \quad (7.28)$$

Where ρ_{air} the air density (kg/m^3), D the pipe's diameter (m), m_{air} the air velocity (m/s) and μ_{air} the kinematic viscosity $[m^2/s]$ of air as proposed (Hanby, 1994):

$$\mu_{air} = 10^{-4}(0.1335 + 0.000925T_{am}) \quad (7.29)$$

The Prandtl number which defines the relationship between the viscosity and the thermal diffusivity of the fluid is evaluated by:

$$Pr = \frac{C_{p,air} \cdot \mu_{air}}{\lambda_{air}} \quad (7.30)$$

Where $C_{p,air}$the specific heat of air $(J/kg\ K)$ and λ_{air} conductivity of air $(W/m\ K)$

The friction coefficient fr for smooth pipes is determined by the following formula:

$$fr = (0.79lnRe - 1.64)^{-2} \quad (7.31)$$

- $r_{pipe,in}$ is the inner pipe radius (m),
- $r_{pipe,out}$ is the outer pipe radius (m),
- L is the pipe length (m)

Now, the overall heat transfer coefficient of earth tube can be determined as:

$$U_{air} = \frac{1}{R_{tot}} \quad (7.32)$$

Where:

$$R_{tot} = R_c + R_p \quad (7.33)$$

As air flows through the pipe, the heat transfer between the soil and the air inside the pipe is equal to the amount of heat loss or gain. If the total length of the pipe is discretised into small elements dL, where i the inlet node and i+1 the outlet in the horizontal axis, n the centreline node and n+1 the node on the wall and k the time, based on the figure 69, the following equations can be used:

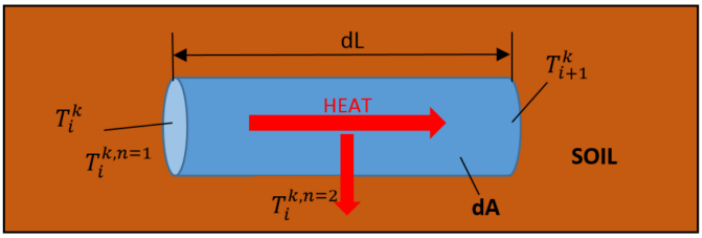

Figure 69: Underground discrete length of the pipe

$$dQ = a_{air} \cdot dA \cdot \left(T_i^n - T_i^{n+1}\right) \cdot dt \tag{7.34}$$

$$dQ = \rho_{air} \cdot \dot{V}_{air} \cdot c_{p,air} \cdot \left(T_i^k - T_{i+1}^k\right) \cdot dt \tag{7.35}$$

Combining these two equations and because $T_i^k = T_i^{k,1}$, the temperature at the outlet of the discrete element can be expressed as:

$$T_{i+1}^k = T_i^k \left(1 - \frac{a_{air} \cdot dA}{\rho_{air} \cdot \dot{V}_{air} \cdot c_{p,air}}\right) + \frac{a_{air} \cdot dA}{\rho_{air} \cdot \dot{V}_{air} \cdot c_{p,air}} T_i^{k,2} \tag{7.36}$$

The air ambient temperature (T_1^k) and the ground temperature $(T_1^{k,2})$ should be known in order to calculate the air temperature at the outlet. Implementing the above equation for a pipe with specific length, which has been discretized in nL elements dL, it is possible to evaluate the cooling performance of the buried pipe.

Heat transfer through the soil

The heat rejection of the air that occurs inside pipe results in a colder air at the pipe's outlet. Therefore, this amount of heat is absorbed by the soil and that effect should be taken under consideration when estimating the sub-soil's temperature. It may happens that, after time elapsed and due to the heat transfer between air and sub-soil, the temperature at the pipe's outer surface is heated up in a high value and meet a steady state situation, where heat transfer will no more be feasible. Consequently, the heat transfer effect presented above should be also evaluated through the time. For this reason, the following algorithm has been developed, referred to a finite length "dL" along the pipe, as illustrated in figure 70.

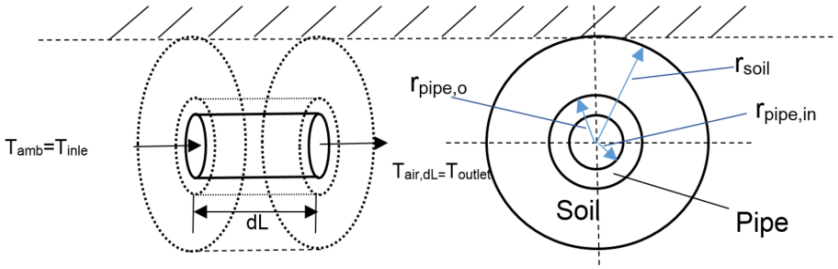

Figure 70: Buried Pipe Discrete Element

Focusing now on a finite element of the soil as depicted below, dividing it by n discrete elements "dr" and analyzing the heat transfer, the followings remarks come out.

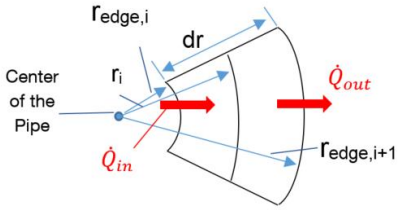

Figure 71: Pipe Cutaway in the vertical axis

On the figure above, n is the number of nodes, dr the radial finite element that discretizes the soil around the pipe, $r_{edge,i}$ are the radiuses of the nodes among which the volume of each element is enclosed, r_I the mean radius and i the node location in the vertical direction.

Given these variables it is possible to define the mean surface of each node and the corresponding volume from the equations present below.

- Mean surface of each node $[m^2]$

$$S_i = 2 \cdot \pi \cdot r_i \cdot dL \tag{7.39}$$

As it is known, the heat equation is derived from Fourier's law and conservation of energy. So the rate of flow of heat energy through a surface is proportional to the change in temperature across the surface. As a result and for a specific time k:

$$\frac{dQ}{dt} = a_{air} \cdot S \cdot \left(T_{i-1}^{k} - T_i^{k}\right) \tag{7.40}$$

For the expression of the heat that is rejected by the air and travels through the soil, the Forward-Time Central-Space (FTCS) method, a finite difference method used for numerically solving the heat equation, has been implemented. The FTCS method applied in this case takes the following form:

$$\frac{T_i^{k+1} - T_i^{k}}{\Delta t} = \frac{a_s}{\Delta x^2}\left(T_{i+1}^{k} - 2T_i^{k} + T_{i-1}^{k}\right) \tag{7.41}$$

Variable a_s corresponds to the soil thermal diffusivity (m²/s) and can be expressed by:

$$a_s = \lambda_s/(\rho_s C_s) \tag{7.42}$$

Where ρ_s is the soil density (kg/m^3) and C_s the specific heat of soil $(J/kg\ K)$.

Combining the above equations and referring to a node in the soil in the vertical direction, the following equation is formed:

$$T_i^{k+1} = \left(-\frac{a_s}{dr^2} \cdot dt\right) T_{i-1}^{k} + \left[1 + a_s \cdot \left(\frac{2}{dr^2} + \frac{1}{r_i \cdot dr}\right) \cdot dt\right] T_i^{k} + \left[-a_s \cdot \left(\frac{1}{dr^2} + \frac{1}{r_i \cdot dr}\right) \cdot dt\right] T_{i+1}^{k} \tag{7.43}$$

The second radial node that corresponds to the wall of the pipe should be treated differently as the node before refers to the air in the center of the pipe. Consequently, the above equations for the second node, based on the (7.40), will be (7.44):

$$T_i^{k+1} = \left(-\frac{dt}{a_{air} \cdot S_i}\right) T_{i-1}^k + \left[1 + \frac{dt}{a_{air} \cdot S_i} + a_s \cdot \left(\frac{2}{dr^2} + \frac{1}{r_i \cdot dr}\right) \cdot dt\right] T_i^k + \left[-a_s \cdot \left(\frac{1}{dr^2} + \frac{1}{r_i \cdot dr}\right) \cdot dt\right] T_{i+1}^k$$

Pressure losses through the buried pipe

The pressure losses while the air flows through the buried pipe can be expressed by (ASHRAE handbook, 2000):

$$\Delta P_{EAHE} = \left(\sum_{J=1}^{5} c_j + \zeta \frac{L_{EAHE}}{d_{in}}\right)\left(\frac{\rho_{air} u_{air}^2}{2}\right) \quad (7.45)$$

Where c_j the pressure loss coefficients for the several fittings and valves that are involved in the installation, ζ the friction factor of the pipe, d_{in} the internal diameter of the pipe, and ρ_{ft} and u_{ft} the density and the velocity of the air that flows through the pipe respectively. The flow of the air through the vertical pipe and its temperature variation is neglected.

The friction factor of the pipe, according to VDI Heat Atlas and the Prandtl-Karman equation, can be evaluated by equation:

$$\frac{1}{\sqrt{\zeta}} = 2log\left(\frac{d_i}{K}\right) + 1.14 \quad (7.46)$$

Where $\varepsilon = \frac{K}{d_{in}}$ is the relative roughness and for plastic tubes has a maximum value of 0.0015.

7.3 Model's Parameters Variation

The equations presented in paragraphs above were combined and inserted into a code in Matlab. In order to go deeper into the model and understand the influence of the several variables, all the main parameters have been varied, while keeping constant the rest. The relative results and their behavior is graphically illustrated below. The main parameters that have been investigated, for given soil condition and on an hourly basis are the pipe length, the pipe radius, the air volume flow rate, the ambient conditions, the depth and the time step of simulation.

First of all, the algorithm that has been developed will be shortly described. After defining all the variables that are required as input, a loop algorithm can be created in order to evaluate the final temperature of the soil and the pipe, after an hourly operation. The air temperature exiting the buried pipe constitutes actually the main evaluation factor and then comes the cost.

The algorithm starts with the division of the total time in specific time steps. At every time step, it is feasible to calculate the air temperature at the outlet of each finite length element "dL" according to equations presented in paragraph 7.2.

Having defined these temperatures, it is now possible to move on the radial or vertical direction and, based on the paragraph 7.4 and the heat rejection that occurs, the temperature profile from the center of the pipe to the ground, through the pipe wall, can be determined. The new wall temperature is equal to the new sub-soil temperature at pipe's surface that is re-defined after the heat absorption. This temperature should be given as input for the next time step, in order to evaluate the new air temperature in the center of the pipe. Same iterations are being made for the whole length of the pipe and the outlet air temperature is finally evaluated.

When the parameters do not vary, then they have the following values:

$$L = 150m, \dot{V}_{air} = 20\, m^3/s\,, R_{pipe,in} = 0.25m, \lambda_{pipe} = 0.33\ W\ /mK,\ \ T_{amb} = 21, T_{soil} = 5^oC$$

Influence of pipe length

Regardless of the installation's location, an increase in the pipe length will contribute in a better performance, meaning that in case of cooling, the inlet air temperature will decrease even more. This occurs, because a longer pipe results in a bigger surface over which heat transfer takes place, for a given overall heat transfer coefficient of earth tube. Of course, factors such as the cost, the soil conditions and the ambient temperature should be taken under consideration. For the same inlet condition in the pipe and varying only its length the following figure comes out:

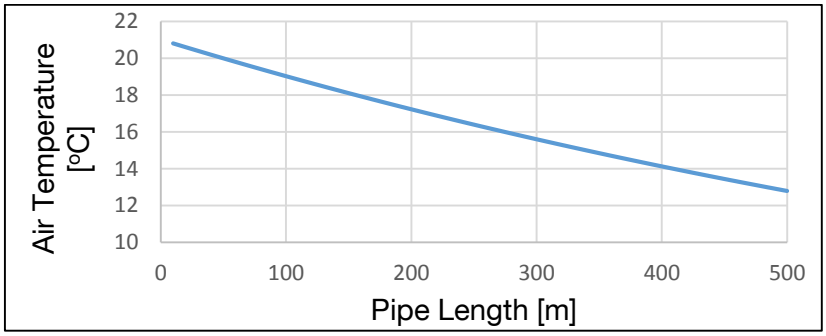

Figure 72: Air temperature at the outlet of the pipe for various pipe lengths

Influence of the pipe's depth

Regardless of the installation's location, increasing the depth of the buried pipe can result in decreasing the outlet temperature of the pipe, as the initial sub-soil temperature is cooler. In this case, also, factors such as the drilling cost have be taken into consideration. The EAHE model was used for a given ambient temperature and variable sub-soil temperatures. It is remarkable that, although after the first minutes the air at the outlet of the buried pipe is cooler, it seems that (figure 73) due to the accumulation of the heat rejected in the soil, after an hourly operation, the air temperature is the same for all cases. As a result the

pipe depth should be selected carefully, depending the installation costs and of course the selected pipe radius.

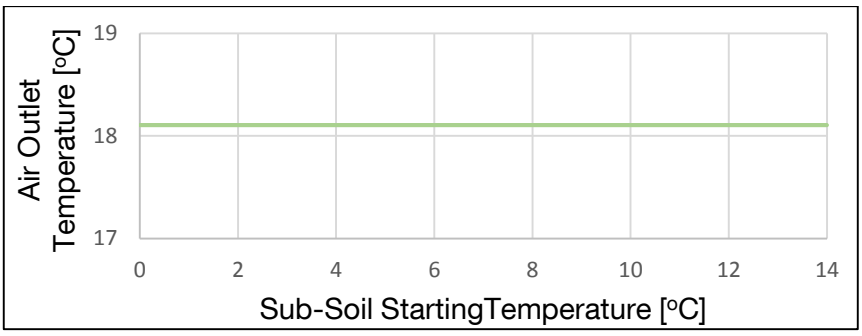

Figure 73: Air temperature at the outlet of the pipe for various initial sub-soil temperatures

Influence of pipe radius

The pipe radius has the same correlation with the outlet temperature as the length, meaning that as the pipe radius increases, the outlet air temperature decreases. This is verified, after having a look figure 74. A larger pipe radius leads to a lower convective heat transfer coefficient and as a result to a lower overall heat transfer coefficient of earth-to-air heat exchanger. Therefore, a pipe with small radius should be selected during design process, or a number of pipes with small radius, whether much air is needed for operational purposes. It has been observed that after a certain value of radius, the improvement in the cooling performance of the buried pipe is not remarkable. This should be taken under consideration when cost factor is also taken into account.

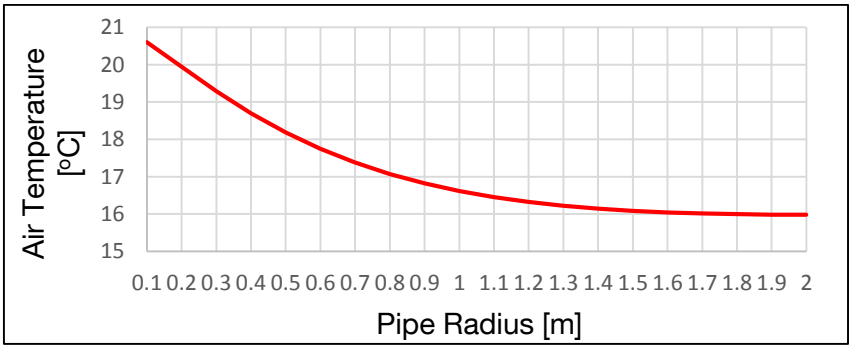

Figure 74: Air temperature at the outlet of the pipe for various pipe radius

Influence of air volume flow rate

Concerning the increase in the air volume flow rate inside the pipe, this would result in an increase in the air temperature exiting the pipe. Consequently, the lower the air flows through the pipe, the better performance characterizes the system, as depicted in figure below, and that is realistic as the air will stay more inside the tube, meaning being more time in contact with the soil temperature affecting it. Of course, the air velocity should be enough to provide with air the cooling tower, overcome the losses and exit from the top of the tower to the atmosphere. The extra pressure losses that are appeared though the pipe

because of the increase of the air volume flow rate should also be considered. For the reason, they are plotted in the same graphic with the cooling performance below.

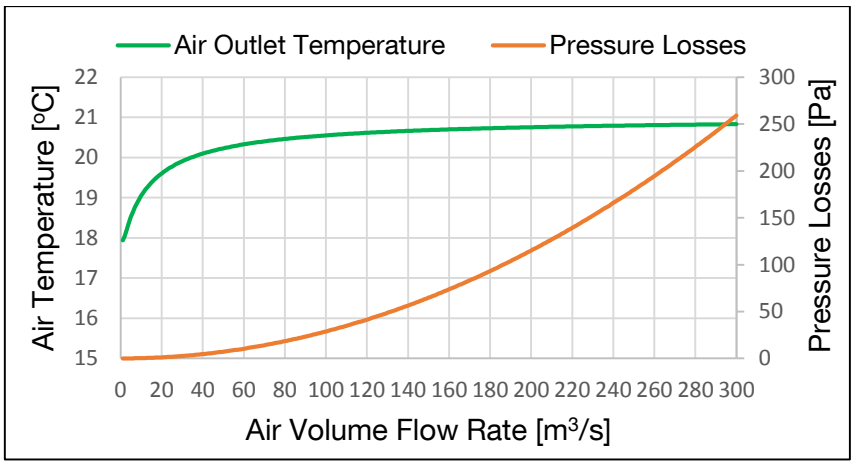

Figure 75: Air temperature at the outlet of the pipe for various air volume flow rates and relative pressure losses through the buried pipe

Influence of ambient air temperature

As it was expected and illustrated in figure 76 the higher the ambient air temperature, the higher the air temperature at the outlet of the buried pipe. It seems that their correlation is linear for specific values for the rest o of the variables and after an hourly operation.

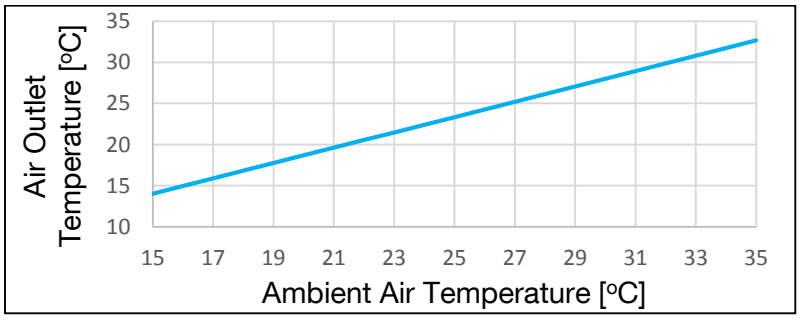

Figure 76: Air temperature at the outlet of the pipe for various ambient air temperatures

Influence of ambient air relative humidity

Using properly this model, it is also possible to evaluate the relative humidity of the air at the outlet of the pipe, given that the mass fraction of water remains the same as it is in the inlet. For a given ambient temperature and various relative humidity, as shown in the figure, the relative humidity at the outlet of the buried pipe is slightly reduced at the outlet. This data is important in order to be able to specify exactly the inlet conditions of the cooling tower.

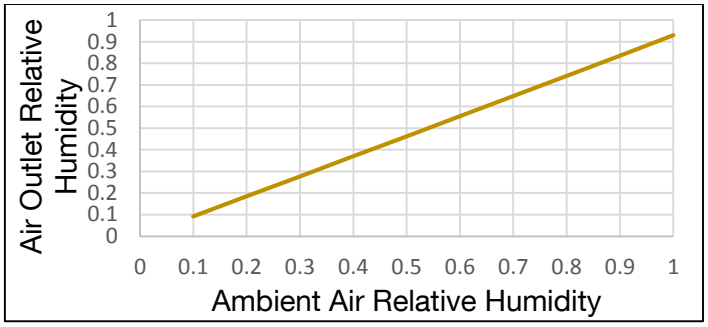

Figure 77: Outlet air relative humidity at the outlet of the pipe for various ambient air temperatures

Influence of the pipe material

The pipe material affects the results of the calculations through the variable of thermal conductivity of the pipe. For this reason, three different materials have been used, PVC carbon steel and stainless steel, and the relative results are in the following graph.

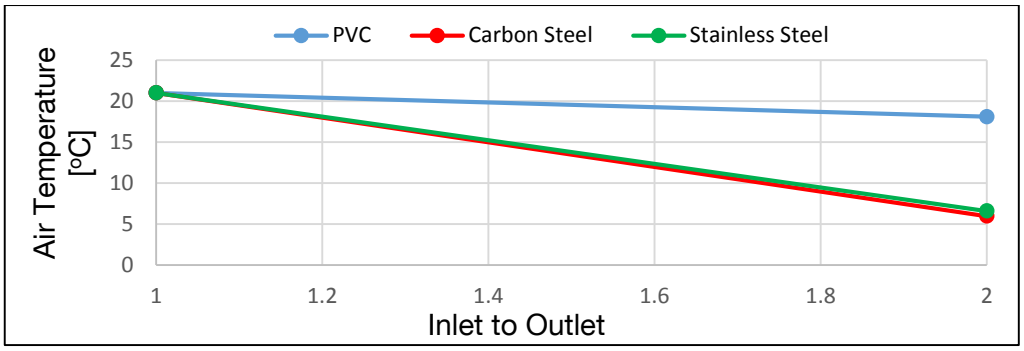

Figure 78: Influence of pipe material on the air outlet temperature

It is easily concluded that the material of the pipe has a great influence on the final temperature of the air at the outlet of the buried pipe. Therefore, two things should be taken into consideration when designing and installing such a system, which are the cost of the material and its corrosion by the earth. These factors constitute carbon steel unsuitable for underground cooling. Of course, stainless steel could be selected to overcome this obstacle, as the cooling performance is almost the same, but then the cost goes really high for the length and the diameter that would be required. Nevertheless, the final results would be compared for both PVC and stainless steel.

Influence of the simulation time step

An investigation on the selection of the simulation time step has been conducted. This constitutes an important factor concerning the total simulation time and the accuracy of the results. As depicted in figure 79 the selection of a high time step results in a higher calculated air outlet temperature. It may happens that a numerical mistake comes up that

is not corrected for a few iterations. So, taking into account the results' accuracy and the simulation time required, a time step of 60sec will be used in the next calculations, which means 3seconds per an hourly operation evaluation.

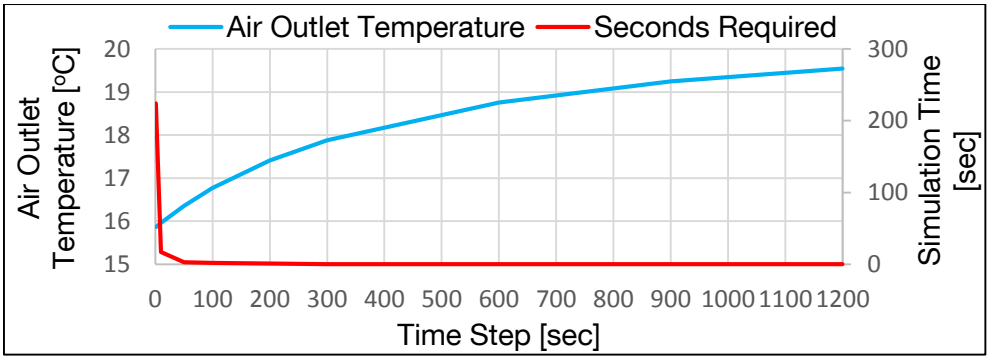

Figure 79: Influence of Time Step Selection on the Air Outlet Temperature and Simulation Time

7.4 Annual operation of the EAHE system

The models presented above concerning the installation of an EAHE system have been combined and configured in order to evaluate the cooling performance of a specific pipe throughout a year.

For this reason weather data were required for each hour of the year. As for the air temperatures, the temperatures of the area of Garching in north Munich for the year 2013 are registered by the TU Munich – Energy Systems Department and have been used as input. The values of the relative humidity were collected from the internet *("whetheronline.co.uk).* As they were available only for per day, it was assumed that the value of relative humidity was the same during the day. This assumption was not negatively affecting the results, as on the one hand during the night it normally is lower and would result in a better cooling performance of the cooling tower, where the air is driven after the buried pipe and on the other hand, as it will be presented below, the heat up of the soil during the day prevents from operating the EAHE during the nighttime. The following graph can confirm the fact of the accumulation of the rejected heat in the soil after an hourly operation, which results in a restricted use of the EAHE system for cooling purposes.

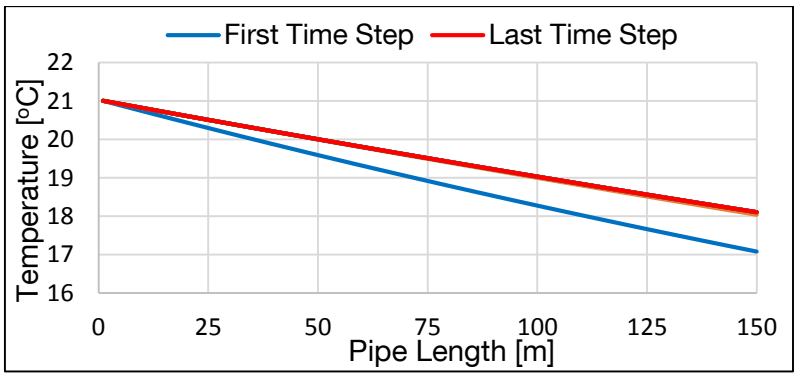

Figure 80: Air in pipe temperature variation due to heat accumulation on hourly operation

The results of the annual operation of the EAHE are depicted in following figures. Firstly, the ambient air and sub-soil temperatures are depicted together in order to have an overview of their fluctuations along the year. It has to be remarked that the year of 2013 was characterized as a remarkably warm season.

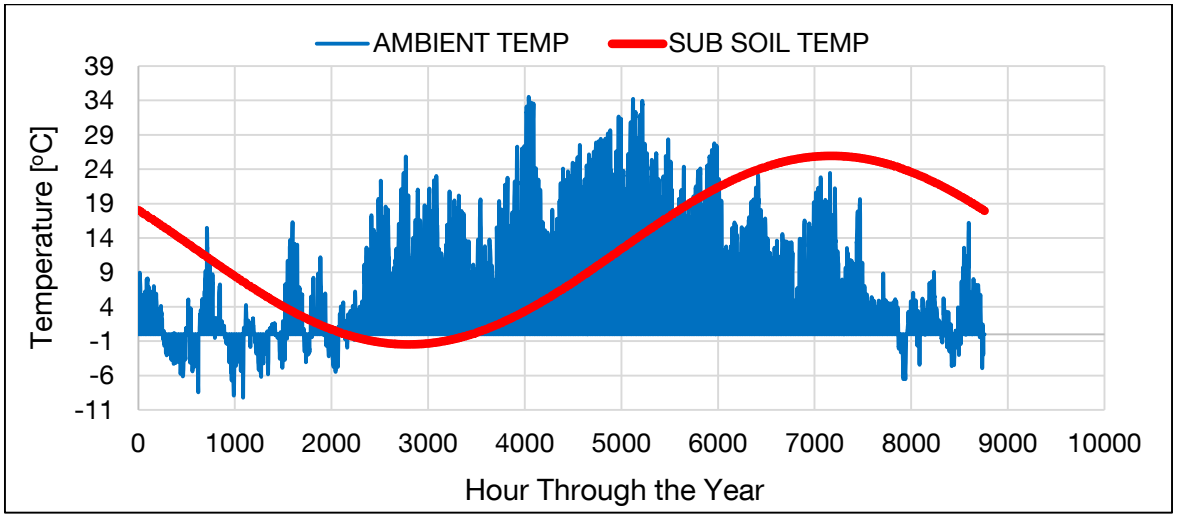

Figure 81: Ambient air temperature and estimated sub-soil temperature, Garching, 2013

From the figure above it is easily to estimate the periods of the year, during which the buried pipe could be useful. Then, the following figure presents the possible reduction of the air temperature depending the corresponding sub-soil temperature.

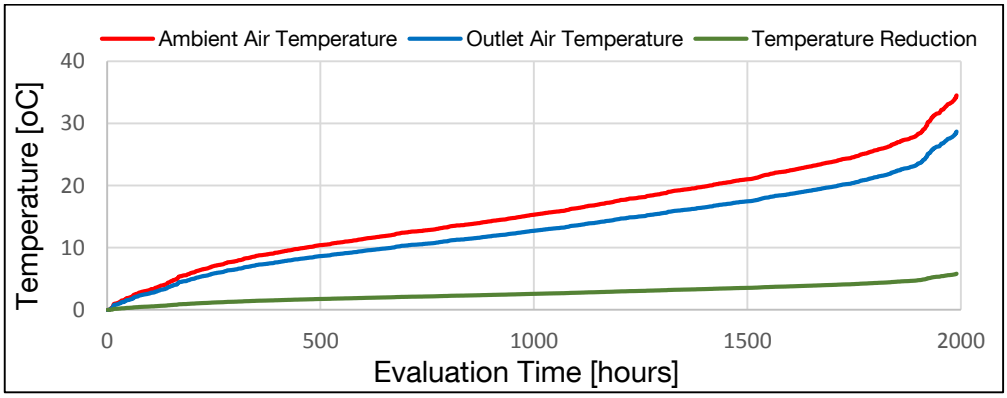

Figure 82: Possible EAHE cooling performance for Garching weather conditions in 2013

It is important also to know how many hours per day would it be possible to use the EAHE system, in order to exploit its cooling effect. As it has been observed, the heat rejected from the air is gradually accumulated in the soil and consequently after a certain amount of hours the use of the EAHE system is no more beneficial. For this reason it has been assumed that at least from the time range between midnight and 5am the air will not pass through the pipe in order to let the soil cool down again. Then, the outlet air temperature is evaluated, as described, until it is equal to the ambient temperature at the specific time. Finally, the possible beneficial operating hours per day are the illustrated in figure below.

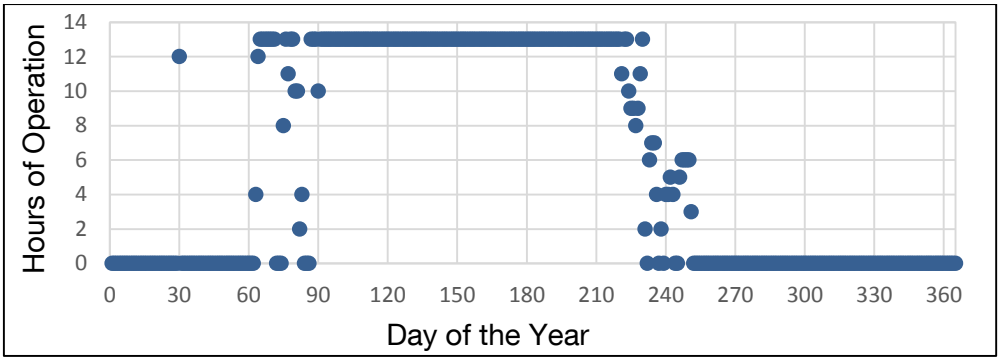

Figure 83: Possible beneficial hours of operation of the EAHE system

In total it has been calculated that the EAHE system could be used for **2125** hours for cooling the ambient air.

7.5 EAHE Simulation, cost factor and optimization algorithm

Using the EAHE simulation model, it is possible to calculate the air temperature at the pipe's outlet, as aforementioned. But, only this result would not mean a lot for a company that is interested in installing such a system and the same happens for Unterhaching Kalina Power Plant in our case. In the real market, where all companies that hunt profit participate, the financial aspect of such systems plays a significant role. For this reason, an effort to insert financial data and estimate the return of such an investment is being undertaken in the next paragraphs. As a first step, relative price values for PVC pipes with several specifications regarding their length, radius and thickness as presented by a typical company, are tabulated below. Of course, these values may vary from company to company.

Table 9: Pipes' diameter [110mm, 355mm], with corresponding thickness and price

Pipe Diameter $2xr_1$ [mm]	110	125	140	160	180	200	225	250	280	315	355
Pipe Thickness r_2 [mm]	4.2	4.8	5.4	6.2	6.9	7.7	8.6	9.6	10.7	12.1	13.6
Price/meter [€/m]	8.45	11.2	13.8	16.5	23.8	26.7	33.8	41.8	56.6	66.2	86.9

Table 10: Pipes' diameter [400mm, 1200mm], with corresponding thickness and price

Pipe Diameter 2xr1 [mm]	400	450	500	560	630	710	800	900	1000	1100	1200
Pipe Thickness r2 [mm]	15.3	17.2	19.1	21.4	24.1	27.2	30.6	34.4	38.2	42.3	45.9
Price/meter [€/m]	111	140	173	217	274	347	440	557	686	866	1,025

An Illustrative overview of these values is also presented, in order to recognize easily the influence of radius and thickness at the price per unit length of the pipe. It seems that for higher values of radius the cost increase much faster. These data will be used for evaluating the optimum, from financially aspect, EAHE system.

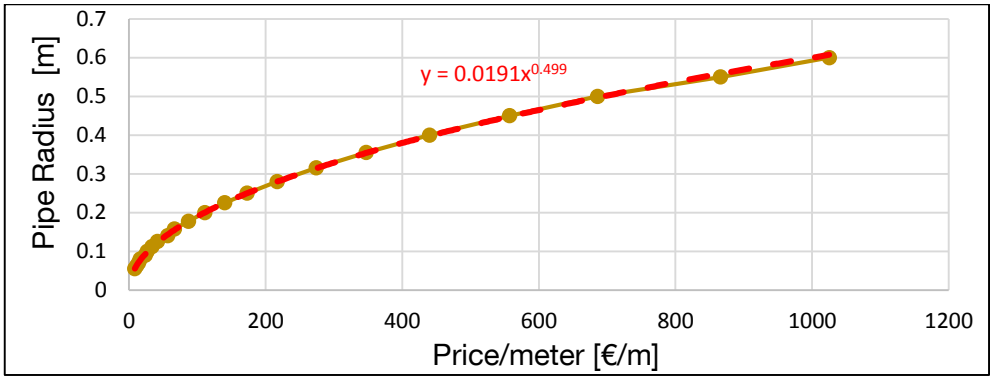

Figure 84: Pipe Cost per meter as a function of Radius

Optimization Algorithm

The purpose of the optimization algorithm, based on the calculations' procedure presented above, is to give sufficient design information, in order to choose the optimum pipe, concerning cost, for given efficiency and time of operation. That means that based on the ambient temperature and a specific cooling performance in conjunction with the minimum cost should be evaluated. The material that has been used was PVC and the cost data are derived from previous paragraph and figure above. The cost function per length based on the radius of the pipe could be:

$$C_{pipe/length} = \left(R_{pipe,in}/0.0191\right)^{2.004} \tag{7.47}$$

A first example that has been evaluated, takes as input: $\dot{V}_{air} = 20\,m^3/s$, $\lambda_{pipe} = 0.33\ W/mK$, $T_{amb} = 21^oC, T_{soil} = 5^oC$, $\Delta T = 2^oC$. The program showed that the required length and radius, in order to achieve a cool down of 2^oC after an hourly operation of the EAHE, would be $L = 89m$, $R_{pipe,in} = 0.2m$ with a cost ranging up to 9,800€. Of course, this algorithm could be used on an annual base in order to specify the best, on the financial aspect, specifications of the pipe in average for a desired cooling performance.

For this purpose, the previous program has been expanded based on the Garching's weather data. Firstly, the days during which the use of any EAHE system can be used, i.e. the sub-soil temperature is lower than ambient, have been defined and the corresponding air inlet temperature has been registered. Then the user can determine the desired cooling performance and operation time at each of these days. Finally, the algorithm calculates the optimum required pipe's dimensions for each occasion, by taking into account the minimum capital cost of the pipe. It would also be possible to run a multi-objective optimization, based on both the best cooling performance and the minimum capital cost. However, analyzing and making decision for each daily different "pareto" that would be extracted is quite time-consuming procedure and not required at this stage, so it was neglected. The

following graph illustrates the fluctuation of the dimensional sizes, the temperature drop of 2°C that was required and the cost of the buried pipe through a week operation.

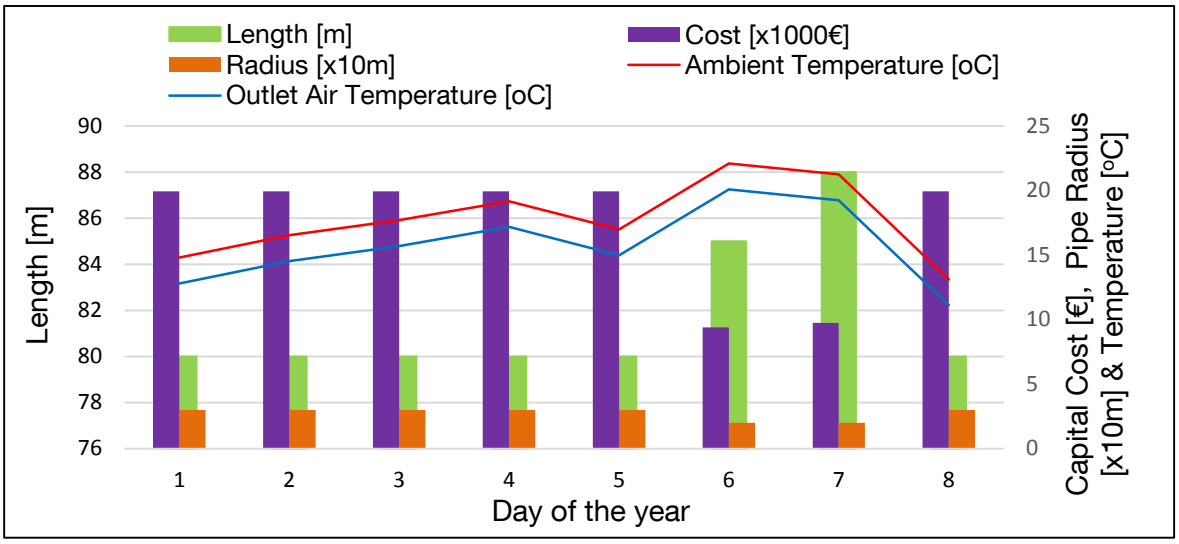

Figure 85: Optimum underground pipe's dimensions for minimum capital cost and required temper-ature drop of 2°C

Based on such data for annual operation, it is possible to estimate the values for the diameter and the length of the pipe that will be able to give the required cooling performance after a specific time of operation. It is worthy to mention that these degrees of temperature drop correspond to the air temperature after the given operational hours throughout the day. Taking into account the fact that heat is being "stored" into the soil, it is clear that during the daily use of the pipe, the cooling performance would be even better. This information is important in case of evaluating the hourly improvement of the cooling towers performance, after the installation of an EAHE system.

7.6 Prospects and improvements of underground cooling

Heating operation

Of course it is quite important to know the performance throughout the year, based on a specific length of pipe. Such a calculation can provide useful information about the EAHE performance during the period of winter, when as expected the EAHE will heat up the ambient air and that is not profitable for the towers' cooling process. Therefore, it is possible to implement an alternative way of exploiting the EAHE system during the cold days. This could happen by supplying the buildings with this available heat, in order to reduce the energy consumption that takes place. Consequently, the EAHE system can be used directly for space heating when low ambient temperatures exist or as a preheating part for existing technologies like heat pumps, in order to improve the ROI of such an investment. Several ways of using the EAHE system have been tested, such as continuous operation

or alternating it any time that can affect beneficially the cooling performance of the cooling towers. The relative results are presented in the following paragraph.

Affecting soil's surface to improve the cooling performance

As it is proposed (Tittelein, 2009) there are some actions that can be made in order to affect the temperature of the ground and as a result its temperature up to a limited depth. The reason that may force someone to undertake such actions is the improvement of the cooling performance of the soil, especially during summer periods, when the solar radiation heats up the soil's surface.

Some treatments that have been proved to be efficient are related with the soil's shading from direct sunlight, as a measure to augment the evaporative heat loss from the surface and eliminate the convective heat gains from the ambient hot air. First and low cost solution would to protect the surface from the sunlight by spreading tree canopy, contributing also to the evaporation of a significant amount of water from the soil's surface and plant leaves. Another efficient but a bit cost consuming treatment could be the irrigation. It has been observed that if the soil is irrigated and the relative humidity at 60-70%, then wet ambient temperatures are being used for modelling purposes. Furthermore, a partial coverage by a layer of straw or wood or gravels, would also enhance the heat losses by evaporation and hamper the convective heat gain. The phenomenon that takes place is based on the dissipation of heat into the ground at a specific depth, which will firstly slightly rise the temperature between the soil and the layer of gravels and subsequently increase the vapor pressure of the soil, fact that in turn enhances the evaporative cooling and prevents the ground from heating up. An example that proves this benefit and qualifies the amount of degrees of Celsius that can be gained through such a treatment is presented graphically in figure 86 below.

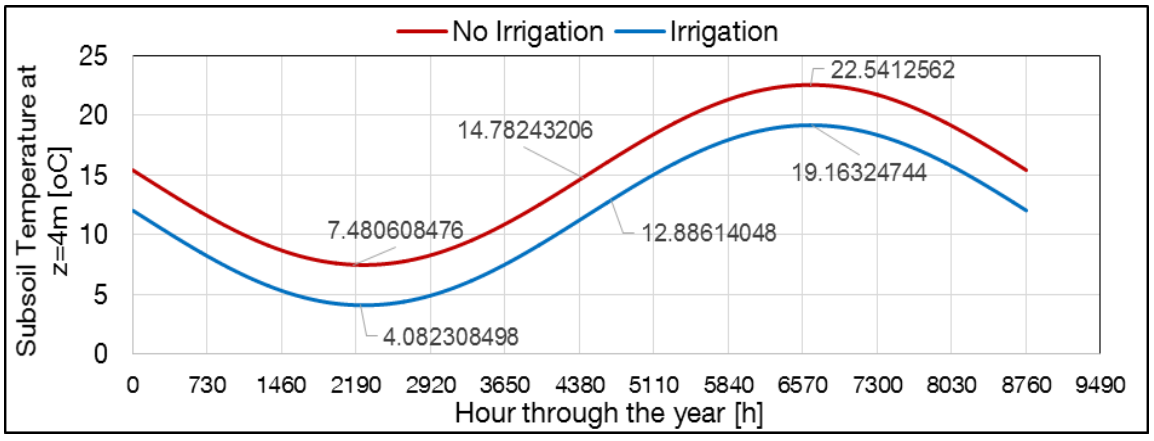

Figure 86: Temperature variation of an irrigated ground at a depth of 4m

Given the results presented above about the new thermodynamic results that can come out after taking under consideration the effect of irrigation it seems interesting that the total beneficial hours of operation is the same as without irrigation and the same happens with

the final cooling performance. Therefore, until the steady state situation takes place every day, the irrigated soil seems to primarily cool down more the air.

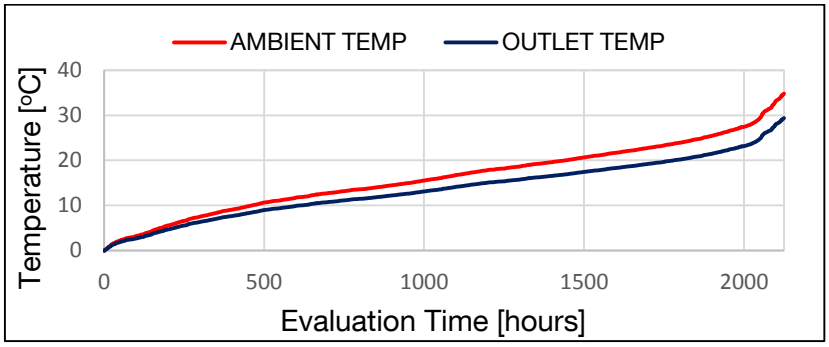

Figure 87: Possible EAHE cooling performance for Garching weather conditions in 2013

7.7 Solution Evaluation - Conclusion

Previous paragraphs have verified that the installation of an EAHE system can be beneficial for the cooling system. Especially during hot periods of the year, when the hot ambient air and the dry conditions influence negatively the cooling performance of the cooling towers.

In entrepreneurship world, such a result must be financially justified that makes profit, in order to convince company's board of directors, "Geothermie Unterhaching GmbH & Co KG" in our case, that such an investment can have an acceptable internal rate of return. For this reason, an algorithm has been created to compare the cooling performance with and without an EAHE. A typical flow of the models that have been used is presented in figure 89. It has to be mentioned that among the comparison, only the ambient temperature was changing. The goal was to evaluate the new water outlet temperature and based on figure 66, to estimate the possible increase in the power production. It was assumed that the water and air flow rates remain constant for both cases. In reality this does not happen as both pump and fan have variable speed drivers, but as their performance curves were not available and in order to simplify the calculations these assumptions were acceptable. In addition, lower ambient temperature, as presented in paragraph 6, eliminates the required air and water mass flow rate. So, such assumptions do not affect positively the results, in contrary they underestimate them.

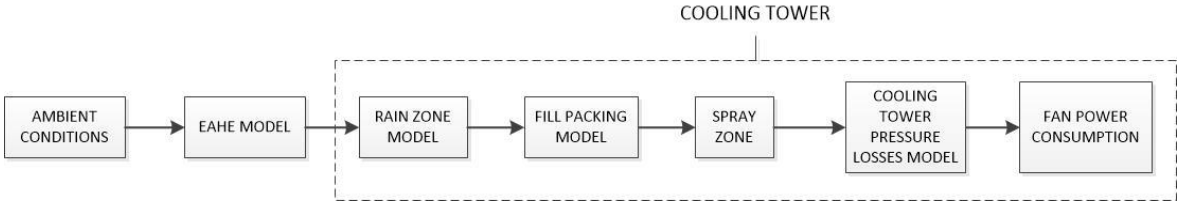

Figure 88: Algorithmic flow for evaluating the cooling performance with an EAHE system

The results that have been extracted are depicted below. Firstly, the reduction in the water temperature at the outlet of the cooling tower is clear in figure 89.

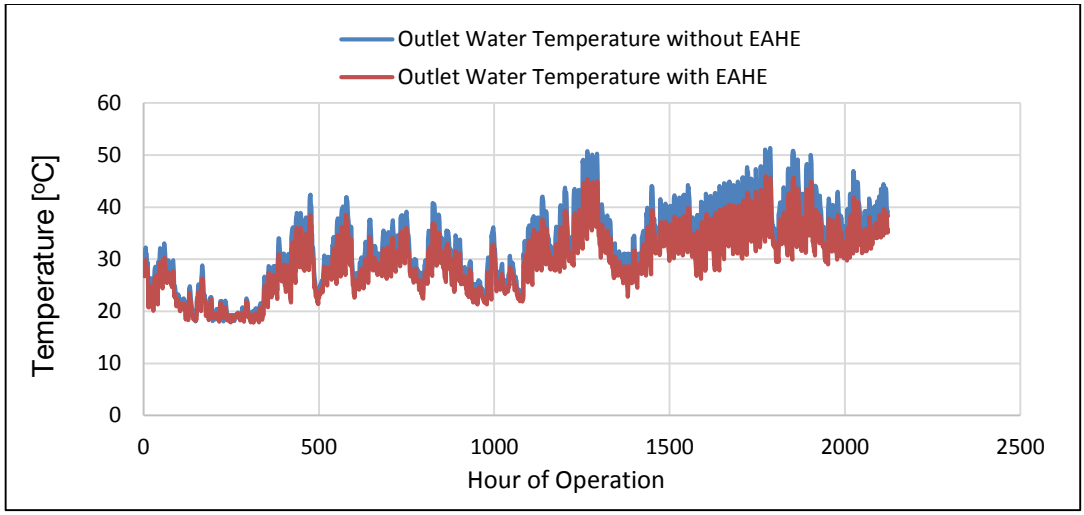

Figure 89: Water temperature at cooling tower's with and without an EAHE system

Combining this result with the possible power production, an estimation of the great power output that can be achieved is illustrated in figure 90.

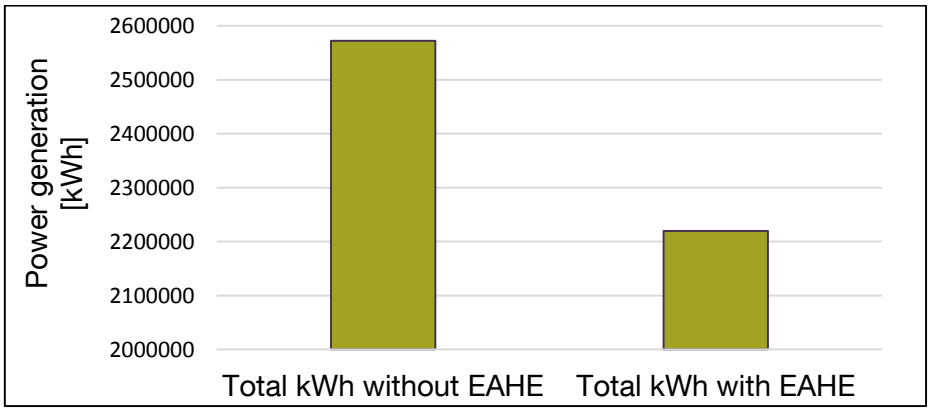

Figure 90: Power production with and without a EAHE system (only for the days that EAHE can be used beneficially)

The pipe that has been selected, has a 150 meters length with a 0.4m diameter. In detail design phase, optimum pipe's specifications should be selected based on the algorithm presented in paragraph 7.5, so that overestimation is avoided and capital cost is eliminated. The pipe that has been used for this first evaluation is able to operate for at least 13hours per day as depicted in figure 83, for almost all of the days that EAHE system can be beneficial for the cooling system. That means that its length can for sure be even less. As for its material, PVC was a first option to avoid corrosion effects from the soil in order to keep the capital cost in low levels, which means around 15000€ for each tower, i.e. 45000€ in order to operate all three the same. Of course a pipe with bigger diameter and length can be selected to supply all cooling towers, a decision that would maybe restrict the capital cost. Furthermore, in this amount, drilling costs, labor and further equipment, such as instrumentation, are not included. If an increasing cooling performance is required,

stainless steel could be also an option but then the capital cost could be up to 5 times higher. Copper could constitute a good option, as it has a thermal conductivity much greater than stainless steel, i.e. around $40W/mK$, but then measures should be taken, such as cathodic protection, to protect it from corrosion.

Figure 90 showed an increase on the power output of about 352,892kWh. From the Geothermie Unterhaching GmbH & Co KG website it is derived that a typical value for selling electrical energy in Germany ranges up to 0.25€/kWh. Taking into account this value, the annual profit for the company, based on all calculations conducted and assumptions declared, can reach up to 90,000€. It is obvious that the internal rate of return could be roughly 200%, constituting the investment more than acceptable and profitable. This profit value gives also a safety margin for all the assumption that have been made and may affect positively the evaluation. To sum up, it is concluded that an EAHE system could increase the coefficient of efficiency of a power plant during the hot periods of the year.

LITERATURE

2011 ASHRAE Handbook: Heating, Ventilating, and Air-conditioning Applications. Atlanta, GA: ASHRAE, 2011.

Al-Ajmi, F., D.l. Loveday, and V.i. Hanby. "The Cooling Potential of Earth–air Heat Exchangers for Domestic Buildings in a Desert Climate." *Building and Environment* 41, no. 3 (12 2006): 235-44. doi:10.1016/j.buildenv.2005.01.027.

Alkhedhair, Abdullah, Hal Gurgenci, Ingo Jahn, Zhiqiang Guan, and Suoying He. "Numerical Simulation of Water Spray for Pre-cooling of Inlet Air in Natural Draft Dry Cooling Towers." *Applied Thermal Engineering* 61, no. 2 (12 2013): 416-24. doi:10.1016/j.applthermaleng.2013.08.012.

Desideri U. and Bidini G. Study of possible Optimization Criteria for Geothermal Power Plants. 1996, In: Proceedings of ECOS 96, Sweden, Jun.25-27, 1996. 313-319. ISBN 91-7170-664-X.

Bourillot, C., TEFERI, Numerical Model for Calculating the Performance of an Evaporative Cooling Tower, EPRI Report CS-3212-SR, August 1983.

Derradji, M. Aiche. “Modeling the soil surface temperature for natural cooling of buildings in hot climates.” The 4th International Conference on Sustainable Energy Information Technology (SEIT-2014) Procedia Computer Science 32 (2014) 615 – 621. Print.

Fisenko, S.p., A.a. Brin, and A.i. Petruchik. "Evaporative Cooling of Water in a Mechanical Draft Cooling Tower." *International Journal of Heat and Mass Transfer* 47, no. 1 (12 2004): 165-77. doi:10.1016/S0017-9310(03)00409-5.

Fu, Wencheng, Jialing Zhu, Wei Zhang, and Zhiyong Lu. "Performance Evaluation of Kalina Cycle Subsystem on Geothermal Power Generation in the Oilfield." *Applied Thermal Engineering* 54, no. 2 (12 2013): 497-506. doi:10.1016/j.applthermaleng.2013.01.044.

Givoni, B. "Performance and Applicability of Passive and Low-energy Cooling Systems." *Energy and Buildings* 17, no. 3 (12 1991): 177-99. doi:10.1016/0378-7788(91)90106-D.

Gnielinski V. New equation for heat and mass transfer in turbulent pipe and channel flow. Int. Chem. Eng. 1976;16: 359–68.

Gruber, “Der Kalina-Cycle zur Stromerzeugung bei Verwendung fester Biomassebrennstoffe.” Diplomarbeit, TUM, Energie Systeme, 2005.

"Heating and Cooling of Buildings: Design for Efficiency." *Choice Reviews Online* 32, no. 03 (12, 1994): 32-1554. doi:10.5860/CHOICE.32-1554.

Incropera, Frank P., and Frank P. Incropera. *Fundamentals of Heat and Mass Transfer*. Hoboken, NJ: John Wiley, 2007.

Kalina, A. I., Leibowitz, H. M., Applying Kalina Technology to a Bottoming Cycle for Utility Combined Cycles, In: Proceedings of the Gas Turbines Conference and Exhibition, Anaheim, California, USA, May 31-June 4, 1987. ASME Paper – No.87-GT-35.

Kloppers, Johannes Christiaan. *A Critical Evaluation and Refinement of the Performance Prediction of Wet-cooling Towers*. 2003.

Krarti, M., C. Lopez-Alonzo, D. E. Claridge, and J. F. Kreider. "Analytical Model to Predict Annual Soil Surface Temperature Variation." *Journal of Solar Energy Engineering* 117, no. 2 (12 1995): 91. doi:10.1115/1.2870881.

Kusuda, Tamami, and Paul R. Achenbach. *Earth Temperature and Thermal Diffusivity at Selected Stations in the United States*. National Bureau of Standards, 1965.

Larsen, Ulrik, Tuong-Van Nguyen, Thomas Knudsen, and Fredrik Haglind. "System Analysis and Optimisation of a Kalina Split-cycle for Waste Heat Recovery on Large Marine Diesel Engines." *Energy*, 12 2013. doi:10.1016/j.energy.2013.10.069.

Lazzeri L. and Bruzzone M. Geothermal Plant Efficiency Enhancement by Means of the Use of Kalina Cycle. In: Proceedings of the 30th Intersociety Energy Conversion Engineering Conference, Orlando Florida, USA Jul.30 – Aug.4, 1995. Vol.2, 453-457. ISSN 0146-955X.

Lolos, “Optimization methods of Kalina cycle”. PhD dissertation, National Technical University of Athens, School of Thermal Engineering, 2010.

Maerefat, M., and A.p. Haghighi. "Passive Cooling of Buildings by Using Integrated Earth to Air Heat Exchanger and Solar Chimney." *Renewable Energy* 35, no. 10 (12 2010): 2316-324. doi:10.1016/j.renene.2010.03.003.

Mlcak, “An Introduction to the Kalina Cycle.” ASME International, Reprinted in 2004 from: PWR- Vol. 30, Proceedings of the International, Joint Power Generation Conference, Editors: L Kielasa, and G. E. Weed, Book No. H01077 -1996.

Pearson, “High Pressure Ammonia Systems – New Opportunities”. International Refrigeration and Air Conditioning Conference, Paper 1111, 2010.

Ranz, Marshall, Evaporation from drops, Chem. Eng. Prog. 48 (1952) 141e146.

Qureshi, Bilal A., and Syed M. Zubair. "A Complete Model of Wet Cooling Towers with Fouling in Fills." *Applied Thermal Engineering* 26, no. 16 (12 2006): 1982-989. doi:10.1016/j.applthermaleng.2006.01.010.

Schiller, Naumann."Uber die grundlegenden berechnungen bei der schwerkraftaufbereitung." Ver. Deut. Ing. 77 (1933): 318-320.

Schlunder, Ernst U. *VDI Heat Atlas*. Dusseldorf: V.D.I.Verlag, 1993.

Shah, R. K., and Dušan P. Sekulić. *Fundamentals of Heat Exchanger Design*. Hoboken, NJ: John Wiley & Sons, 2003.

Shankar Ganesh, T.Srinivas, “Processes assessment in binary mixture plant.” International Journal of Energy and Environment, Volume 4, Issue 2, 2013, pp. 321-330.

Stull, Roland. "Wet-Bulb Temperature from Relative Humidity and Air Temperature." *Journal of Applied Meteorology and Climatology* 50, no. 11 (12 2011): 2267-269. doi:10.1175/JAMC-D-11-0143.1.

Tittelein, Pierre, Gilbert Achard, and Etienne Wurtz. "Modelling Earth-to-air Heat Exchanger Behaviour with the Convolutive Response Factors Method." *Applied Energy* 86, no. 9 (12 2009): 1683-691. doi:10.1016/j.apenergy.2009.02.010.

Turton, Richard. *Analysis, Synthesis, and Design of Chemical Processes*. Upper Saddle River, NJ: Prentice Hall PTR, 1998.

Uchida, Toshihiro. "Present State and Future of Geothermal Energy Technology." *The Journal of the Institute of Electrical Engineers of Japan* 133, no. 4 (12 2013): 226-29. doi:10.1541/ieejjournal.133.226.

Valdimarsson, “Factors influencing the economics of the Kalina power cycle and situations of superior performance.” International Geothermal Conference, Reykjavik, Sept. 2003.

Zhang, Xinxin, Maogang He, and Ying Zhang. "A Review of Research on the Kalina Cycle." Renewable and Sustainable Energy Reviews 16, no. 7 (12 2012): 5309-318. doi:10.1016/j.rser.2012.05.040.

Articles

Allison TR. Heat gains in Kuwait buildings, a simplified code, Kuwait Institute for Scientific Research (KISR) -PPI/110 ENGPT-G-7931, 1979

Black and Veatch (2012), Cost and Performance Data for Power Generation Technologies, Black and Veatch Corporation, Kansas.

Bloomberg New Energy Finance (BNEF) (2012), Q1 2012 Clean Energy Policy & Market Briefing, BNEF, London.

Duffie, John A. "Solar Engineering of Thermal Processes." American Journal of Physics 53.4 (1985): 382. Print.

Energy Recearch Centre of the Netherlands (ECN) (2011), Properties of the O&M Cost Estimator, ECN, Petten

EPRI, Technology Assesments of Advanced Power Generation Systems II-Kalina Botomming Cycle. 1986a. Palo Alto USA: Electrical Power Research Institute. EPRI AP-4681 Project 2528-4, Final Report.

EPRI, State of the art Survey of Diesel Botomming Cycle. 1986b. Palo Alto USA: Electrical Power Research Institute. EPRI AP-4420 Project 2528-2, Final Report.

EPRI, A Comparison of Humid Air Turbine (HAT) Cycle and Combined Power Plants. 1991. Palo Alto USA: Electrical Power Research Institute. EPRI IE-7300, Project 2999-7, Final Report.

Hance, C.N. (2005), Factors Affecting Costs of Geothermal Power Development, Geothermal Energy Association, for the U.S. Department of Energy, Washington, D.C.

Geothermal Technologies Program (GTP) (2008), Geothermal Tomorrow 2008, DOE-GO-102008-2633, Geothermal Technologies Program of the U.S. Department of Energy, Washington, D.C.

Kagel, the State of Geothermal Technology, Part II: Surface Technology, a Publication by the Geothermal Energy Association for the U.S., Department of Energy, 2008

Labs, in: J. Cook (Ed.), Passive Cooling, MIT Press, Cambridge, Massachusetts, 1989.

Maloney J.D. and Robertson R.C., ORNL Report CF-53-8-43, Oak Ridge, TN, 1953.

Zhou, Cheng, Elham Doroodchi, and Behdad Moghtaderi. "An In-depth Assessment of Hybrid Solar–geothermal Power Generation." Energy Conversion and Management 74 (2013): 88-101. Print.

WEBSITES

[1] URL: www.geo-energy.org

[2] International Geothermal Assocation (IGA) (2012), http://www.geothermal-energy.org/.

[3] International Renewable Energy Agency (IRENA) (2012). IRENA Renewable Cost Database. IRENA, Bonn.

[4] International Geothermal Assocation (IGA), website:http://www.geothermal-energy.org/.

[5] URL: http://www.industry.siemens.com

[6] URL: http://www.geothermie-unterhaching.de

[7] URL: http://www.wasabienergy.com/